

Requirements Evaluation for the Implementation of Offshore Electrolysers in Green Hydrogen Production: An Approach for the Marine Industry

Auteur : Aranda Marquez, Alejandro

Promoteur(s) : Rigo, Philippe

Faculté : Faculté des Sciences appliquées

Diplôme : Master : ingénieur civil mécanicien, à finalité spécialisée en "Advanced Ship Design"

Année académique : 2024-2025

URI/URL : <http://hdl.handle.net/2268.2/25049>

Avertissement à l'attention des usagers :

Tous les documents placés en accès ouvert sur le site le site MatheO sont protégés par le droit d'auteur. Conformément aux principes énoncés par la "Budapest Open Access Initiative"(BOAI, 2002), l'utilisateur du site peut lire, télécharger, copier, transmettre, imprimer, chercher ou faire un lien vers le texte intégral de ces documents, les disséquer pour les indexer, s'en servir de données pour un logiciel, ou s'en servir à toute autre fin légale (ou prévue par la réglementation relative au droit d'auteur). Toute utilisation du document à des fins commerciales est strictement interdite.

Par ailleurs, l'utilisateur s'engage à respecter les droits moraux de l'auteur, principalement le droit à l'intégrité de l'oeuvre et le droit de paternité et ce dans toute utilisation que l'utilisateur entreprend. Ainsi, à titre d'exemple, lorsqu'il reproduira un document par extrait ou dans son intégralité, l'utilisateur citera de manière complète les sources telles que mentionnées ci-dessus. Toute utilisation non explicitement autorisée ci-avant (telle que par exemple, la modification du document ou son résumé) nécessite l'autorisation préalable et expresse des auteurs ou de leurs ayants droit.



POLITÉCNICA



Universität
Rostock



Traditio et Innovatio



SOLENT
UNIVERSITY
SOUTHAMPTON



Zachodniopomorski
Uniwersytet
Techniczny
w Szczecinie



With the support of the
Erasmus+ Programme
of the European Union



Requirements Evaluation for Implementation of Offshore Electrolysers in Green Hydrogen Production: An Approach to Marine Industry

submitted on 31 August 2025

by

ARANDA MARQUEZ Alejandro | Av. de la Memoria 4 | Madrid | 28040 | Spain |

alex_aranda123@hotmail.com

ULiège Student ID No.: S2300903

First Reviewer:

Dr. Lionel Gentaz

École Centrale de Nantes

1 Rue de la Noë

44300

Nantes, France

Second Reviewer:

^B Dr. Vladimir Meca López

Supervisors:

^A Dr. Sara Oliveira da Costa

^B Dr. Rafael d'Amore Domenech

^A Navantia Seanergies

Ctra. Algameca, s/n, 30205

Cartagena, Spain

^B Universidad Politécnica de Madrid

Av. De la Memoria 4, 28040

Madrid, Spain



[This page is intentionally left blank]

TABLE OF CONTENTS

ABSTRACT	xiv
1. INTRODUCTION.....	1
1.1. Background	1
1.2. Problem Analysis and Research Questions	5
1.3. Thesis Structure.....	6
2. STATE-OF-THE-ART: GREEN HYDROGEN PRODUCTION TECHNOLOGIES AND THEIR APPLICABILITY TO THE OFFSHORE ENVIRONMENT	8
2.1. Electrolysis Technologies.....	8
2.1.1. Alkaline Water Electrolysis (AWE).....	9
2.1.2. Proton Exchange Membrane Electrolysis (PEM)	14
2.1.3. Anion Exchange Membrane Electrolysis (AEM).....	19
2.1.4. Solid Oxide Electrolyser Cell Electrolysis (SOEC).....	22
2.1.5. Summary of Electrolysis Technologies	26
2.2. Suitability of Hydrogen Production on Offshore Platforms.....	31
2.2.1. Types of floating offshore foundations.....	31
2.2.1.1. TLP	33
2.2.1.2. Semi-Submersible	34
2.2.1.3. Spar.....	36
2.2.1.4. Barge	37
2.2.2. Connection Schemes	39
2.2.2.1. Centralized Onshore Electrolysis	39
2.2.2.2. Centralized Offshore Electrolysis	40
2.2.2.3. Decentralized Offshore Electrolysis.....	41
2.3. Offshore electrolysis demonstrations and pilot projects	45
2.4. Regulatory frameworks	48
3. CASE STUDY: EUROPE	51
3.1. Justification of implementation zone	51
3.2. Implementation scenarios.....	67
3.3. Impact and specific requirements of electrolyzers in offshore environments	70
3.3.1. Dynamics and maximum tilt of platform	71
3.3.2. Intermittency and variability of energy	80
3.3.3. Marine environment	82

3.3.4. Water quality	82
3.3.5. Summary of requirements	83
4. TECHNO-ECONOMIC EVALUATION FOR INTEGRATION OF HYDROGEN PRODUCTION WITH FLOATING OFFSHORE WIND	85
4.1. Methodology for Techno-Economic Model	85
4.1.1. Economic Model Estimation.....	87
4.1.1.1. CAPEX.....	87
4.1.1.2. OPEX	99
4.1.1.3. DECEX.....	102
4.1.2. Technical Model Estimation.....	103
4.2. Case Analysis and Results.....	108
4.3. Sensitivity Analysis.....	114
5. CONCLUSIONS AND FUTURE WORK.....	119
5.1. Future Work and Recommendations	121
6. ACKNOWLEDGEMENTS	122
7. REFERENCES.....	123
8. APPENDICES	137
8.1. Electrolyser Commercial Database	137
8.2. Hydrogen Carriers Storage and Transportation.....	141
8.3. Demonstration and Pilot Projects Overview	145
8.4. Semi-Submersible Centralized Platform 2D Layout.....	148
8.5. Semi-Submersible Centralized Platform RAOs for Motion and Acceleration ...	152
8.6. LCOH Calculations for Case Study	158

LIST OF FIGURES

Figure 1.1: New Wind Power Capacity in the EU – WindEurope’s Outlook.	4
Figure 1.2: European maps of European (a) yearly energy production and (b) LCOH in 2030.	4
Figure 2.1: Alkaline Electrolysis Technology: Cell Level.	11
Figure 2.2: Alkaline Electrolysis Technology: Stack Level.	13
Figure 2.3: Alkaline Electrolysis Technology: BoP Level.	14
Figure 2.4: PEM Electrolysis Technology: Cell Level.	15
Figure 2.5: PEM Electrolysis Technology: Stack Level.	17
Figure 2.6: PEM Electrolysis Technology: BoP Level.	18
Figure 2.7: AEM Electrolysis Technology: Cell Level.	19
Figure 2.8: AEM Electrolysis Technology: Stack Level.	21
Figure 2.9: AEM Electrolysis Technology: BoP Level.	22
Figure 2.10: SOEC Electrolysis Technology: Cell Level.	23
Figure 2.11: SOEC Electrolysis Technology: Stack Level.	25
Figure 2.12: SOEC Electrolysis Technology: BoP Level.	26
Figure 2.13: Commercial Database: Electrolyser Power Boxplot.	29
Figure 2.14: Commercial Database: Electrolyser Electrical Efficiency.	29
Figure 2.15: Trade-offs between efficiency, durability, and cost for electrolyzers.	30
Figure 2.16: Types of Floating Foundations.	33
Figure 2.17: TLP foundation in Float4Wind by SBM Offshore.	34
Figure 2.18: Semi-Submersible foundation in WindFloat Atlantic.	35
Figure 2.19: Spar foundation in Hywind Tampen.	36
Figure 2.20: Barge Platform in Floatgen by BW-IDEOL.	38
Figure 3.1: Map of total planned hydrogen consumption in the industry by 2030 in EU+EFTA+UK region.	53
Figure 3.2: Forecasted hydrogen demand clusters in Germany until 2030.	54
Figure 3.3: The Hydrogen Map. Sweden and Finland 2025-02.	55
Figure 3.4: Hydrogen Valleys in Netherlands.	56
Figure 3.5: Production capacity by region in France per year.	56
Figure 3.6: Hydrogen Project Census in Spain.	57
Figure 3.7: Hydrogen Infrastructure Map for European Hydrogen Backbone in 2040.	58
Figure 3.8: Site-selected location Viana do Castelo for case study.	67
Figure 3.9: Semi-submersible Hull Mesh for Centralized Electrolysis Platform at Waterline.	75
Figure 4.1: Evolution of electrolyser rated costs with scaling effect and learning rates.	91
Figure 4.2: String-based wind farm layout with inter-array cables for centralized configurations.	93
Figure 4.3: Radial-based wind farm layout with inter-array pipelines for decentralized configurations.	94
Figure 4.4: Power Curve approximation through Equation (4.54). Parameters adjusted for Vestas V236-15.0.	104
Figure 4.5: Lifetime cost structure and LCOH overview across all implementation scenarios in Viana do Castelo Case Study.	113

Figure 4.6: LCOH sensitivity analysis with Water Depth parameter for implementation scenarios.	114
Figure 4.7: LCOH sensitivity analysis with Distance to Shore parameter for implementation scenarios.	115
Figure 4.8: HVAC vs. HVDC comparison in Onshore Centralized Scenario.	116
Figure 4.9: LCOH sensitivity analysis with Distance to Port parameter for implementation scenarios.	116
Figure 4.10: LCOH sensitivity analysis with Wind Potential parameter for implementation scenarios.	117
Figure 8.1: Commercial Database: Stack Power Boxplot.	137
Figure 8.2: Commercial Database: Electrolyser Power Boxplot.	137
Figure 8.3: Commercial Database: Nominal H ₂ Production Boxplot.	138
Figure 8.4: Commercial Database: Specific H ₂ Production Boxplot.	138
Figure 8.5: Commercial Database: H ₂ Output Pressure Boxplot.	139
Figure 8.6: Commercial Database: Electrolyser Electrical Consumption Boxplot.	139
Figure 8.7: Commercial Database: Minimum Load Boxplot.	140
Figure 8.8: Commercial Database: Electrolyser Electrical Efficiency.	140
Figure 8.9: Deck #1 2D Layout at 23 meters (Cable Deck).	148
Figure 8.10: Deck #2 2D Layout at 28 meters (Main Deck).	149
Figure 8.11: Deck #3 2D Layout at 38 meters (PEM Deck #1).	150
Figure 8.12: Deck #4 2D Layout at 43 meters (PEM Deck #2).	151
Figure 8.13: Centralized platform Hydrostar RAO for surge.	152
Figure 8.14: Centralized platform Hydrostar RAO for sway.	152
Figure 8.15: Centralized platform Hydrostar RAO for heave.	153
Figure 8.16: Centralized platform Hydrostar RAO for roll.	153
Figure 8.17: Centralized platform Hydrostar RAO for pitch.	154
Figure 8.18: Centralized platform Hydrostar RAO for surge.	154
Figure 8.19: Centralized platform Hydrostar RAO for acceleration in surge.	155
Figure 8.20: Centralized platform Hydrostar RAO for acceleration in sway.	155
Figure 8.21: Centralized platform Hydrostar RAO for acceleration in heave.	156
Figure 8.22: Centralized platform Hydrostar RAO for acceleration in roll.	156
Figure 8.23: Centralized platform Hydrostar RAO for acceleration in pitch.	157
Figure 8.24: Centralized platform Hydrostar RAO for acceleration in yaw.	157
Figure 8.25: Detailed LCOH calculations across the project's lifetime at Viana do Castelo case study for Centralized Onshore scenario.	158
Figure 8.26: Detailed LCOH calculations across the project's lifetime at Viana do Castelo case study for Centralized Offshore scenario.	159
Figure 8.27: Detailed LCOH calculations across the project's lifetime at Viana do Castelo case study for Decentralized Offshore scenario.	160

LIST OF TABLES

Table 1.1: Colors of hydrogen production according to Hydrogen Europe	2
Table 2.1: Overview of types of electrolyzers.....	28
Table 2.2: Overview of main floating foundation types.....	39
Table 2.3: Overview of main connection schemes.....	43
Table 3.1: Overview of Leading Countries according to Hydrogen Potential Consumption, Off-takers and Infrastructure.	59
Table 3.2: Objective and Exclusion Criteria for MCDM.	60
Table 3.3: Site-Selection Decision Matrix for MCDM method in the European Atlantic Coast.	60
Table 3.4: Scales of Pairwise Comparisons.....	61
Table 3.5: Comparison among criteria for AHP Method.	65
Table 3.6: Normalized decision matrix P_{ij} for Entropy Method.	65
Table 3.7: Criteria Weights for AHP, Entropy and Combined Methods with balancing factor $\alpha = 0.8$. See Table 3.2 for abbreviations of parameters.	65
Table 3.8: Weighted and normalized decision matrix V_{ij} , ideal solutions and rank of TOPSIS Method.	66
Table 3.9: Characteristics of the site selected for techno-economical evaluation.....	67
Table 3.10: Equipment weight and quantity assumptions for a 500 MW centralized electrolysis plant.....	73
Table 3.11: Estimated total weights for a 500 MW centralized electrolysis plant mounted on a semi-submersible platform.....	74
Table 3.12: Semi-submersible Design Parameters for a 500 MW Centralized Electrolysis Plant.	74
Table 3.13: Semi-submersible Mass and Inertia Properties.	77
Table 3.14: Semi-submersible Parameters for Static Stability Check.....	77
Table 3.15: Historical waves of buoy at Costera de Silleiro from 1996-2006.	77
Table 3.16: PEM Modules Relative distance to CoG of platform.....	78
Table 3.17: Peak Response Check for Maximum Tilt and Linear Accelerations in PEM Modules.....	79
Table 4.1: Wind Turbine Installation Parameters.	89
Table 4.2: Installation parameters for offshore floating platform foundations.	90
Table 4.3: Techno-economic costs for 66 kV inter-array cables.	93
Table 4.4: Pipeline Inter-array radial configuration.	94
Table 4.5: Pipe size and miscellaneous cost factors for pipelines.....	95
Table 4.6: Pipe size and number of connection slots factors for manifolds.	96
Table 4.7: Techno-economic assumptions for site-specific HVAC export cables.....	98
Table 4.8: Recommended Pipeline Diameters for pure hydrogen (IN: 30 bar, OUT: 24 bar).	99
Table 4.9: Major wind turbine repair vessel parameters.	102
Table 4.10: Vestas V235-15.0 main parameters for power generation.....	104
Table 4.11: PEM Electrolyser Parameters: Siemens Silyzer 300.....	105
Table 4.12: Failure rates and repair times for transmission components.	106
Table 4.13: Efficiency values along the hydrogen production chain for conversion.	107

Table 4.14: Cost breakdown of sub-systems for each implementation scenario.....	108
Table 4.15: Lifetime cost overview without NPV correction for each implementation scenario.	110
Table 4.16: Technical Performance and Hydrogen Output across implementation scenarios.	110
Table 4.17: LCOH results comparison with and without stack degradation across implementation scenarios.	111
Table 4.18: Sensitivity methodology for site-specific parameters.	114
Table 8.1: Pairing of Storage and Transportation of Hydrogen	143
Table 8.2: State-of-the-art in industry for hydrogen production platforms.	145

LIST OF ABBREVIATIONS

AEM	Anion Exchange Membrane
AHP	Analytic Hierarchy Process
AHTS	Anchor Handling Tug Supply Vessel
AHV	Anchor Handling Vessel
AWE	Alkaline Water Electrolysis
BoP	Balance of Plant
CoG	Center of Gravity
CTV	Crew Transfer Vessels
DLC	Design Load Cases
DoF	Degrees of Freedom
e ⁻	Electron
EEZ	Exclusive Economic Zone
GBS	Gravity Based Structures
GIS	Geographic Information System
H ⁺	Hydrogen Ions
H ₂	Hydrogen Gas
H ₂ O	Water
HER	Hydrogen Evolution Reaction
HHV	High Heating Value
HLCV	Heavy Lift Cargo Vessel
HVAC	High Voltage Alternating Current
HVDC	High Voltage Direct Current
KOH	Potassium Hydroxide
LHV	Low Heating Value
LOHC	Liquid Organic Hydrogen Carrier
LSCF	Lanthanum Strontium Cobalt Ferrite
LSM	Lanthanum Strontium Manganite
MCDM	Multi-Criteria Decision Making
MRL	Manufacturing Readiness Level
NaOH	Sodium Hydroxide
NPV	Net Present Value
O ₂	Oxygen Gas
OER	Oxygen Evolution Reaction
OH ⁻	Hydroxide Ions
PEM	Proton Exchange Membrane
PFSA	Perfluorosulfonic Acid
PGM	Platinum Group Metals
RAO	Response Amplitude Operator
SOEC	Solid Oxide Electrolyser Cell
SOFC	Solid Oxide Fuel Cells
TLP	Tension Leg Platforms

TOPSIS	Technique for Order of Preference by Similarity of Ideal Solution
TRL	Technology Readiness Level
YSZ	Yttria-stabilized Zirconia

LIST OF SUBSCRIPTS AND SUPERSSCRIPTS

A	Arrays
BA	Base
D	Decentralized
DS	Desalinators
EC	Export Cable
EL	Electrolyser
EP	Export Pipe
EQ	Equipment Costs
Gen	Generated
IAC	Inter-Array Cables
IAP	Inter-Array Pipelines
IC	Installation Costs
inst	Installation
load	Loading
maj	Major
MF	Manifold
min	Minor
misc	Miscellaneous
OFF	Offshore
PC	Power Converter
PF	Platform
RC	Repair Costs
S	Section of Cable
s	Slots
SD	Stack Degradation
sp	Pipe Size
SR	Stack Replacement
SS	Substation
TE	Turbine Equipment
TF	Turbine Foundation
TR	Transmission
u	Units
WF	Wind Farm
WT	Wind Turbine

LIST OF VARIABLES

c	Coefficient	-
CAPEX	Capital Expenditures	€
DECEX	Decommissioning Expenditures	€
DP	Distance to Port	km
DR	Day Rate	€/d
DS	Distance to Shore	km
E	Total Amount of Hydrogen Produced	kgH ₂
L	Project's Lifetime	yr
LCOH	Levelized Cost of Hydrogen	€/yr
N	Number of Elements	-
OPEX	Operational Expenditures	€
P	Power	kW
P*	Equivalent Electric Power	kW
r	Rate of Return	%
RC	Rated Costs	€/kW
t	time	h
UC	Unit Cost	€
v	Velocity	m/s
VC	Vessel Capacity	units/lift
WD	Water Depth	m
WP	Wind Potential	h/yr
V _{H2O}	Nominal Flow Rate of Water	m ³ /h
LC	Linear Cost	€/m
L	Length of Element	m
D	Mean Distance	m
CD	Capacity Density	MW/km ²
LIC	Linear Installation Cost	€/m
CF	Cost Factor	-
d	Pipeline Diameter	m
A	Area of Downstream Turbines	km ²
Q	Maximum volumetric flow rate	Nm ³ /h
LoC	Logistics Costs	
λ	Probability of Failure	f/yr
U	Cable Tension	kV
R	Cable Resistance	ohm/km

[This page is intentionally left blank]

DECLARATION OF AUTHORSHIP

I, ALEJANDRO ARANDA MARQUEZ, declare that this thesis and the work presented in it are my own and have been generated by me as the result of my own original research.

Where I have consulted the published work of others, this is always clearly attributed.

Where I have quoted from the work of others, the source is always given. With the exception of such quotations, this thesis is entirely my own work.

I have acknowledged all main sources of help.

Where the thesis is based on work done by myself jointly with others, I have made clear exactly what was done by others and what I have contributed myself.

This thesis contains no material that has been submitted previously, in whole or in part, for the award of any other academic degree or diploma.

I cede copyright of the thesis in favour of Universidad Politécnica de Madrid

Date: 30 August 2025

Signature:

A handwritten signature in dark ink, appearing to be 'Alejandro Aranda Marquez', written over a series of horizontal lines.

[This page is intentionally left blank]

ABSTRACT

The marine industry is increasingly evaluating offshore green hydrogen production as a pathway to decarbonize key energy-intensive sectors. However, offshore electrolyzers face unique technical, economic, and operational challenges that require adaptation to withstand harsh marine conditions. This thesis evaluates the requirements, feasibility, and techno-economic performance of integrating offshore electrolysis and wind resources. It combines a comprehensive state-of-the-art of electrolyser technologies and floating offshore foundations with a European case study and a techno-economic framework.

The state-of-the-art identifies key strengths and limitations of the main types of electrolysis technologies, as well as the current market trends and gaps of floating platforms concepts, connection schemes, demonstration projects, and regulatory frameworks. It highlights that PEM offers the greatest offshore readiness due to its compactness, pressurized hydrogen output, low minimum load, and fast dynamic response despite its reliance on precious metals.

The case study applies a multi-criteria site-selection which identified Viana do Castelo as the optimal Atlantic location for a 500 MW offshore hydrogen project. It is based according to market demand, infrastructure and resource availability for the 3 configuration schemes considered. Experimental testing and hydrodynamic modelling of a semi-submersible platform with PEM modules confirm an acceptable performance under marine motions with mitigation and operational strategies, including ramping controls, buffering, marine-grade protection, and integrated water treatment.

Finally, a techno-economic evaluation estimates LCOH of 4.00 €/kg for centralized onshore, 4.57 €/kg for centralized offshore, and 4.82 €/kg for decentralized offshore electrolysis at the case study site. A sensitivity analysis shows that wind availability appears as the dominant cost driver. Export distances over ~120 km favor HVDC or hydrogen pipelines due to electrical losses in HVAC, while port distance increase O&M significantly until SOVs become viable at ~150 km. Water depth does not influence results significantly for the deep-water range considered. Centralized onshore electrolysis remains the most cost-effective for near-shore sites with strong wind and proximity to shore, while offshore configurations gain advantage when long export distances or space limitations occur.

1. INTRODUCTION

The aim of this chapter is to present a description of the foundation and groundwork of this research. Section 1.1 highlights the comprehensive background and context to determine the key requirements for the implementation of offshore electrolyzers in green hydrogen production offshore. Section 1.2 details the critical problem analysis as well as the research questions that are driving this study by identifying the opportunities, challenges, and gaps in current technologies, regulations, and market dynamics. Lastly, Section 1.3 overviews and briefly explains the contents of the chapters covered during this study.

1.1. Background

Currently, excessive consumption of fossil fuel resources caused by the rapid industrialization and urbanization has led to an increase in greenhouse gas (GHG) emissions. This has caused the reach of new records in clear signs of human-induced climate change in the year 2024, with an increase in the global near-surface temperature to be more than 1.55 ± 0.13 °C above the pre-industrial era [1]. Approximately about three-quarters of the GHG emissions are produced by the energy sector, which makes it a crucial player against the challenge of the effects of climate change. To achieve net-zero emissions of global carbon dioxide (CO₂) by 2050 and limit the global temperature rise, it requires a transformation towards a greener economy of how the energy is produced, transported and used [2].

Hydrogen (H₂) is the most simple and abundant element in the universe, which consists of only one proton and electron in its composition. However, hydrogen exists always bound with one or many elements and does not exist as pure gas naturally on Earth [3]. One of the benefits that hydrogen can provide is to be used as an energy carrier, which can deliver and store a large amount of energy and used when and where it is needed. A way to extract the energy stored in the H₂ molecule can be done using fuel cells or other energy systems such as internal combustion engines or generator sets. This is possible since it has the highest energy per mass of any fuel at 120 MJ/kgH₂ but has a downside of having a low volumetric density of only 8 MJ/L in the form of liquid hydrogen and even less for compressed hydrogen at 350 bar pressure with 2.7 MJ/L [4]. Nonetheless, their high efficiency and zero-emission capabilities have a real potential to reduce the GHG emission in its many applications to be used [5]. H₂ global production has reached 97 Mt in 2023, from which only 1% is accounted to be produced by means of low emission sources. According to planned projects, the low emission production could rise to 49 Mt by 2030 [6].

Hydrogen can be classified into different types according to their method of production, necessary raw material and the amount of GHG emissions. One of these classifications is by the “color” of the hydrogen production by Hydrogen Europe as shown in Table 1.1 [7]. Some of these colors like black, brown and grey hydrogen are produced using traditional methods which rely on fossil fuels and are responsible for significant CO₂ emissions. A way to mitigate these emissions and their impact is through using carbon capture and sequestration techniques (CCS), which turns it into a blue hydrogen production. Another method that is still in its experimental stage is the turquoise hydrogen, which removes the carbon in a solid form and reduces the impact of CO₂ emissions. Additionally, hydrogen can be produced by using nuclear-based methods using electricity or high temperature or a combination of both for the color’s red, pink and purple hydrogen production respectively, but has the disadvantage of creating nuclear waste. Considering all these types of production, green hydrogen stands out as the most sustainable option by using renewable energy for the electrolysis process on water, which results in a zero-carbon emission production.

Table 1.1: Colors of hydrogen production according to Hydrogen Europe
Source: [7].

Hydrogen Type “Color”	Production technology	CO ₂ Emissions
Black / Brown	Produced from coal gasification depending on coal type: bituminous (black) and lignite (brown).	19 tCO ₂ /tH ₂
Grey	Produced from fossil fuel and commonly uses steam methane reforming	10 – 19 tCO ₂ /tH ₂
Blue	Produced from natural gas by steam gas reforming paired with carbon capture and sequestration (CCS)	9-12 tCO ₂ /tH ₂
Turquoise	Extracted by thermal splitting of methane through pyrolysis (experimental)	Removes carbon in a solid form instead of CO ₂ gas
Red	Produced by high-temperature catalytic splitting of water using thermal nuclear power.	Zero CO ₂ emissions but generates nuclear residue.
Pink	Produced by electrolysis of water using electricity from a nuclear power plant	Zero CO ₂ emissions but generates nuclear residue.
Purple	Produced by using nuclear power and heat for chemo-thermal water electrolysis	Zero CO ₂ emissions but generates nuclear residue.
White	Naturally hydrogen occurs within Earth’s crust. (No strategies to exploit)	Zero CO ₂ emissions
Green	Produced by water electrolysis using renewable energy sources.	Zero CO ₂ emissions

It is necessary to invest in green hydrogen technology to support global climate goals and reduce industrial emissions by developing new technologies and improving efficiency in the production of green hydrogen. There are various initiatives in Europe that are working to accelerate the transition into green technologies through the development of clean hydrogen technologies. The EU Hydrogen Strategy has as its main purpose to create a roadmap for building a fully integrated hydrogen economy by recognizing its use as a feedstock, fuel and energy carrier to decarbonize key sectors. Another initiative is the European Commission's Next Generation EU recovery plan, which prioritizes all investments made into hydrogen technologies to enhance technological developments while creating economic growth and local jobs for the community while positioning EU as a global leader in hydrogen [8]. These initiatives align with several of the United Nations Sustainable Development Goals (SDGs). Green hydrogen specifically contributes by promoting the use of renewable energy use to obtain affordable and clean energy (SDG 7), by driving technological advancements in clean energy (SDG 9) to reduce GHG emissions (SDG 13). It also contributes as mentioned before by creating new job opportunities (SDG 8) while enabling cleaner transportation and energy systems (SDG 11), which has a key role in achieving a sustainable future [9].

Additionally, the REPowerEU Plan sets indicative green hydrogen production goals which targets 10 million tons of hydrogen production for both domestic production as well as imported renewable hydrogen by 2030. The plan outlines a set of six key measures to be able to achieve this, which consists of raising targets for renewable hydrogen use in industry and transportation, increasing investments by €200 million in clean hydrogen, refining methodologies for measuring GHG emissions, assessing the IPCEIs for clean hydrogen, accelerate the missing standards and infrastructure in the industry, and committing to the report of hydrogen uptake and use in both industry and transportation [10].

To transition into utilizing renewable energy and achieving a greener economy, Europe has been investing and making significant strides to expand its offshore wind energy capacity. During 2024, an increase of 16.4 GW in wind power capacity was installed, with 2.6 GW corresponding to offshore wind power connected to the grid to achieve a total of 37 GW in its offshore capacity. Expectations for Europe according to WindEurope's outlook indicates that there would be an increase of offshore wind power capacity of approximately 50 GW to reach expected agreements by EU member states of 87 GW offshore as shown in Figure 1.1 [11].

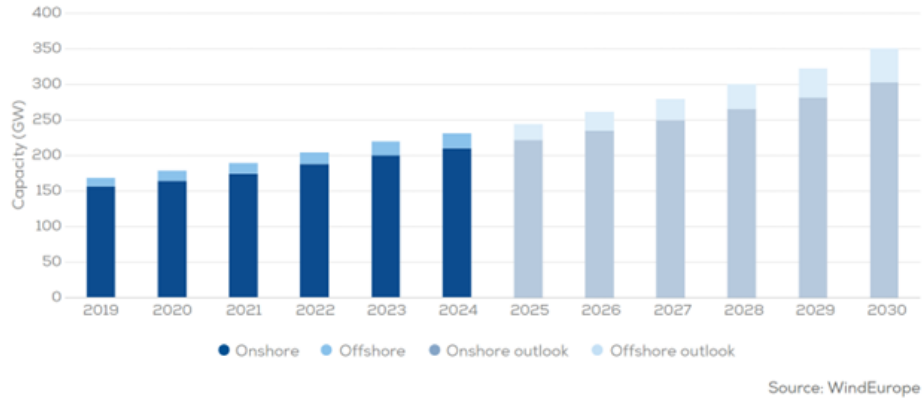


Figure 1.1: New Wind Power Capacity in the EU – WindEurope's Outlook.
Source: [11].

With an increase in the capacity and efficiency of renewable energy and higher wind resource coming from offshore wind power, considering offshore hydrogen production can be viable. This, when paired with pipeline transport or carriers to shore, presents a more cost-effective solution than onshore electrolysis in many scenarios as the technology and infrastructure involved advances. When considering pipeline transport, studies show that while in 2020 offshore hydrogen was mainly viable when paired with deep-water and with great distances from shore, the estimated projections by 2050 indicate that it will become feasible economically in all scenarios except on nearshore and shallow locations. Additionally, assessments made by considering the variations determine that about 200 TWh of supply of energy corresponding to offshore electrolysis can compete with onshore scenarios. This potential is calculated considering the wind patterns, the seafloor depth, as well as the port and shore distance as seen in Figure 1.2, which gives an indication that offshore hydrogen production can be a potential strategic path forward to achieve a sustainable and scalable green economy [12].

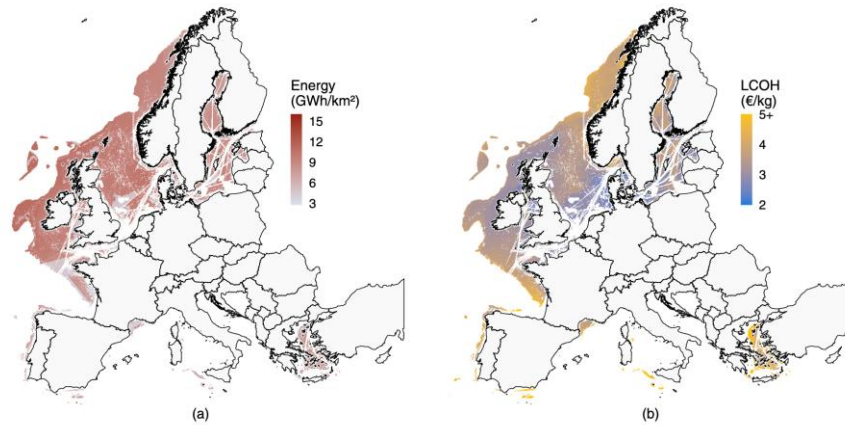


Figure 1.2: European maps of European (a) yearly energy production and (b) LCOH in 2030.
Source: [12].

1.2. Problem Analysis and Research Questions

The marine industry is increasingly exploring the possibility of developing offshore green hydrogen production to support the decarbonization of certain key industries and the energy sector. However, utilizing offshore electrolyzers for the use of green hydrogen production by means of wind power presents a set of technical, economical, and operational challenges that are not present when considering onshore electrolysis technology. This produces a need to adapt electrolysis systems in their Balance of Stack (BoS) and Balance of Plant (BoP) to withstand the harsh marine environment as well as the intermittency present when using wind energy.

This key challenge of differentiating the conditions and the necessary specific requirements related to the offshore environment is necessary to be addressed and understood. This includes optimizing the materials, the system design, and the technology to fight against corrosion, saltwater exposure, temperature fluctuations and wave forces, especially with floating platforms. Additionally, to address the intermittency of wind energy when integrating it into the offshore hydrogen production system, an efficient coupling must be achieved while managing any issues that can be presented like the energy storage, grid connection, and power fluctuations.

Furthermore, the economic feasibility of implementing these offshore electrolysis systems needs to be considered and analyzed accordingly. This depends on various factors like the cost and type of offshore foundations, considering both fixed versus floating platforms, the distance to shore and ports, and costs associated with the installation, operation, and maintenance. For this, understanding the Levelized Cost of Hydrogen (LCOH) can help to determine if a project is viable by being able to compare various scenarios and determine which are the best options. The goal is to determine under what conditions offshore green hydrogen can become economically and technically competitive by using a techno-economic analysis that incorporates the choice of electrolyser technology, platform type, connection schemes, and the choice of the optimal location according to site-specific parameters.

The following main and sub research questions will guide this research and will be answered during the thesis:

1. What are the technical requirements and challenges for implementing offshore electrolysis systems in the marine industry?

- a. How do the BoS and BoP requirements for offshore electrolysis differ from those for onshore systems in terms of efficiency, durability, and resistance to

harsh marine conditions and what is necessary to withstand marine conditions?

- b. How can offshore electrolysis systems be integrated effectively with intermittent wind energy to optimize hydrogen production while managing energy fluctuations and storage?
- c. Which are the best alternatives for implementation scenarios to integrate green hydrogen production with floating offshore wind according to the economic and technical aspects?

2. What are the economic feasibility and cost factors associated with offshore green hydrogen production, and how do platform and location affect this?

- a. How do the costs of floating foundations impact the economic feasibility of offshore hydrogen production, including installation, operation, and maintenance costs?
- b. What are the regulatory challenges and international compliance requirements that affect the economic competitiveness and deployment timeline of offshore electrolysis technology?
- c. How do offshore location factors, such as foundation type, distance to shore and renewable energy resource availability, influence the LCOH across different implementation scenarios?

1.3. Thesis Structure

This work is split into five chapters along with several appendices to with the objective of answering the main and sub research questions proposed.

Chapter 0: Introduction gives an overview of the importance of this study and presents a description of the foundation and groundwork for context. It highlights why implementation of offshore electrolysers in green hydrogen production is in demand and gives a preview of the objectives to be followed later in the work

Chapter 2: State-of-the-art presents a comprehensive overview of the current state-of-the-art for green hydrogen electrolysis technologies as well as its suitability for production in offshore environments. It begins by examining the four main technologies of electrolysers by highlighting their operational principles, efficiencies, material requirements, and suitability for offshore environments by exploring in the levels of cell, stack, and balance of plant. It then explores the structural and functional characteristics of offshore floating platforms and the

various connection schemes to integrate offshore wind energy with electrolysis. Additionally, current demonstrations and pilot projects worldwide are detailed to offer insights into technological readiness and practical challenges, as well as the current regulatory frameworks that govern hydrogen production to identify existing gaps for safe, efficient, and scalable implementation.

Chapter 3: Case Study details a European case study aimed at identifying and evaluating a strategic location for offshore green hydrogen production using floating offshore wind resources. It begins by analyzing the regional demand of hydrogen and potential industrial off-takers and infrastructure to justify a suitable implementation zone. A multi-criteria approach is then applied to assess potential sites along the Atlantic coast and selecting an optimal site. It proceeds to define and compare the three implementation scenarios considered and finally explores the specific technical impacts and requirements of operating electrolyzers to withstand the offshore environment and intermittency and variability of the wind resource.

Chapter 4: Techno-economic Evaluation develops and presents a techno-economic model to evaluate the performance and cost-effectiveness of the three implementation scenarios at the selected site. It then compares the scenarios in terms of lifetime costs, hydrogen output, and the Levelized Cost of Hydrogen (LCOH) and conducts a sensibility analysis to assess the influence of key location parameters such as water depth, wind potential, and proximity to shore and port, and how they affect the economic viability of each configuration.

Chapter 5: Conclusions recapitulate the key findings and relevant conclusions achieved by offering a comprehensive review of the technical and economic viability of integrating floating offshore wind with green hydrogen production. This chapter highlights the trade-offs between each of the implementation scenarios and outlines future research directions with the recommendations for future research.

2. STATE-OF-THE-ART: GREEN HYDROGEN PRODUCTION TECHNOLOGIES AND THEIR APPLICABILITY TO THE OFFSHORE ENVIRONMENT

The aim of this chapter is to cover the most recent stage of research and development in the field of green hydrogen production technologies, as well as its applicability to the offshore environment. Section 2.1 highlights the 4 main electrolyser technologies and current developments in a database with commercial data and compares its main characteristics to apply in an offshore environment. Section 2.2 briefly describes the types of floating offshore platforms and their current developments, as well as the types of transmission connection schemes to determine the suitability of hydrogen production offshore. Section 2.3 details current demonstration and pilot projects for offshore electrolysis to determine current trends and market demands in the field and its development. Lastly, Section 2.4 overviews the current regulatory frameworks and identifies possible gaps for hydrogen production and offshore platforms to ensure safety, reliability and compliance with international standards.

2.1. Electrolysis Technologies

Water electrolyser systems are electrochemical devices that are used to split water molecules to produce hydrogen and oxygen by the passage of an electric current, causing the following reaction in Equation (4.1):



The principle of water electrolysis is simple, but the technologies to achieve this vary in physical, chemical and electrochemical aspects. One of the main parameters of the operation of a cell or stack electrolysis is the current density applied, which is directly proportional to the quantity of gases produced and measured by the amperage by squared centimeters of surface at the electrode. Another parameter is the voltage at the cell, which varies according to the current density and creates a polarization curve to characterize the operation and behavior of the cell. The use of renewable energy sources in the electrolysis process results in the production of clean and renewable high purity (99.99%) green hydrogen and oxygen [13]. The electrolysis process can be divided into three levels of increased complexity divided into cells, stacks and balance of plant levels [14].

The cell is the central component of the electrolyser, in which the electrochemical reaction takes place. The cell is made of two electrodes (anode and cathode) in contact with an electrolyte in liquid form or as a solid membrane, two porous transport layers which promote the transport of reactants and product removal, and the bipolar plates that offer mechanical support as well as to distribute the flow.

The stack includes multiple electrochemical cells electrically connected in series and hydraulically connected in parallel, spacers which insulate the two opposite electrodes, seals, frames for mechanical support and end plates to avoid leaks and collect fluids.

The system level or balance of plant (BoP) extends beyond the stack to incorporate equipment for cooling, hydrogen processing for purity and compression, electricity conversion with transformers and rectifiers, water supply treatment and gas output. Pumps or gravity are used to introduce purified water into the system. The process occurs once the water reaches the electrodes by flowing through the bipolar plates and through the porous transport layers. At the electrode, the water is split into oxygen and hydrogen, with hydrogen ions (H^+) or hydroxide ions (OH^-) crossing through the electrolyte. The membrane or diaphragm is responsible for keeping gases produced separated and avoiding a mixture.

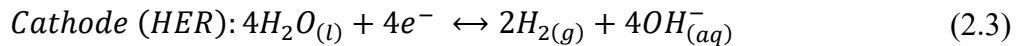
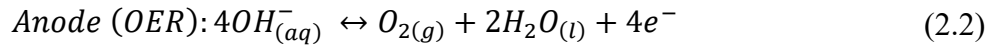
Electrolysers are typically divided into four main technologies, distinguished by the type of electrolyte and temperature of operation, materials, and components. The four main types of electrolysers are Alkaline (AWE) and Proton Exchange Membrane (PEM) in a commercial development stage, while Anion Exchange Membrane (AEM) and Solid Oxide (SOEC) are at lab scale with a promise of a major step forward.

2.1.1. Alkaline Water Electrolysis (AWE)

Alkaline water electrolysis (AWE) is a well-established and most mature electrochemical process for electrolytic hydrogen production and is characterized by its large single-cell stacks, hydrogen production capacity, durability, and low cost, especially in large-scale industrial applications [15]. When an electric current is applied to the electrolysis cell, the water molecules get reduced into H^+ ions which become hydrogen gas (H_2) when gaining an electron, and OH^- ions. The hydroxide ions move towards the anode, where they are oxidized and release oxygen gas (O_2). This flow of charge carriers depends on the ionic conductivity of the electrolyte and is driven by hydroxide ions between the cathode and anode, and electrons are transferred via an external circuit from the anode to the cathode.

To produce this reaction, an external DC power supply is required to kick start the process by a difference in potential in between the two electrodes. Since liquid water is

characterized as having poor electrical conductivity at room temperature, a way to improve the conductivity is to use alkaline compounds like potassium hydroxide (KOH) or sodium hydroxide (NaOH) as electrolyte. KOH electrolyte disassociates into K^+ and OH^- ions and enables electricity conduction between the electrodes typically made of nickel, while the ion conductive membrane permits the transport of hydroxide ions and prevents gas crossover. With the addition of a current density and voltage, two half reactions for hydrogen evolution reaction (HER) and oxygen evolution reaction (OER) occur.



Equation (2.2) outlines the cathodic reaction occurring at the electrode wired to the negative terminal of the DC source, while Equation (2.3) outlines the anodic reaction at the positive terminal. This process yields gases with high purity, making it an efficient method for hydrogen production. A key component in this process is the separator membrane, which prevents mixing between gases and any potential combustion due to mixing of the produced gases.

The AWE process is an endothermic reaction, meaning it requires external energy. The reactions produce two hydrogen molecules for each oxygen molecule and do not consume any alkaline ions, which suggests that its only role is to enhance the solution's conductivity directly [16].

AWE electrolyzers have a simple stack and system design that are relatively easy to manufacture. Figure 2.1 illustrates the AWE electrolyser and its fundamental principles within the technology at the cell level. They generally operate between 0.2 to 0.8 A/cm² with a system efficiency of 50% to 90% according to literature [14], [15], [16], [17], [18], [19], [20] with the current lowest installed cost but a larger footprint between 100 to 170 m²/MW. It uses a high concentrate KOH, typically in solutions of 30% as an electrolyte as well as Nickel based electrodes for the electron flow [15]. The use of a liquid electrolyte results in a bulky stack configuration and represents an additional ohmic loss and a longer start up time due to the resistance, viscosity and thermic mass of the own electrolyte. Having a high concentration of electrolyte, as well as increasing the current density and voltage may improve efficiency but can lead to increased deterioration of the electrodes [21].

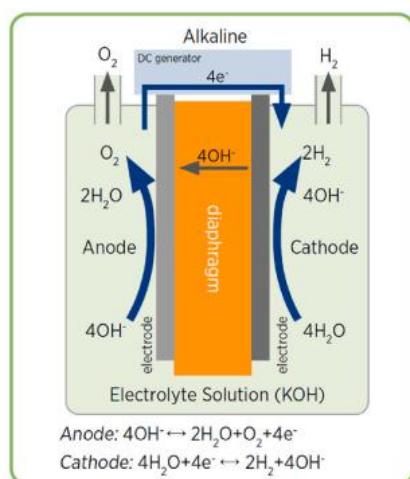


Figure 2.1: Alkaline Electrolysis Technology: Cell Level.
Source: [14].

Due to the alkaline environment, electrodes must be corrosion-resistant, conductive, and catalytically active. Nickel is widely used for both the HER and OER due to its effectiveness in basic media, while stainless steel is suitable for OER. Importantly, AWE electrodes typically avoid critical raw materials like platinum group metals. Ni or Ni-Raney is commonly used for the cathode due to its high HER activity, though its performance can degrade over time due to Ni hydride formation. To address this, nickel is alloyed with metals such as Mo, Zn, Fe, or Co, or combined with metal oxides. For the anode, nickel is also used, often with added iron to enhance OER performance and reduce overpotential. Catalysts, both precious and non-precious metals can be deposited to decrease the activation of overpotential for water splitting [15].

A porous separator plays a critical role by preventing short-circuiting, stopping gas mixing, and enabling ion transport. Some of its main characteristics are high porosity and wettability to promote the surface affinity and electrolyte filling through the pores, high electrical resistance to prevent parasitic currents, minimum thickness to avoid ohmic losses, corrosion resistance to highly concentrated alkaline solutions, mechanical stability and flexibility [21]. Zirfon-type materials, around 460 μm thick, are commonly used, which uses polysulfone membrane with ZrO_2 to combine the flexibility of the polymer with the rigidity and wettability of the ceramic component. Maintaining minimal pressure differences between the anode and cathode is important to prevent gas crossover, though challenging due to the density differences between oxygen and hydrogen. AWE systems operate either at atmospheric or differential pressure, the latter preferred for high-pressure hydrogen production. Gas bubbles affect pressure drops and electrolyte flow, and at high current densities, electro-osmotic flow may increase species crossover, impacting efficiency and safety. Over time, separators can

degrade due to corrosion, and while the filter-press design saves space, failure in one cell can affect the entire stack [15].

The local distribution of bubbles in AWE influences the amount of energy required for hydrogen production. Reducing the electrode gap in AWE can lower ohmic resistance but may increase overall resistance if gas bubble accumulation and electrolyte tortuosity are high. Studies show that applying centrifugal force can assist in bubble removal, leading to reduced activation overpotentials and more stable cell performance, highlighting the potential of body forces to enhance efficiency [14].

In AWE systems, cells are arranged in stacks that can be either monopolar or bipolar. Figure 2.2 illustrates the AWE electrolyser technology within the stack level with bipolar plates. Monopolar stacks connect all anodes and cathodes separately, allowing for easier cell replacement, while bipolar stacks link the anode of one cell directly to the cathode of the next, creating a compact design with lower ohmic losses and greater efficiency at various temperatures and pressures [22]. Due to these advantages, bipolar configurations are preferred in most commercial electrolyzers. The zero-gap cell configuration is the typical configuration of modern alkaline electrolyzers. This minimum distance between electrode and diaphragm minimizes overpotentials resulting from electrolyte resistance and bubble formation on the electrode surface [23].

Some of its main advantages is that the lifetime that has been stated for AWE systems is generally about 80,000 hours and has lower annual operating costs compared to other electrolysis techniques. Additionally, the use of liquid electrolyte guarantees a homogeneous distribution of flow, which translates into a more efficient transport of OH^- ions. Since it is an alkaline environment, it is normally less aggressive and permits the use of cheaper and more available materials as well as not being that sensitive to the quality of the water [24].

Some limitations are that it needs to be operated in between a range of 20%-100% of their installed capacity to minimize the amount of gas-crossover in between the cathode and anode, which may impact the purity of the hydrogen product, and even lead to an explosive mixture of oxygen in hydrogen [25]. Since the maximum current density it presents is not too high compared to other technologies, it usually means it needs a bulkier stack for higher H_2 production. This translates into requiring higher start-up time and higher response time against changes in current compared to other technologies as a bulkier stack needs more heating time for the optimal operational temperature.

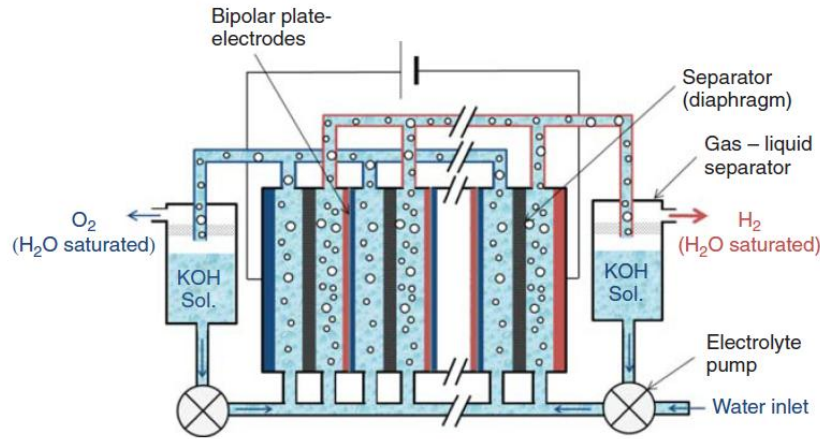


Figure 2.2: Alkaline Electrolysis Technology: Stack Level.
Source: [26].

The BoP in alkaline electrolyzers plays a crucial role in supporting system efficiency and functionality and ensuring stable operation. Figure 2.3 illustrates the AWE electrolyser technology at the BoP level. A key component is the raw water treatment unit that treats the water before feeding it into the electrolysis process by producing deionized water with the quality required for the stack. This water enters through a gas scrubber tower to eliminate any residual KOH present in the hydrogen gas and cools it down, as well as helping regulate water flow based on the liquid level in the gas separator and scrubber tower. The stack is fed electrically by a system composed of a transformer and rectifier to supply the required DC voltage and current for the stack.

The electrolyte circuit of the stack is another crucial system that consists of a heat exchanger to remove residual heat from the stack to control the operating temperature. Depending on the configuration, the circuit could include or not a recirculation pump, since a minimum flow rate is needed to limit the temperature difference in the stack. This thermal regulation ensures that the stack remains operational in a stable and efficient way. Additionally, it includes a KOH injection system which is used during the initial filling of the system and to replenish the electrolyte as needed for the stack.

At the outlet of both the anode and cathode, the gas-liquid separators are used to separate the mixture of electrolyte with the oxygen and hydrogen respectively before returning it to the stack circuit. In some designs, a second gas scrubber tower to further clean the oxygen from any KOH traces. For pressurized alkaline systems, a compression system could be used on both the hydrogen and oxygen to reach the required pressure. The purification and drying unit consist of a deoxo reactor used to remove any traces of oxygen and a temperature swing adsorption to dry the hydrogen stream and reach the desired hydrogen purity.

The two electrolyte loops at the anode and cathode are normally interconnected and mix at the outlet of both gas separators to guarantee a uniform and homogeneous concentration of electrolyte. However, this configuration limits the stack's ability to operate on differential pressure and limits the minimum load for operation due to the risk of gas crossover. Overall, the AWE BoP is robust, well established and operate best under balanced pressure conditions due to its interconnected gas-liquid handling design. Operating at high pressure is achievable but requires reinforced BoP components and pressure-resistant designs, increasing system complexity and CAPEX [14], [21].

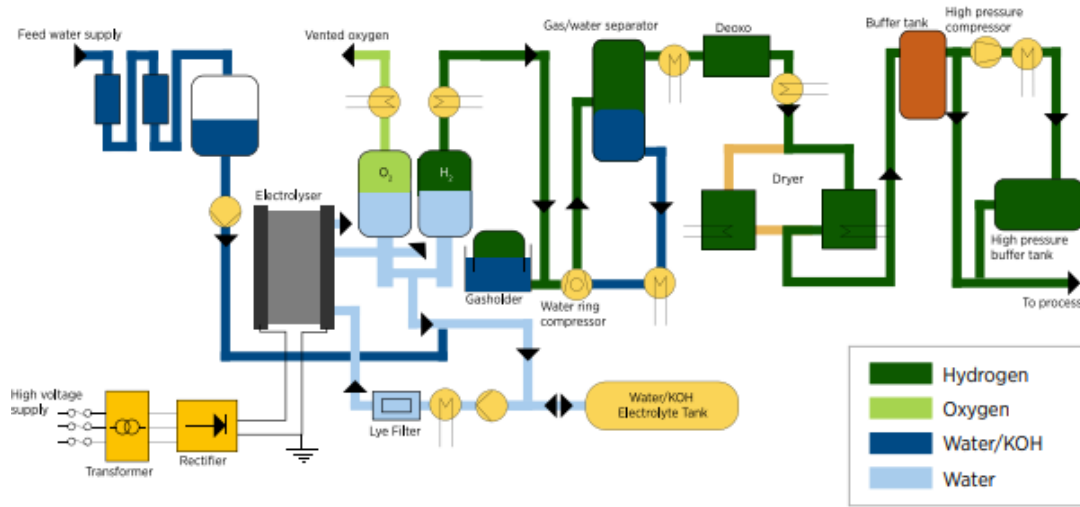


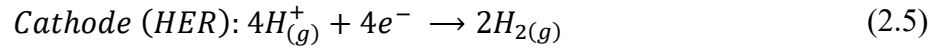
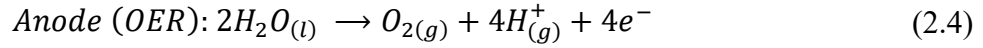
Figure 2.3: Alkaline Electrolysis Technology: BoP Level.
Source: [14].

2.1.2. Proton Exchange Membrane Electrolysis (PEM)

The proton exchange membrane (PEM) electrolysis system is based on the design of a reverse hydrogen fuel cell, making it especially compatible with fluctuating renewable energy sources. What sets PEM electrolysis apart is its use of protons to carry electrical charge during the reaction. The core of the process happens at the catalyst surfaces of both the anode and cathode, which include flow channels, porous transport layers, and catalysts. These layers help manage the flow of reactants and ensure water is evenly distributed across the anode surface. Typically, platinum is used on the cathode, while iridium is used on the anode due to its effectiveness in facilitating the OER which demands a higher potential than HER. To further support durability and performance, noble metals like titanium are used in the anode structure.

An electrical current is introduced into the system, while water is pumped into the anode side. There, the water splits into oxygen, protons, and electrons, as seen in Equation (2.4). The electrons travel through the external circuit, while the protons move across the membrane to

the cathode side. At the same time, oxygen exits through the anode channels, mixed with any remaining water, and hydrogen is formed on the cathode side as it moves through the membrane. The HER then takes place at the cathode, where electrons and protons from the anode combine to create hydrogen gas, as seen in Equation (2.5) [27].



The generated hydrogen gas mixes with water and a small amount of oxygen diffuses through the membrane. Figure 2.4 illustrates the PEM electrolyser and its fundamental principles within the technology at the cell level. PEM electrolyzers use a thin perfluorosulfonic acid (PFSA) membrane in the range of 100 to 400 μm as a solid electrolyte which has a high conductivity of protons and has advanced electrode designs to achieve higher efficiency by reducing resistance [28]. The PFSA membrane, also commonly known as Nafion[®], is both chemically and mechanically durable, allowing the cells to operate at pressures up to 50 bar, with the oxygen side at atmospheric pressure. However, the harsh oxidative conditions at the anode demand the use of titanium-based materials, noble metal catalysts, and protective coatings to ensure long-term stability and high efficiency. While PEM systems are compact and straightforward, they are highly sensitive to water impurities like iron, copper, and sodium, and can suffer from calcination. Currently, electrode areas are approaching 2,000 cm^2 , but they still fall short of the future goal for large MW stack units. Additionally, the reliability and lifetime of large-scale PEM stacks are still under evaluation [29].

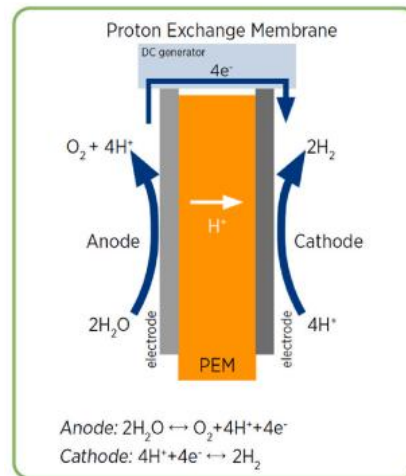


Figure 2.4: PEM Electrolysis Technology: Cell Level.
Source: [14].

The main appeal of PEM electrolysis is that it has the capability to produce high-purity hydrogen with values higher than >99.99% with high efficiencies in the range of 45 to 90% according to literature, with a high current density of around 1 to 2.2 A/cm². They operate at lower temperatures in between 30 to 80 °C and with higher pressures in the range of 15 to 50 bar, with the most common being around 30 bar [14], [15], [16], [17], [18], [19], [20]. Being able to produce high-pressurized gases in the electrolysis process without the use of additional energy reduces costs as the pressure required to store hydrogen is about 350 to 700 bar in its compressed state. Additionally, while operating with high pressure it is necessary to also have a high current density, as when operating with low current density the gas crossover increases, making it an explosion risk of having a mixture with hydrogen exceeding 4% [30].

Another advantage is that they feature faster response time even when being subjected to variable power conditions, as well as only needing a lower minimum load of approximately 5 to 10% of the maximum rated capacity, making it more suitable for working with the supply conditions coming from renewable energy sources [15]. As PEM electrolyzers tend to have compact size and low maintenance requirements, they are also suitable for small-scale applications such as fuel cell vehicles and portable power systems and since a solid electrolyte is used in the membrane, they avoid having to work with a highly corrosive liquid like KOH [31]. Since PEM electrolyzers tend to display high-efficiencies, adaptability, fast response time and compact size, it has started to gain popularity for decentralized connection schemes offshore [16], [18].

The downside of PEM electrolyzers is the heavy reliance on using platinum group metals (PGM) for the electrocatalysts, which can mean various problems with both the high costs for using them as well as the quantity of available resources, as this is classified as a critical material with a limited supply [32]. Another disadvantage is with the composition of the membrane used, since it consists of fluorinated polymers. These materials end up having a heavy impact on the environment when being produced as well as when disposing. The effects of these materials may soon cause them to be banned on all applications for which it can be substituted for another material with less impact. Although significant efforts have been made to develop and assess various experimental materials as a substitute to Nafion® in the membrane, none have had any significant results as the durability of the non-or partially fluorinated materials to this date is poorer [20]. This could potentially represent a barrier that can affect the implementation of PEM technology. Despite this, PEMs are currently considered as the most promising electrolysis technology in the marine environment and have become very

competitive against AWE as substantial research has been devoted into improving its components and the efficiency of the process [33].

Even though the stack uses ionized water, the electrodes suffer highly acidic corrosion due to the acidic nature of the PEM caused by the H^+ ionomer in the cathode exchange. Figure 2.5 illustrates the PEM electrolyser within the technology at the stack level. To be able to withstand this corrosive environment, the electrocatalysts must use PGM-based materials, normally having iridium at the anode and platinum in the cathode. Using these types of materials can be quite costly, accounting for 24% of the total cost of the cell. Also, it is common to apply that the catalyst coating is applied directly over the membrane instead of the catalyst surface [34].

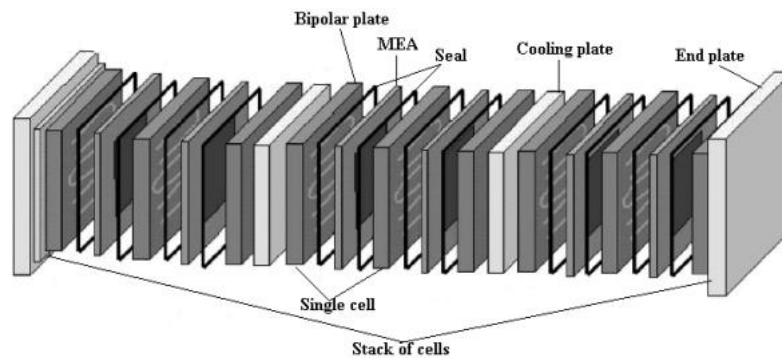


*Figure 2.5: PEM Electrolysis Technology: Stack Level.
Source: [35].*

PEM systems are simpler compared to the BoP of alkaline electrolyzers since they use less components in their design. PEM systems have different types of design choices for the functioning of the stack with atmospheric pressure, balanced pressure between the cathode and anode, and differential pressure with a typical pressure of 30 bar. Figure 2.6 illustrates the PEM electrolyser within the technology at BoP level. One of the essential subsystems is the electrical supply system, which uses a transformer and rectifier to regulate the DC voltage and current needed to supply into the PEM stack. This ensures that the electrochemical reaction in the cell is performing as optimized as possible and avoids excess degradation of the stack.

Another key subsystem is the water circuit of the stack which is composed of a recirculation pump, heat exchanger, and an ion exchanger resin bed. The recirculation pump is needed to limit any gradients of temperature in the stack by keeping a minimum water flow. The heat exchanger refrigerates the water and controls the operational temperature by dissipating any excess heat from the stack. The ion exchanger resin bed is used to catch any heavy metals and contaminants coming from the corrosion of any other components or piping

in the system. Additionally, a raw water treatment unit is used to feed the system with deionized water of the required quality for the stack.

At the output of the electrolysis stack of both the cathode and anode, gas-liquid separators are used to separate the mixture of hydrogen and oxygen respectively from the residual water. This separated residual water is then returned to the water circuit of the stack and the gases are routed downstream for the purification process. A purification and drying unit are often included for hydrogen purification to eliminate any remaining traces of oxygen via a deoxo reactor and reduces the water content using temperature swing adsorption to meet hydrogen purity required. In the case of differential pressure configuration, the de-oxygenation component at the cathode may be removed due to minimal crossover of oxygen into the hydrogen stream but requires a thicker membrane for mechanical stability. Having a thicker membrane decreases gas permeation and reduces the efficiency of the stack.

The oxygen stream exits through the gas-liquid separator, and its flow rate determines the feed water flow. In case the configuration intends to also produce oxygen, additional units such as a compression system and a purification and drying units may be included to reach the required purity and dryness. Finally, the cathode pressure of operation can be regulated and fixed via a backpressure valve to ensure a correct system operation [14], [21].

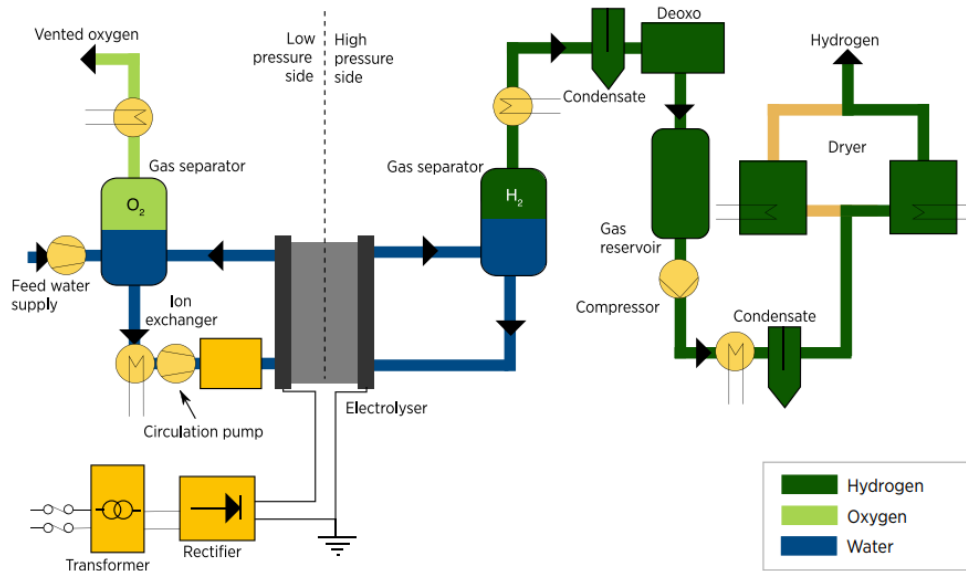


*Figure 2.6: PEM Electrolysis Technology: BoP Level.
Source: [14].*

2.1.3. Anion Exchange Membrane Electrolysis (AEM)

Both AWE and PEM electrolyzers have a series of disadvantages and barriers that need to be solved to be able to scale-up hydrogen production to achieve decarbonization goals for 2050. Therefore, research and developments of these last years have started to investigate the replacement of the AWE diaphragm for an anion exchange membrane to create a technology that could combine the advantages of both AWE and PEM electrolysis. The objective is to create a technology with the advantage of AWE for low capital costs while combining it with PEM's advantages of low operational costs and greater safety producing pressurized and ultrapure hydrogen [36].

The electrochemical reaction for AEM electrolyzers is similar to the reaction given by the conventional alkaline electrolysis but more complex [18]. Figure 2.7 illustrates the AEM electrolyser and its fundamental principles within the technology at the cell level. In the case of AEM, water enters through the cathode side to form H_2 gas as shown in Equation (2.6) for HER and the anode side oxidizes to form O_2 gas as shown in Equation (2.7) for OER [37].

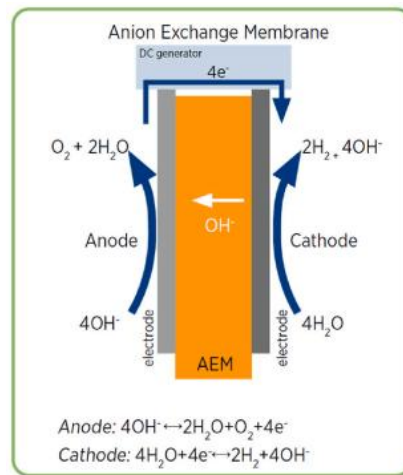
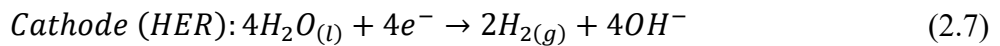
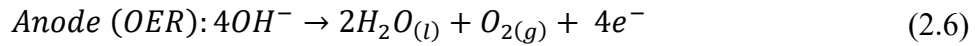


Figure 2.7: AEM Electrolysis Technology: Cell Level.
Source: [14].

The main appeal of AEM is that it could combine the advantages of both AWE and PEM electrolysis while producing high-purity hydrogen. According to literature, AEM is currently in a research and development stage, with some prototypes built with efficiencies in the range of 52 to 90% according to literature, and a high range of current densities of around 0.1 to 2.5

A/cm². They operate at temperatures comparable to AWE in between 50 to 90 °C and with pressures around 30 bars, which is comparable to PEM [14], [15], [16], [17], [18], [19], [20].

The key difference between AWE and AEM is that the diaphragm for AWE does not have ionic conductivity and is provided by means of the electrolyte filling its pores. In the case for AEM's polymeric membrane it is not porous and possesses an intrinsic anionic conductivity. These membranes are typically composed of a polymer matrix of polysulfone or divinylbenzene that is chemically modified with quaternary ammonium functional groups that support the conductivity of OH⁻. Some commercial products for such membranes are Sustainion[®] and Fumasep[®] [19]. These quaternary ammonium groups are particularly vulnerable to attack by OH⁻ ions in the operation which leads to their degradation and resulting in reduced conductivity and membrane brittleness. Also, polymer backbones can split under alkaline conditions, which may accelerate chemical degradation and weaken the membrane which facilitates gas crossover and compromises electrode adhesion [38].

This makes it not necessary to use a highly corrosive electrolyte like KOH for the electrolysis reaction. Nevertheless, currently a big portion of studies use a diluted KOH electrolyte at 1% as a support to achieve a higher performance as a high ionic conductivity is needed [39]. On the other side, the use of these membranes permits the use for the zero gap, which refers to porous electrodes pressed directly onto the diaphragm which reduces the ohmic losses and achieving higher current densities and efficiencies [40].

The key difference between PEM and AEM is that it allows the use of non-noble catalysts like Ni-Mo alloys for the cathode and Ni-Fe for the anode, which presents promising results comparable to platinum-based catalysts. It also presents a less harsh environment while still being able to have differential pressure and the same simplicity and efficiency as PEM [41]. Ni-based oxides have demonstrated good electrochemical activity and stability in alkaline environments and represent a cost-effective path for long-term operation. This reduces significantly the material costs while still being able to achieve a compact and pressurized stack design. However, currently AEM membrane have chemical and mechanical problems which lead to unstable lifetime profiles and performance is still lacking due to poor AEM conductivity, poor electrode architectures and slow catalyst kinetics [21].

Performance can be enhanced by tuning the properties of the membrane or adding the diluted electrolyte solution of KOH but having the drawback of reducing the durability and expected lifetime. This trade-off between performance and membrane stability is one of the main design challenges that limit the AEM electrolyser. Moreover, OH⁻ ions are intrinsically 3 times slower than H⁺ ions because of their lower conductivity, which forces AEM membranes

to be thinner or have higher charge density [14]. Moreover, membranes must maintain optimal hydration on the membrane to facilitate ion transport since excess water uptake in elevated temperatures can lead to swelling and weakening. Studies show that thermal operations around 70 to 90 °C improve ionic conductivity and electrode kinetics but presents a drawback of accelerating membrane degradation due to chemical attacks and physical strain [42].

This is why ongoing investigations and development for new AEM designs focus primarily on improving both the chemical and mechanical properties and robustness to enable longer lasting components that operate more efficiently [43]. Figure 2.8 illustrates the AEM electrolyser within the technology at the stack level. To address these challenges, research is exploring nanomaterials like silica into the polymer matrix to strengthen the mechanical properties while creating additional transport channels [44].

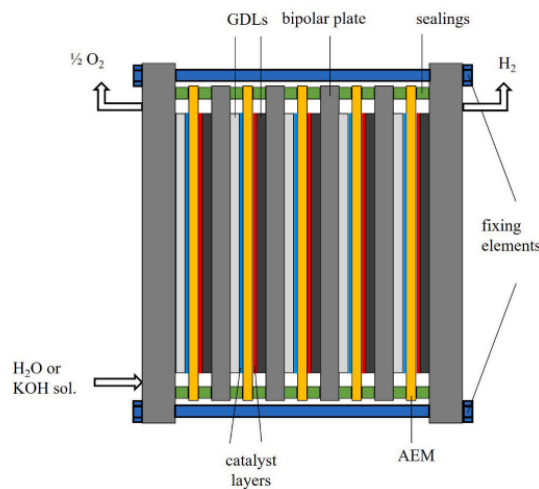


*Figure 2.8: AEM Electrolysis Technology: Stack Level.
Source: [19].*

AEM electrolyser have a similar BoP design concept as that of PEM electrolyser and include several key subsystems. Figure 2.9 illustrates the AEM electrolyser within the technology at the BoP level. Firstly, an electrical supply system that conditions the input power to the required conditions of the DC voltage and current needed for an optimized performance of the stack. Upstream of the system, a water treatment unit is needed to produce deionized water of the adequate quality for the stack functioning. The core of the BoP is the electrolyte circuit for the stack, which incorporates a recirculation pump that provides a flow rate to limit the differential temperature that the stack experiences during operation. A heat exchanger is also used to refrigerate the electrolyte and dissipate the residual heat from the stack and control the operation temperature. An ion exchanger resin bed is used to trap the heavy metals cations

that can exist from the flow of water passing through the piping and auxiliary equipment or any byproducts of from corrosion of the stack itself.

At the outlet from the anode side, a gas-liquid separator removes the oxygen from the electrolyte before recirculating the electrolyte back to the stack. In a dry cathode configuration, water is only introduced into the anode and is transported to the cathode by means of diffusion and electro-osmotic drag, which translates into less water content in the hydrogen exiting the cathode compared to PEM systems. This permits the elimination of the liquid-gas separator in the cathode side but may still need a dedicated drying system depending on the degree of purity requirements and flow rate needed in the hydrogen [14], [21]. Currently there is limited information about the challenges that come with high differential pressure operation due to the low technological maturity. Improvements for AEM membranes are expected in the mechanical stability, gas purity and high-pressure differentials that it can withstand. Moreover, AEM electrolyzers are still limited in the range of power input, which means that the limitation is not only in the stack itself, but on the whole balance of plant [45].

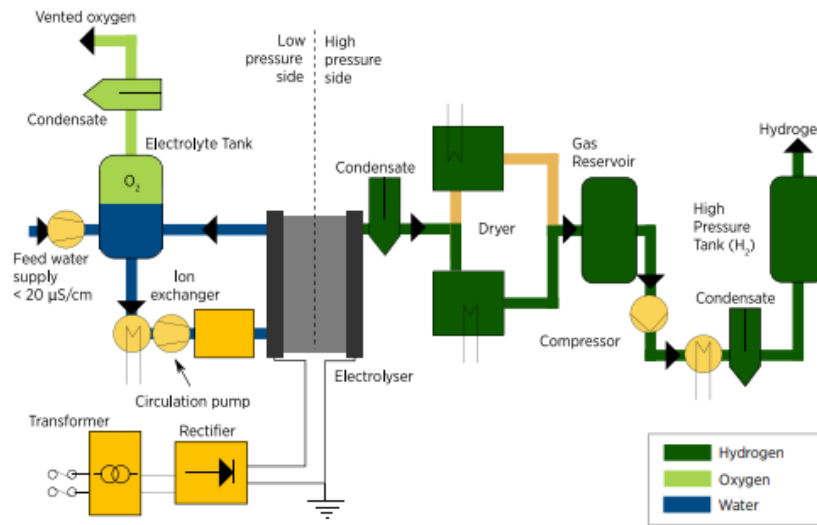


Figure 2.9: AEM Electrolysis Technology: BoP Level.
Source: [14].

2.1.4. Solid Oxide Electrolyser Cell Electrolysis (SOEC)

The solid-oxide electrolysis system is a water electrolysis technology that operates at high temperatures in the range of 700 °C and 1,000 °C while using a solid oxide ceramic electrolyte that conducts oxygen ions O^{2-} . At these elevated temperatures, it is possible to use steam instead of using water in liquid and translate into a higher electrical efficiency as part of the energy to split the water is supplied as heat instead of electricity and makes the reaction easier to drive.

This makes SOEC well-suited when integrated to use any high-temperature waste heat generated during industrial processes or concentrated solar power, as it improves the overall system efficiency [21].

The core of a SOEC is its solid-oxide cell composed of three layers of cathode, dense ceramic electrolyte and anode. Figure 2.10 illustrates the SOEC electrolyser and its fundamental principles within technology at the cell level. Some of the most common materials that are used are nickel-based cermets and perovskite-type mixed oxides for the cathode and anode respectively and an yttria-stabilized zirconia (YSZ) for the ceramic electrolyte. The electrochemical reaction for SOEC consists of a reduction reaction when steam is introduced into the cathode and generates hydrogen and oxygen ions as shown in Equation (2.8) for HER. The oxygen ions are transported through the solid electrolyte and into the anode, where they are oxidized and released as oxygen gas as shown in Equation (2.9) for OER [46].

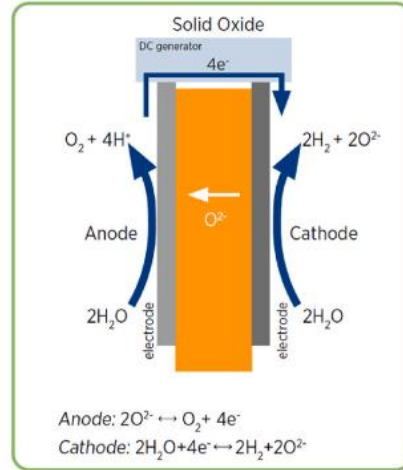
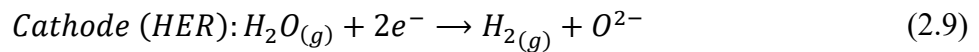
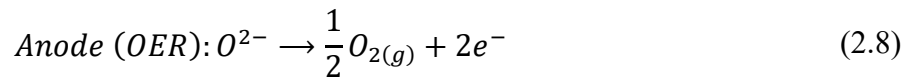


Figure 2.10: SOEC Electrolysis Technology: Cell Level.
Source: [14]

These cells can be stacked in a series and connected via metallic interconnects and seals to ensure that there is no gas crossover and ensure the mechanical integrity of the stack, while end plates internal hardware make up the full electrolysis system. The electrolyte material is typically YSZ due to its high oxygen-ion conductivity above 800 °C and its thermal and chemical stability. However, one of the key challenges for this material is to broaden the

application of SOECs and reduce the thermal stress of the components by lowering the operating temperature and maintaining conductivity and mechanical resilience [47].

The cathode is commonly composed of a Ni-YSZ cermet and offer high porosity and conductivity while remaining cost-effective. However, it presents the trade-off of requiring a continuous presence of hydrogen stream to avoid reoxidation of nickel that leads to irreversible degradation. At high current densities higher than 1 A/cm^2 , the stability of the electrode is compromised due to nickel agglomeration and depletion, limiting the durability of the SOEC stack [48].

On the anode side, materials like lanthanum strontium manganite (LSM) and lanthanum strontium cobalt ferrite (LSCF) are commonly used, with the latter presenting a lower risk of delamination and higher performance. However, the migration of strontium and cobalt can degrade the interface between the electrode and electrolyte, since both LSM and LSCF are incompatible with YSZ. This incompatibility between the materials brings the need to use a barrier interlayer to prevent any chemical interactions and improve the durability of the components. Additionally, interconnect materials such as Inconel and Crofer with ceramic coatings are used to transport electrical current and manage thermal expansion and guarantee the distribution of gases while separating the anode and cathode from adjacent cells [47].

One of SOEC's most distinguished advantages and appeal is that it can achieve very high electrical efficiencies for hydrogen production close to 75 to 100% according to literature, when the thermal integration is properly applied with industrial and nuclear settings in which high-grade excess heat is produced as waste from the process and is available for use [14], [15], [16], [17], [18], [19], [20]. Figure 2.11 illustrates the SOEC electrolyser within the technology at the stack level. Additionally, SOECs can co-electrolyze water and CO_2 to produce syngas, which consist of a mixture of H_2 and CO . Moreover, SOEC systems are reversible and can operate as solid oxide fuel cells (SOFC) to generate electricity from hydrogen when needed, which provides flexibility in grid applications [46]. However, SOEC presents technical challenges due to the high operating temperatures. These cause material stress and degradation due to thermal cycling which affects the long-term durability of the electrolyser [20]. The ceramic components must be able to withstand repeated changes in temperature along their whole life cycle which translates into a constant cycle of expansion and contraction. This requires precise material matching and structural support from a specialized BoP. These constraints may present hurdles in scalability and deployment, especially in environments with dynamic or extreme conditions like offshore. Nevertheless, SOEC electrolysis remains a promising option when integration with heat-intensive processes is available.

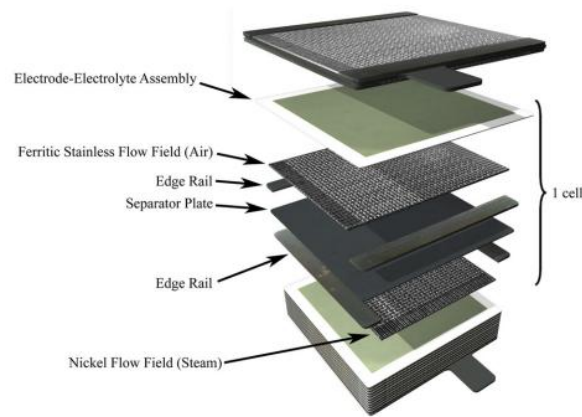


*Figure 2.11: SOEC Electrolysis Technology: Stack Level.
Source: [49].*

The BoP in SOEC electrolyzers play an essential role in the system to ensure stable, efficient, and durable operation of the stack at high temperatures. Figure 2.12 illustrates the SOEC electrolysis technology at the BoP level. One of the key components of the system is the steam generation system, which supplies the necessary steam to the cathode side of the stack. This can be produced by either using an electric heater evaporator or preferably by using waste heat from an industrial process to improve the overall efficiency of the system and reduce electric consumption [14]. The system also needs a raw water treatment system located upstream of the stack to protect from contaminants and ensure optimal performance. This unit purifies the feedwater to produce deionized water with sufficient quality by removing any impurities and mineral buildup that could damage the ceramic components of the stack.

Another subsystem needed for electrolysis is the electrical power supply system, which conditions the electricity input by means of a transformer and rectifier if needed, to match the specific requirements of the stack with the proper voltage and DC current to ensure stable and controlled conditions for electrochemical reactions. Thermal efficiency is enhanced using heat recover exchangers, which use the hot exhaust gases coming from both the cathode and anode side to preheat the input gases to maintain the stack's internal temperature and reduce the energy required, increasing the system's overall efficiency. Additionally, flow of air is fed continuously to the anode to ensure a homogeneous temperature distribution along the whole stack and facilitate the removal of oxygen produce during the electrolysis process.

The SOEC stacks are housed inside a hot box, which works as a high-temperature furnace that maintains the optimal operating temperature according to the stack and insulates the system. A unique characteristic corresponding to SOEC electrolysis is that the gas coming

out from the outlet of the cathode contains no oxygen since the ions transported across the electrolyte react with hydrogen at high temperatures. This eliminates the need for a Deoxo reactor in the purification unit downstream in the final gas handling of hydrogen. Depending on the final application and the amount of purity required, the BoP may include a compression system to increase the pressure of the hydrogen and a gas drying unit using temperature swing adsorption to remove residual moisture. Additionally, part of the hydrogen that is produced is recirculated back into the cathode inlet. This recirculation creates a reducing gas mixture of both hydrogen and steam in a 10% concentration that helps to maintain the stability of the Ni-based cathode material and prevent its oxidation. Finally, the anode exhaust is composed of a stream of oxygen-enriched air that can be either vented or recovered for industrial use depending on the configuration [14], [21].

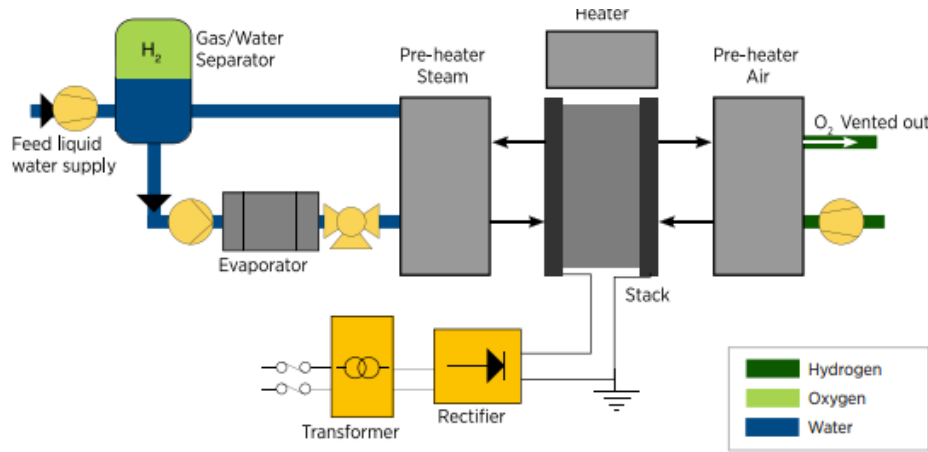


Figure 2.12: SOEC Electrolysis Technology: BoP Level.
Source: [14].

2.1.5. Summary of Electrolysis Technologies

An overview of the different electrolysis technologies reviewed in this section is shown in Table 2.1. The capabilities for the types of electrolysis were extracted from literature sources and were compared with the capabilities compiled from the commercial database available for the commercial electrolyzers, which are shown in the boxplots shown in Figure 2.13 for the power available in the electrolyser system and Figure 2.14 for the efficiencies of the electrolyser system. Other parameters are compared in between the types of electrolyzers according to the compiled commercial database in Appendix 8.1.

AWE electrolyzers are currently the most established electrolysis technology and with the highest technological maturity. It is known for being a simple, robust, and cost-effective

system in large-scale hydrogen production. It uses a KOH liquid electrolyte and nickel-based electrodes. The main advantages are its durability of approximately 80,000 hours, low capital costs, and using non-precious metals as catalysts. However, AWE systems are bulky, slow to respond to fluctuations in power, and have a minimum load above 20% capacity to avoid gas crossover. Additionally, their low current density leads to larger footprints, which becomes a challenge for deployment with offshore renewables because of space and power intermittency.

PEM electrolyzers use a solid electrolyte polymer to conduct H^+ ions from the anode to the cathode. Some of their main advantages lie in its low operating temperatures, high current density, fast response times and compact designs while producing pressurized hydrogen. However, PEM relies heavily on PGM-based metals and fluorinated polymers which affect its investment cost and environmental impacts. Despite these drawbacks, PEM is currently the most promising technology offshore and is well suited to be integrated with renewable energy sources.

AEM electrolyzers are an emerging hybrid technology that aims to combine the main advantages of both AWE and PEM. It uses a solid anion-conducting membrane that allows the use of non-precious metals catalysts, while keeping the compactness and pressurization of PEM, which reduces costs and environmental concerns. However, research is still ongoing to improve durability since AEM membranes still suffer from chemical and mechanical stability issues. AEM can be a potential technology to be used offshore if some of its main challenges can be resolved.

SOEC electrolyzers operate at high temperatures and use a ceramic electrolyte that conducts oxygen ions. This operation at high temperature allows for achieving electrical efficiencies near 90% and having the possibility of integrating it with industrial or nuclear heat sources that can provide heat. SOECs can also co-electrolyze CO_2 and H_2O to produce syngas and can work in reverse as fuel cells. However, this high temperature leads to material degradation due to thermal cycling and presents slower startup times, which limits its suitability for dynamic offshore conditions.

Table 2.1: Overview of types of electrolyzers.

Sources: [14], [15], [16], [17], [18], [19], [20]. Full references for the Commercial Database sources are available upon request.

Technology	AWE	PEM	AEM	SOEC
Electrolyte Type	Liquid KOH (~30%)	Solid PFSA membrane (Nafion®)	Solid anion-exchange membrane	Solid ceramic (YSZ)
Operating Temp [°C]	60 - 90	30 - 80	50 - 90	700 - 1000
Current Density [A/cm²]	~0.2 - 0.8	~1 - 2.2	~0.1 - 2.5	~0.1 - 1
Efficiency (literature) [%]	~50 - 90	~45 - 90	~52 - 90	~75 - 100
Efficiency (Commercial Database) [%]	~70 - 78*	~50 - 79*	~65 - 74*	~88 - 95*
TRL	8 - 9	7 - 9	2 - 7	4 - 7
Material Use	Non-PGM (Ni, SS)	PGM (Pt, Ir)	Non-PGM (Ni-Mo, Ni-Fe)	Ni-YSZ, LSM/LSCF, Inconel
Pressure Output	Atmospheric to ~30 bar	15 - 50 bar	1 – 30 bar	Low (<5 bar, typically)
Advantages	Low CAPEX. Mature. Durability. No PGMs.	Compact. Fast response. High purity H ₂	Low-cost potential. Non-noble catalysts.	Very high efficiency. Co-electrolysis. Reversible.
Limitations	Bulky. Slow response. Use of KOH. Higher minimum load.	High material cost. Sensitive to water purity	Unstable membranes. Short lifetime	High-temperature fragility. Slow ramp-up. Costly
Offshore Suitability	Moderate. Large footprint. Less flexible	High. Best for dynamic systems	Promising. Needs maturation	Very limited. Better suited with industrial heat integration

*: Efficiency for AWE, PEM, and AEM is calculated with HHV and SOEC used LHV.

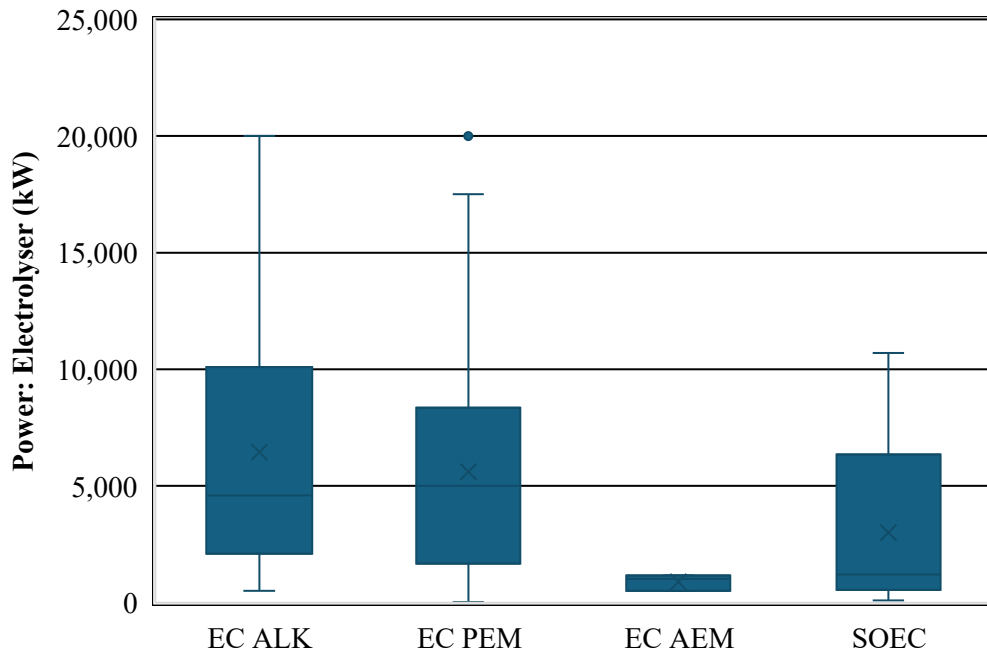


Figure 2.13: Commercial Database: Electrolyser Power Boxplot.
Sources: All references for the Commercial Database sources are available upon request.

*: Efficiency for AWE, PEM, and AEM is calculated with HHV and SOEC used LHV.

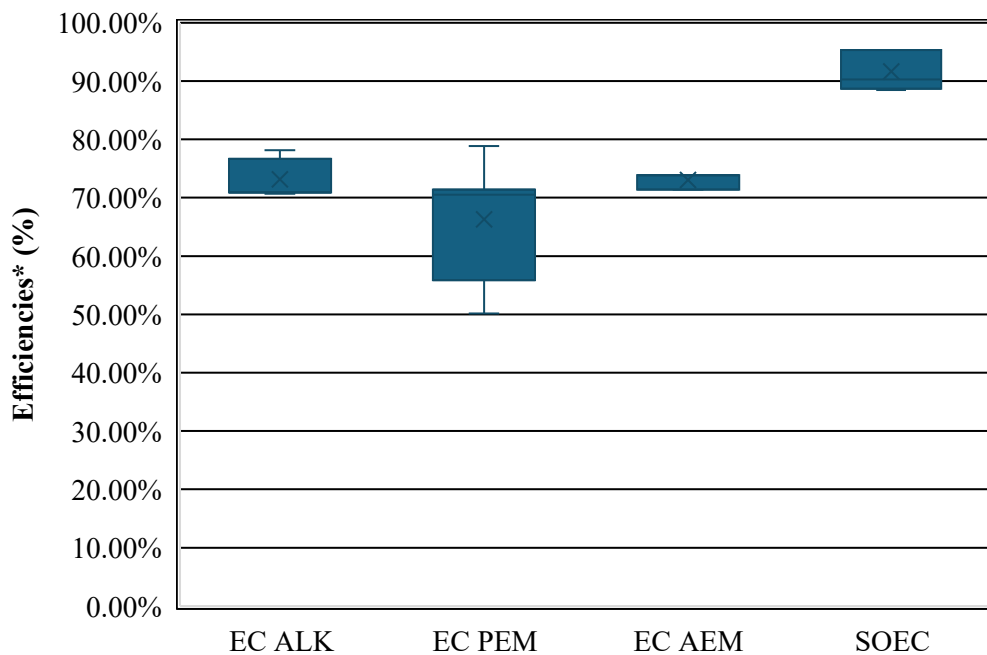


Figure 2.14: Commercial Database: Electrolyser Electrical Efficiency.
Sources: All references for the Commercial Database sources are available upon request.

Figure 2.15 illustrates the different trade-offs between efficiency, durability, and cost in both CAPEX and OPEX in electrolyser design and operations. It means to show how modifying a component, design, manufacturing or research direction for a material can improve in one dimension but affect negatively in another parameter. An example of this can be that working with higher efficiencies can create a direct impact on OPEX and reduce the total costs, but it may compromise durability if it involves less robust materials. Similarly, trying to enhance efficiency by using larger stacks, advanced manufacturing and better-quality control may induce an increase in the CAPEX of the project. This interconnected framework emphasizes that it is important to find a balance between all aspects of durability, efficiency and costs to optimize the electrolyser performance for offshore hydrogen production, where these parameters can be critical.

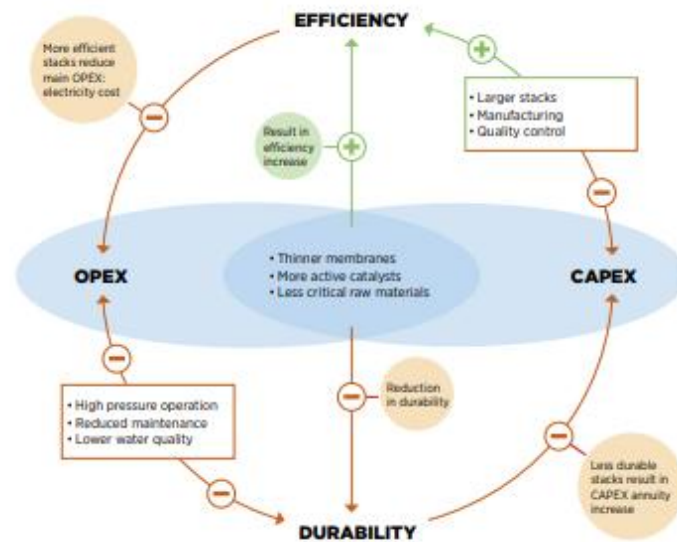


Figure 2.15: Trade-offs between efficiency, durability, and cost for electrolyzers.
Source: [14].

Each of these technologies presents a different trade-off between their maturity, efficiency, costs, and offshore adaptability. Currently PEM leads to offshore readiness due to compact design and dynamic capability, while AWE remains a cost-effective choice for stable, centralized systems where space is not a constraint and intermittency can be compensated. AEM offers great future potential but still requires research and development to solve durability challenges and SOEC is the most efficient but presents certain constraints in regards its high-temperature usage and slow response times that can pose incompatibility with a dynamic offshore environment.

2.2. Suitability of Hydrogen Production on Offshore Platforms

Assessing the suitability of hydrogen production offshore according to the highly demanding environmental conditions is essential to determine the viability of the project. For this, understanding the various types of platforms that are currently in operation in different hydrogen projects and their characteristics is important, as platforms can vary widely in design, infrastructure and their suitability vary with certain factors like depth, sea states, soil conditions, besides others. All these differences are key players in determining feasibility and efficiency when integrating it into hydrogen production technologies. Moreover, the possibilities in the connection schemes greatly influence accordingly with the supply, storage and transportation of energy, in both the form of electricity for supply in hydrogen production and the hydrogen product as an energy vector.

2.2.1. Types of floating offshore foundations

Offshore platforms can be classified into two main types based on the structural foundation, which can be either fixed or floating platforms. Each of these types presents different characteristics like stability, space availability, seabed depth and conditions, and energy integration. Fixed platforms are placed directly into the seabed and are present normally in shallow and intermediate water depths, for which they offer a stable base for heavy equipment. In the case of floating platforms, they are designed specifically for deeper waters in which fixed foundations are not viable or economically feasible to install. They rely mainly on buoyancy and mooring systems for positioning depending on the type of platform, which introduces various challenges in terms of motion and maintenance according to the harsher conditions.

Fixed foundations are widely used in most offshore environments in shallow to intermediate water depths due to their robust structural stability and their ability to support heavy industrial operations. All fixed foundations share certain characteristics despite any variations that exist between the different types of structures. The three main types of fixed foundations are monopiles, jackets and gravity-based structures (GBS). They are anchored and in contact with the seabed, which makes it important to know the characteristics of the soil. Additionally, they provide a stable platform for any equipment installation and maintenance while providing a high structural rigidity. However, the main drawback for fixed foundations come from becoming not economically viable when reaching deeper sites in which a higher wind resource may be present. The current deepest fixed foundation corresponds to a jacket

installation in the Seagreen Offshore Wind Farm in Scotland, in which the water depth is equal to 58.6 meters [50].

Conversely, floating foundations are a rapidly evolving solution for various offshore renewable energy sources, having been proved for their functionality and long-lasting working life in harsh operating environments in the oil and gas sectors. These foundations are particularly suitable in deep sea waters where fixed foundations are not economically or technically feasible to install, operate or maintain [51]. These foundations are particularly favorable for depths ranging from 100 to 600 meters and have the capacity to support generations between 200 MW to 1200 MW with offshore wind resources. Currently, there are four main classifications for floating foundations which include Tension-Leg Platforms (TLP), Semi-Submersible, Spar, and Barge, as seen in Figure 2.16. There are a variety of different designs for offshore foundations but only a few projects have reached to a pre-commercial deployment, which include the concrete Spar used in Equinor's Hywind Tampen in Norway [52] and the Principle Power Inc. system of WindFloat for both Kincardine Offshore Wind by Cobra Group in Scotland [53] and WindFloat Atlantic by Ocean Winds in Portugal [54]. Most of the current designs are still in the conceptual or into only a demonstration phase with scaled models by using steel and concrete materials.

The biggest difference between the design characteristics of fixed and floating platforms is that floating platforms must account for the complex interactions between the hydrodynamic and aerodynamic forces that affect the platform. It must ensure that the platform resists the varying climatic environment and ensure stability during operation. Some of the key design elements needed to ensure this are mooring systems, ballast systems and dynamic cables adapted for offshore conditions. Despite that floating foundations lack standardization and have longer lead times of approximately seven years from start to installation, it currently offers a flexible and scalable solution for offshore hydrogen production in deep-water locations [55].

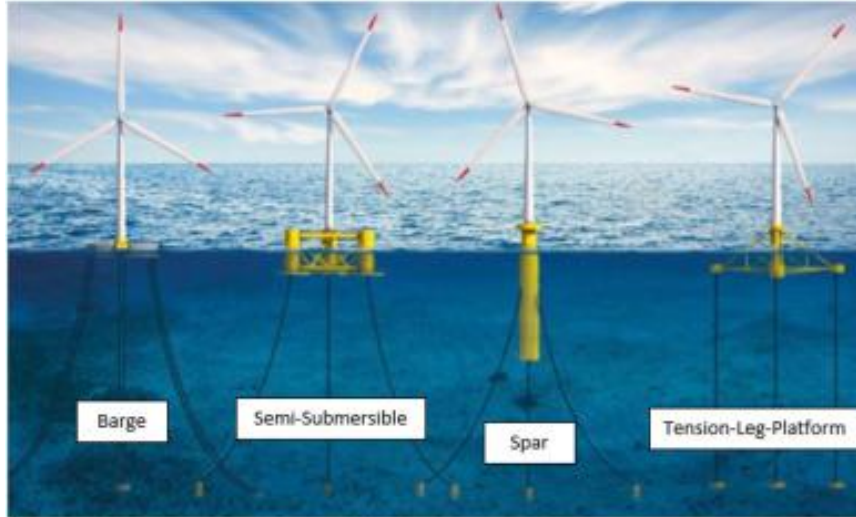


*Figure 2.16: Types of Floating Foundations.
Sources: [51].*

2.2.1.1. TLP

TLP foundations are a type of floating foundation designed for offshore wind turbines for deep water applications exceeding depths up to several hundred meters. These platforms maintain a positive buoyancy and can be stabilized by a mooring system consisting of a series of vertical and taut tendons anchored to the seabed. This mooring system is necessary since TLPs are not self-stable because of the excess buoyancy of the platform [56]. This buoyancy needs to be counteracted by the vertical tension in the mooring lines, and it helps to keep the platform in place and maintain its vertical position. The unique design results in a slender and lightweight structure that significantly reduces the vertical and horizontal motions of the platform but induces high tensions into the mooring lines [57].

Several TLP designs are currently during development or demonstration phase, including the Float4Wind concept by SBM Offshore [58], as seen in Figure 2.17, and CT-bos concept by Acciona and Bluenewables [59]. These systems are characterized by a large, submerged footprint which gets minimized in space at the seabed by the taut mooring configuration. This configuration helps reduce and limit the out-of-plane motions of roll, pitch, and heave motions of the platform with its partially rigid system that ensures high stiffness and great positioning capabilities [60]. The design is made to effectively reduce the impacts of mooring for first-order wave loads and for an efficient operation for wind turbines, since excessive platform motions can impact energy generation and structural integrity [61]. Additionally, they are recognized for their compact and lightweight design since the buoyancy for the TLP foundation can be provided by a relatively smaller waterplane area, which in turn reduces steel usage and cost for this structural material [62].

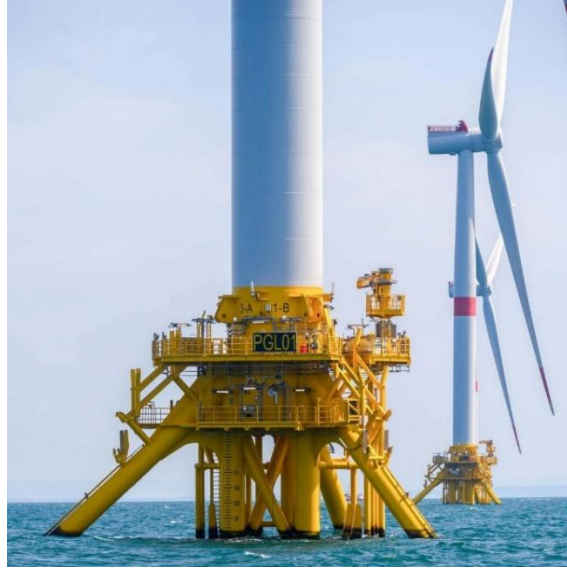


*Figure 2.17: TLP foundation in Float4Wind by SBM Offshore.
Source: [58].*

However, the TLP design comes with some challenges and technical and economic difficulties. Since stability depends entirely on the integrity of the taut mooring system, even the failure of one single tendon or tethers can jeopardize the entire structure, representing a higher risk compared to using catenary moored systems. Additionally, the complex procedure needed for transportation and installation to deploy the structure as well as anchoring the mooring system in deep waters is still a significant logistical hurdle to accomplish, as positive and precise tension is needed to install the tethers. These difficulties make TLP foundations a technically promising but still maturing option for floating offshore wind deployment [60].

2.2.1.2. Semi-Submersible

Semi-submersible foundations are among the most developed and widely demonstrated floating foundations and are designed for deep water sites that are above 55 meters of depth. These platforms are characterized by being massive slender structures composed of multiple buoyancy columns or pontoons connected by a structure above the waterline. Each of these columns contains a water ballast which is used to reach the operational draft of the platform once positioned and combined with the wide waterplane area and mooring system achieves self-stability. This stability allows the platform to remain upright without relying only on its mooring system, making the design relatively robust and reliable under high and varying sea conditions [56]. Nonetheless, as semi-submersibles typically have a large area exposed to wave action and significant wave loading, higher order wave loading effects must be considered in the design of the foundation [63].

Technologies such as concepts used for some notable pre-commercial projects that used semi-submersibles foundations include Kincardine [53] and WindFloat Atlantic [54], as shown in Figure 2.18, which indicate that it has progressed to have a maturity for Technology Readiness Level (TRL) 7-8 [64]. These platforms typically have the flexibility to choose between catenary or semi-taut mooring systems according to the seabed conditions depending on the option that best adapts to the situation. One of the many advantages of semi-submersible is their ability to remain afloat and operational even with the loss or failure of a mooring line, as the design is made to be robust and resilient and to still be able to function with the failure of one tendon, but taking into consideration in the overall wind farm design that this does not produce any impacts with any other nearby platforms [65].



*Figure 2.18: Semi-Submersible foundation in WindFloat Atlantic.
Sources: [54].*

Despite its many strengths and advantages, semi-submersibles have some trade-offs. They present logistical challenges during fabrication, transport, and installation and a large quantity of high steel requirements due to their large footprint and significant structural mass. Additionally, flexible mooring and its large, submerged portion cause notable horizontal displacements or excursions, which must be accounted during the overall wind farm design for spacing between platforms as well as for dynamic cable design. Nevertheless, their proven performance in both pilot and demonstration projects currently place them as a leading option for any commercial-scale floating wind projects [66].

2.2.1.3. *Spar*

Spar foundations are highly stable platforms for offshore wind turbines that are characterized by a long, slender cylindrical structure that is mostly submerged below the water surface. The way this structure achieves its high stability is by means of a combination from a low center of gravity of the structure plus a heavy ballast located at the bottom of the structure. With this, it is possible to counteract the center of buoyancy of the structure and minimize the motion of the platform. Compared to other floating platforms, spars have a relatively small waterplane area, which reduces any wave-induced motion and improves the wind turbines performance in harsh offshore environments [56].

These types of self-stabilizing platforms typically use flexible mooring systems like catenary or semi-taut anchored to the seabed to help maintain its position. The concept of technology for spar foundations that reached pre-commercial status corresponds to the Hywind Series developed by Equinor which includes projects like Hywind II and Hywind Tampen [52], as shown in Figure 2.19. This led to the development of technology and to showcasing their ability to operate in challenging environments at deep-water sites. These foundations can be constructed with flexibility in the material selection, be they concrete or steel, depending on project needs as well as regional capabilities and availability of resources.



*Figure 2.19: Spar foundation in Hywind Tampen.
Sources: [52].*

However, one of the main limitations for the installation and transportation for spar foundations is their requirement for very deep-water depths of approximately over 100 meters in the whole process. The large draft of the foundation makes it a requirement for deep harbors or fjords for the final assembly of the foundation as well as for towing of the foundation. This makes spar foundations well-suited for countries like Norway in which such infrastructure is

available for construction, but not suitable in locations which does not cover this requirement, making it a very big limiting factor in other locations. While the deployment and use of this foundation is heavily constrained by logistical challenges, spar foundations remain as one of the most technically stable and mature solutions for floating wind for regions with suitable conditions for the water depth and bathymetry required [56].

2.2.1.4. Barge

Barge foundations are ship-like floating structures used to support offshore wind structures with their stability being provided by their broad floating surface. Unlike other solutions like spar foundations with large drafts, barges maintain their equilibrium through their wide, flat-bottomed design with a large waterplane area, allowing them to remain upright and have high stability even with shallower waters. This design makes it ideal for moderate depths starting from 40 meters and has the flexibility of being able to be fabricated in both steel and concrete depending on construction capabilities and costs [56].

One of the most important barge foundation designs is the patented concept Damping Pool published by BW-IDEOL. It has been used for demonstration projects such as Floatgen for 2 MW in concrete [67], as shown in Figure 2.20 as well as Hibiki for 3 MW in steel [68] which have validated successfully the barge concept in real marine sea states offshore. Currently the pre-commercial EOLMED project is under construction which features three 10 MW turbines for a total of 30 MW located 18 km from the offshore in Occitane, France with a water depth of 55 meters [69]. As of April 2025, the float fabrication has been completed and the painting is in process to be finished, which points that installation is close [70]. These projects showcase the potential scalability and versatility of the barge foundation, progressing towards commercial readiness.



*Figure 2.20: Barge Platform in Floatgen by BW-IDEOL.
Source: [67].*

Barge foundations are self-stable using their own structure buoyancy and ballast system and are typically moored into position by using catenary or semi-taut systems. However, one of its downsides is their large footprint and waterplane area on the water surface that may pose challenges for dense wind farm layouts, since they can be prone to excessive motion in harsh weather conditions. Additionally, their construction involves complex processes to ensure durability and balance under loads [56]. Despite these challenges, barge foundations offer a solution for intermediate water depths where deep-draft or heavy lifting infrastructure is limited.

In summary, floating foundations are well suited for deep waters beyond the scope of fixed foundations to deploy offshore wind and hydrogen infrastructure. Each of the different technologies offer diverse designs, concepts, and characteristics that are tailored to each specific site and project conditions, as shown in comparison in Table 2.2. TLPs use taut vertical mooring which is ideal for installation with sensitive stability and minimal motion. Semi-submersibles offer versatility and commercial readiness for a range of sea-states. Spar platforms provide excellent stability through deep ballast but require special installation conditions like fjords. Barges offer a simplified, ship-like structure with easy fabrication potential but is more influenced by wave loading. As floating concepts develop and mature, they unlock new possibilities and potential for renewable energy deployment to reach farther and deeper offshore areas. It also helps to accelerate decarbonization goals and innovations in mooring systems, structural optimization and offshore electrolysis. These platforms mark a critical step toward scalable, flexible, and global offshore renewable energy deployment.

Table 2.2: Overview of main floating foundation types

Type	Principle	TRL & MRL [64]	Advantages	Limitations
TLP	Platform with positive buoyancy retrained by vertical tendons to seabed. (Mooring-tension)	TRL 4-5 MRL 4	Low overall risk. Onshore / drydock assembly. Shallow draft. Well understood supply chain.	Large and heavy structure. Columns likely will need inspection every 10 years by specialized technicians.
Semi-Submersible	Slender structures with several buoyancy tanks filled with water, serving as ballast for stability. (Hydrostatic)	TRL: 7-8 MRL: 7	Suitable for high sea states. Low steel weights. Low operational risks.	Large draft. Limits in ports and transport routes. Attachment of topside could be complex. Heavy lift is likely needed.
Spar	Self-stabilizing platform with deep draughts and ballasted at bottom to compensate CoG. (Ballast)	TRL: 7-8 MRL: 7.5	High stability. Lower still weight. Onshore / drydock assembly. Suitable for deep waters.	Sensitive to waves and currents. Not self-stable during towing. Expensive mooring system.
Barge	Ship-like concept which stability comes from a large floating surface. (Hydrostatic)	TRL: 6-7 MRL: 6.5	Moderate draft. Onshore / drydock assembly.	Bigger influence of wave loading.

2.2.2. Connection Schemes

When considering the connection schemes of the different typologies for electrolyser placements, it is necessary to consider certain factors and key drivers like the offshore distance, the capacity of the farm for the most suitable transport of energy. These connection schemes can be categorized into three different types, from which in one the electricity is transported via power cables to land to perform the water electrolysis onshore, or in the other 2 methods in which the electrolysis is done directly offshore and then transported via pipelines or tankers. These three connection schemes are explored in depth in this section as well as some of its implications for infrastructure and characteristics.

2.2.2.1. Centralized Onshore Electrolysis

The onshore electrolysis scheme consists of generating electricity by offshore wind turbines and transmitted using submarine cables to shore where hydrogen production by means of electrolysis is done on land. This configuration collects the electrical output from all turbines by using inter-array cables and transmitted to an offshore substation, where the voltage is

stepped up to reduce transmission losses. From there, the power is transmitted to shore via high-voltage submarine export cables using either HVAC for shorter distances or HVDC for longer distances with a turning point of around 100 and above from shore since HVAC presents cable-generated reactive power [71]. This power is collected at an onshore substation, where voltage is adjusted to match the requirements of operation of the electrolyser.

Once onshore, electricity is fed into a centralized hydrogen production system where electrolysis takes place. This layout permits greater flexibility in design as it avoids having hydrogen production on offshore platforms which means a reduction in weight and space constraints. As a result, both AWE and PEM electrolysis could become a cost-effective option for onshore deployment as it is easier to deal with the space constraint onshore and with AWE electrolysis having a relatively lower capital cost [17]. This electrolyser facility should typically be located close to shore to minimize any further transmission on land and include auxiliary systems like cooling units and water supply infrastructure. The water required can be sourced from local supply networks or any desalination systems near shore if there are limits in freshwater sources. It may be necessary to also to include a compressor for the hydrogen in case of requirement for its integration into storage or distribution systems [72].

One of the major advantages of this connection scheme is that it reduces the infrastructure footprint offshore since the electrolysis system is on land. This means the offshore substation only needs to accommodate the necessary equipment for electrical conversion and transport, avoiding the complexity and high cost of installing and maintaining the electrolysers at sea. However, the trade-off for this type of scheme comes from the higher costs for subsea cable costs, getting even higher if dynamic cables are needed and the transmission losses related to the cable over long distances [12]. This makes this configuration most suitable for coastal regions with strong grid connections or for remote floating offshore wind applications in deep waters using spars where hydrogen will be used locally or exported [73].

2.2.2.2. Centralized Offshore Electrolysis

The centralized offshore electrolysis scheme consists of having all hydrogen production done directly at sea using as power source all the electricity collected from all the wind turbines in the offshore wind farm. The individual power outputs from each wind turbine are gathered through medium voltage dynamic cables and collected into an offshore substation, where the voltage is stepped up [72]. This electric current is transmitted to the offshore hydrogen production facility installed either on an offshore platform or a floating vessel (FPSO) to perform the electrolysis using desalinated seawater as feedstock.

This centralized configuration has the advantage of avoiding the use of high-voltage electrical cables all the way to shore. Instead, hydrogen is produced offshore and can be stored and transported in various ways according to the project and site characteristics. It can be compressed and transported via submarine hydrogen pipelines, which are typically more cost-effective for long distances, avoiding electrical transmission losses. An alternative would be to use tankers or FPSOs to storage and transport by chemically bound hydrogen carriers or in their liquified form and shipped to shore [17].

The offshore electrolysis plant consists of electrolyzers, seawater desalination units, cooling units, cooling systems, compression equipment, hydrogen buffers, and a backup battery system for critical components, and all needs to be considered in the space and weight necessary for the platform and its footprint. Both AWE and PEM electrolysis technologies are initially viable for this, considering that AWE is more cost-effective but has a limited hydrogen output pressure and may require additional compression. On another note, PEM technology has a higher output pressure and better response times but comes at a higher capital cost [73].

From an operational perspective, centralized offshore scheme reduced the wind turbine maintenance complexity, as the turbines remain electrically connected to an offshore substation and do not have embedded electrolysis units [12]. However, it has some disadvantages as it does introduce an operation risk as failure in the electrolysis systems can mean no hydrogen production for the entire farm, introducing the need of on-site personnel for turbines and electrolysis plant maintenance. Additionally, environmental impacts must be considered as there is a risk coming from managing the resulting brine discharge from seawater desalination [73].

While this scheme simplifies logistics compared to a decentralized design and benefits from pipeline transport efficiency which avoids electrical transmission losses, it requires a significant investment cost for floating infrastructure. It is more suitable for deep-water installations or where island-based electrolysis is not feasible. The trade-off between operational and economic conditions must be evaluated according to any site conditions, infrastructure costs, and distribution requirements.

2.2.2.3. Decentralized Offshore Electrolysis

The decentralized offshore electrolysis scheme consists of having hydrogen production in each individual wind turbine within the offshore wind park. These systems include typically an electrolyser, cooling system, seawater desalination unit, hydrogen buffer and a battery system as backup. This whole setup must be integrated into each of the wind turbine platforms,

considering the space and weight for the platform design [72]. This way, all electricity generated by the wind turbine is used on-site directly for electrolysis, which eliminates the need for complex AC-DC conversion steps associated with the centralized power transmission and lower energy losses related to power electronics.

One of the biggest advantages of the decentralized scheme is the redundancy of the system, since electrolysis occurs independently at each unit. This distribution makes the system inherently robust, as failure of one turbine or electrolyser does not disrupt the overall hydrogen production from the rest of the wind farm. PEM technology is considered as a strong candidate for this type of scheme due to its compact footprint, high efficiency and the ability to output pressurized high purity hydrogen, eliminating the requirement for additional compression for hydrogen export [73].

The hydrogen produced at each of the electrolyzers is collected by a series of flexible pipelines that connect a group or array of turbines into a subsea manifold system. The subsequent transmission is done by a larger main export pipeline which is static and fixed to transport the hydrogen to shore for its storage and distribution. With this layout, it is possible to avoid using massive offshore platforms for an offshore substation or an offshore electrolysis plant, which can significantly reduce CAPEX [12]. Furthermore, the design is modular and enables deployment and installation by phases and makes it easier to scale up the hydrogen production capacity. Looking at the environmental implications, this scheme distributes spatially the brine discharge coming from desalination, which means less impact compared to centralized scheme [73].

Since electrolysis systems must be placed on each wind turbine, platforms must have enough deck area and stability to not compromise the turbine's efficiency, making semi-submersibles or barges well suited for deepwater sites. Flexible hydrogen pipes must be used in this scheme to allow dynamic and reliable interface between floating structures and fixed seabed infrastructure and allowing high-pressure hydrogen transport. This scheme is defined by the trade-off of having system scalability, resilience and robustness against a higher equipment duplication and greater maintenance complexity, as each turbine needs its own electrolysis system.

These three different electrolysis schemes differ mainly from their configuration regarding the location of hydrogen production as well as the method of storage and transport of energy or hydrogen to the shore. Centralized onshore electrolysis places all electrolyzers on land and relies of high-voltage power cable to transport electricity from offshore wind farm,

which simplifies offshore infrastructure but has power losses and high cable costs. Centralized offshore electrolysis locates the electrolysis system on a platform or vessel offshore, reducing transmission losses by transporting hydrogen via pipeline or tankers but requires costly offshore infrastructure. Decentralized offshore electrolysis distributes electrolysis to each individual wind turbine and uses flexible and static pipelines through a manifold for hydrogen transport, which eliminating electric transmission adds redundancy and dispersion of brine discharge at the expense of adding system complexity. Each of these approaches balance different trade-offs and is suitable for different site characteristics and requirements, as shown in Table 2.3, with each of them having their own advantages and disadvantages in terms of infrastructure complexity, CAPEX and OPEX costs, scalability, and environmental impact.

Table 2.3: Overview of main connection schemes

Scheme	Configuration	Advantages	Limitations
Centralized Onshore	Electricity is transmitted to shore via HVAC / HVDC cables and hydrogen is produced at a single centralized land-based facility.	Easier installation and lower costs onshore. Simple onshore maintenance. Electrolysis technology does not need further validation.	High cable and converter costs. Power losses in long-distance transmission.
Centralized Offshore	Centralized electrolysis on an offshore platform or vessel with transportation via pipeline or shipped to shore.	Reduced electrical losses. Efficient hydrogen pipeline uses. Smaller land footprint. Relatively quicker repair times.	Expensive offshore infrastructure. O&M complexity. Environmental impact of brine. Operation risk due to all electrolyzers being in single location.
Decentralized Offshore	Each turbine integrates an electrolyser, and hydrogen is transported via dynamic and fixed pipelines.	High system redundancy. No power transmission losses. No separate additional structure needed. Distributed brine discharge.	High equipment replication. Complex control & maintenance. Higher turbine integration cost.

Another aspect to consider for each connection scheme is how hydrogen will be stored and transported safely with the lowest possible cost to shore. Offshore environments have the constraint of space, weights, motion, long export distances, and harsher conditions compared to onshore. Some of the different technologies that can be suitable for storage of hydrogen consist of compressed, cryogenic hydrogen, and solid-state hydrogen or through chemical carriers such as LOHCs, ammonia and methanol. Each of them presents certain advantages and

disadvantages, with trade-off in energy density, infrastructure complexity, and safety. On the transport side, it is possible to have the use of dedicated hydrogen pipelines or retrofitted oil & gas pipelines that are no longer in use. Additionally, the use of tankers and carriers may be used in some cases to transport produced green hydrogen into shore. Appendix 8.2 presents the main characteristics of the storage types and their pairing with the most suitable transportation method for hydrogen carriers. Considering that the use of tankers for transportation for hydrogen carriers is advantageous when considering very long distances of around ~1000 km, compressed hydrogen pipelines will be considered as the potential method of storage and transportation.

Pipelines represent a promising and efficient method to deliver hydrogen from offshore production sites like offshore wind farms from large distances from shore, where electrical transmission becomes unfeasible economically or technically. For hydrogen transport at sea, two key categories of pipeline infrastructure are considered depending on the marine environment in the way of static and dynamic pipelines. Additionally, retrofitting existing natural gas pipelines may be a cost-effective pathway to accelerate hydrogen deployment offshore where such infrastructure is available for use [74].

Static pipelines are rigid subsea pipelines that remain fixed to the seabed by being laid or slightly buried under it. They are commonly used for transporting hydrogen from stationary offshore platforms like fixed-bottom wind farms or offshore electrolyzers to connect it directly to shore or collection hubs [75]. They feature durable, rigid steel or composite construction to withstand the seabed pressure and corrosion while transporting hydrogen with high efficiency and low maintenance. However, it required careful material selection, as well as coatings to resist hydrogen embrittlement and diffusion and may need compression stations for long distances [76].

Dynamic pipelines are flexible flowlines or risers typically designed to handle the continuous motions due to the wave, current, and wind loads, which makes it suitable to use in floating offshore wind or hydrogen production platforms and follow its motions of the floating foundations. For this, it needs to be built using flexible, layered materials to handle movement and fatigue, often having a reinforcement of armor layers and pressure containment systems. However, it requires specialized anchoring and buoyancy systems to manage the stress suffered by the continuous motion, as well as to maintain its position. Dynamic pipelines present a more complex design and higher cost compared to static pipelines but remain essential for a safe and reliable operation for floating platforms which present deep water and high-motion environments [77].

In some cases, it is possible to retrofit existing subsea and onshore natural gas pipelines into infrastructure viable for hydrogen transport. This can be a cost-effective strategy to accelerate the infrastructure development of green hydrogen production. This process involves ensuring material compatibility assessment to prevent hydrogen embrittlement in certain steels and welds [78], as well as replacing seal and valves since these components may not be suitable for hydrogen as it is a small molecule and can cause diffusivity. It is also necessary to adjust the flow and pressure of the pipeline, as hydrogen has a lower volume density than natural gas and requires higher flow rates or compression and in some cases include internal coating to improve hydrogen resistance and reduce permeability. These adaptations offer a significant cost savings opportunity with costs of 10% to 35% compared to a new pipeline build, making it relevant in North Sea offshore hydrogen projects located near decommissioned or underutilized natural gas infrastructure exist [79].

2.3. Offshore electrolysis demonstrations and pilot projects

Detailing and analyzing current demonstration and pilot projects for offshore electrolysis is essential to understand the feasibility and progression that support offshore green hydrogen production according to the market. These initiatives and early projects serve as practical testing grounds that will help in the future to validate the systems performance, durability, and integration with offshore renewable energy sources and give way to any necessary technological advancements needed to reach decarbonization goals. These projects play a critical role for technology readiness and maturation by identifying any challenges that can present themselves in commercial projects on a bigger scale and improving the operation and performance. It also contributes to any risk identification and mitigation that was not previously considered by exposing any potential technical, logistical and environmental issues that may arise when scaling up. Furthermore, these projects are a necessary step to determine and comply with regulatory requirements for this evolving technology and demonstrating its market readiness and inspiring confidence in stakeholders. Testing innovation and improvements under actual offshore conditions and marine environment accelerate the path towards being ready for commercial-scale projects and contribute towards a green energy transition.

Several offshore electrolysis demonstration and pilot projects have currently been completed, commissioned or have been planned across the globe to assess this technical feasibility, economic viability, and its environmental impact to produce green hydrogen at sea, as shown in Appendix 8.3. The first offshore hydrogen production pilot developed by Lhyfe in

2022 was the initiative of SeaLhyfe, which was installed off the coast of Le Croisic in France and successfully produced its first kilograms of green hydrogen in 2023. This project was pivotal in validating the functionality of a 1 MW PEM electrolyser under real marine conditions, as it provided valuable insights into technical and environmental aspects and difficulties producing hydrogen offshore. The tests were done for 14 months producing hydrogen at sea with real marine conditions, going through extreme conditions in terms of platform motion and environmental stress. It faced 5 important storms, with one of them being Ciaran that went through the Atlantic coast in October 2023 with waves of above 10 meters and winds above 150 km/h. These tests repeatedly tested the versatility and response time in a variety of configurations, reaching the same performance as compared when on land [80].

The OceanH2 project coordinated by ACCIONA in Spain, focused on designing and experimentally validating the integration of floating wind, solar and hydrogen production to support the country's commitment to renewable energy [81]. Similarly, PosHYdon in Netherlands is a pioneering project that aims to integrate offshore wind, gas, and hydrogen production on an existing operational gas platform in the Dutch North Sea by installing a 1 MW electrolyser. This unique approach of combining existing energy systems offshore helps examine the electrolyser technical performance and durability under offshore conditions and create a fully electrified platform [82]. Over in Asia, the Yantai Offshore Platform is China's first offshore platform with integrated production of green hydrogen, ammonia, and methanol with the goal of demonstrating that clean fuels can be generated offshore, off the grid and refuel ships at sea [83]. The Green Hydrogen Shore Power Demonstrator at the Port of Leith showcases the potential of green hydrogen to support decarbonizing port activities by integrating water treatment, waste heat utilization, and green hydrogen production to provide clean shore power for maritime operations [84]. The OYSTER Project in the UK aimed to develop a marinized electrolyser to integrate with offshore wind infrastructure. Although the project was recently terminated in 2025 following Orsted's withdrawal from the project, it contributed valuable insights towards the hydrogen technology and challenges involved [85].

Meanwhile, some planned initiatives and projects in the short term are currently underway to contribute towards reaching EU's green hydrogen targets like the HOPE project coordinated by Lhyfe which involves developing, building, and operating a 10 MW offshore hydrogen production unit in the North Sea. It corresponds to the second stage following the success of SeaLhyfe and aims to demonstrate viability in both technical and financial aspects of large-scale offshore hydrogen and pipeline transport [86]. In Germany, the H2Mare project is part of their national strategy to directly link offshore wind turbines with hydrogen generation

and aims to reduce the costs associated with this [87]. The same can be said about Norway's Deep Purple Project, which focuses on also integrating storage solution for hydrogen and offering a vision for stable offshore energy systems [88].

Some of the projects have bigger ambitions in regards of the capacity of the project, having in Belgium the Hyport Oostende project with tap into the country's wind resources to fuel green hydrogen production with a 50 MW electrolyser onshore using offshore wind as power source [89]. GET H2 Nukleus in Germany sets its ambitions to focus on developing large-scale commercial production with a 300 MW electrolyser capacity with offshore power, after commissioning in 2024 a 10 MW AWE and 4 MW PEM electrolysers onshore [90]. The Salamander Project in Scotland will use DOLPHYN technology to achieve integration of 100 MW in offshore wind plus 100 MW in onshore batteries to hydrogen production, desalination and transport via pipeline to power sectors that are hard to electrify [91].

Farther out, some initiatives include the HØST PtX Esbjerg project in Denmark that categorizes as a leading Danish Power-to-X project planning to produce green hydrogen and ammonia with primarily offshore wind and solar power with a total capacity of 1 GW by 2029 [92]. Other large-scale efforts are underway in Netherlands, with projects like H2opZee by 2030 looking for developing green hydrogen production in the Dutch North Sea with a capacity of 500 MW [93], as well as NorthH2 project, looking to achieve 10 GW in Netherlands between 2030 and 2035 [94]. Some of the most ambitious and larger-scale initiatives also proposed for 2035 are the DOLPHYN project which plans phased deployments of floating wind turbines equipped with electrolysers, currently conducting sea trials with a PEM electrolyser and with planned phases ranging between 10 MW until 4 GW [95]. Finally, the AquaVentus initiative in Germany aims to scale up to 10 GW of green hydrogen capacity through a set of coordinated projects [96] such as AquaPrimus, which serves as a demonstrator for electrolyser of 1 MW and 5 MW capacity, AquaSector, which aims to establish 300 MW in the German North Sea as a first large-scale offshore hydrogen park, and AquaDuctus, which aims to install a hydrogen pipeline network to efficiently transport hydrogen produced from offshore wind farms [97]. These projects are not only demonstrating the pathways necessary to take for offshore hydrogen production, but also laying ground for any regulations, infrastructure, and economical models needed to accelerate green hydrogen deployment at scale.

2.4. Regulatory frameworks

Regulatory frameworks are necessary for offshore hydrogen production systems by ensuring a safe, efficient, and scalable deployment and operation. They are used to provide a guide of rules and standards on design, environmental, and safety compliance for a certification. This certification demonstrates commitment to achieving a certain standard and quality and provides assurance to stakeholders and the public that operations meet regulatory requirements [98]. Offshore electrolysis can become complex in terms of regulations since it integrates renewable power, desalination, and hydrogen storage and transport, which makes it a requirement to harmonize regulations across the different sectors and jurisdictions necessary.

Several international and regional regulatory initiatives are currently in development or early implementation stage. In the European Union, regulatory standards have been increasing with the EU Renewable Energy Directive RED II and RED III, which defines the sustainability criteria that renewable hydrogen must comply with. These directives determine the greenhouse gas emissions thresholds, as well as the rules for the sourcing of electricity [99]. Additionally, the Delegated Acts introduced by the European Commission in 2023 establishes the legal criteria to certify hydrogen production as part of the Renewable Fuels of Non-Biological Origin (RFNBOs) under these directives. It defines specifically the conditions of additionality to ensure it comes from new renewable installations that are not already supplying to the grid, the temporal and geographical correlation which determines electricity must be generated close in time and location to the hydrogen production, as well as the minimum GHG savings of a minimum threshold of 70% to ensure that it contributes to climate goals [100].

Some complementary initiatives are the TEN-E Regulation which aims to support the development of cross-border energy infrastructure and its integration into the EU's energy system [101] and the European Hydrogen Backbone which aims to establish a dedicated hydrogen pipeline network [102]. The International Energy Agency compiles an annual report in the Global Hydrogen Review 2024 which provides a detailed global track and comparison of all the hydrogen related regulation and certification systems. This report plays a crucial role in assessing the progress of technology, infrastructure development, and market trends to help regulations and industry leaders take decisions and guide investment strategies and policy frameworks accelerate hydrogen deployments. For example, several EU countries like Germany, Netherlands and France are developing their own certification systems, which must arrive to a mutual recognition of certification schemes instead of a full harmonization between them to facilitate cross-border trade. Another focus goes to Latin America and the Caribbean, since it has strong potential for low-emissions hydrogen production with abundant renewable

resources and industry demand. Currently its deployment is limited by high capital costs and the need for a significant expansion in renewable energy that can be remedied by energy security improvements and hydrogen hubs to scale production and balance domestic use with export ambitions [103].

Technical codes and standards are currently in development and being defined. The ISO 22734:2019 standard is currently an active standard that focuses on the general requirements involved in hydrogen generators using water electrolysis and covers all industrial, commercial, and residential applications [104]. This standard is applicable for electrolyzers using AEM, PEM, aqueous acids or bases for ion transport medium and covers general guidance on its safe constructions of its components, minimum requirements for safe operations, routine tests according to operation, leakage and basic electrical installation, mechanical integrity, performance and reference conditions [105]. It is expected that the standard be replaced and extended by the ISO 22734-1 and ISO/AWI TS 22734-2, which will guide the performance testing and its protocols to determine if the electrolyser has the minimum capabilities to provide electricity in grid-integrated scenarios with the focus on alkaline and PEM electrolyzers [106]. The ISO 19880-1:2020 focuses on gaseous hydrogen fueling stations and defines its safety, design, installation, and operational requirements mainly for land applications. This can be adapted towards offshore hydrogen production, specifically for hydrogen bunkering in maritime applications by referencing aspects in its safe storage, compression, dispensing and transport in offshore environments [107].

Other organizations like the IEC are currently working on establishing electrical safety and performance standards with the IEC 62282 series which covers the fuel cell technologies including offshore applications [108]. In the case for certification services, DNV has issued the first global standard for electrolyser systems with the code DNV-ST-J301. This standard provides the technical requirements and guidance for the certification of electrolyser systems. It addresses risk management for relevant hazards and safety requirements associated with hydrogen production. It also establishes design verification in both system and component level requirements to be met to ensure the safety of the operation in all phases including design, manufacturing, installation, commissioning, and operation [109].

In the United States, regulatory efforts are currently led by organizations such as ASME, NFPA, and CSA to provide standards in different fields of pressure vessels, hydrogen piping, and electrolyser certifications in terms of safety and mechanical integrity. Some of the key codes and standards from ASME consist of TPG-1 – Guidelines to ASME Standards in Hydrogen Value Chains serves as a guidance for existing hydrogen-related standards, B31.3,

B31.8, and B31.12 which deal with the requirements for piping, gas transmission, distribution and handling of gas and hydrogen pipelines and lastly for pressure vessels the rules for construction can be seen in BPVC.VIII.1 and BPVC.X including fiber-reinforced plastic pressure vessels [110], [111]. In the case of NFPA, NFPA 2 covers the guidelines for safety in production, storage, and transportation of hydrogen technologies, NFPA 55 deals with compressed gases and cryogenic fluids safety including hydrogen, NFPA 67-69 deals with explosion protection and prevention systems in gaseous mixtures in pipe systems, and NFPA 70 provides guidelines for electrical installations involving hydrogen systems [112]. Lastly, CSA/ANSI B22734:23 is a standard that mirrors the ISO 22734 specifically for the North American markets, CSA/ANSI HGV series deals with hydrogen fueling stations and CSA/ANSI B107-24 addresses safety requirements for enclosed hydrogen equipment [113], [114]. Additionally, the U.S. Hydrogen Safety Panel and Hydrogen Tools database known as H2tools offers comprehensive guidance for hazard assessment and design practices with regards to best practices on hydrogen production [115], [116].

Despite progress in the development of regulatory frameworks, significant gaps remain. Offshore-specific frameworks currently are lacking in various fields like floating hydrogen platforms, marine integration, hydrogen pipeline safety, and brine discharge regulations. Additionally, the fragmentation of certification schemes and lack of mutual recognition in between different national certifications affect cross-border projects. These regulations must constantly be evolving and must keep pace with the current innovations regarding electrolyzers, subsea pipeline and hydrogen offshore energy hubs. These regulations must keep international coordination to close these gaps by using regulatory sandboxes, pre-commercial demonstrations exemptions, and shared certification platforms. Additionally, integrating hydrogen regulations with maritime laws, offshore wind regulations, and environmental regulations will be key to ensure a safe, efficient, and sustainable deployment in a cohesive hydrogen economy.

3. CASE STUDY: EUROPE

The aim of this chapter is to present and select a detailed European case study that establishes chosen scenarios for a specific potential location for offshore green hydrogen production using offshore wind resources, taking into consideration the impact and specific requirements of electrolyzers in offshore environments. Section 3.1 examines the regional market demands for the biggest industrial off-takers, hydrogen pipelines infrastructure and projects, existing port infrastructure and its location, available wind resources, and socio-political constraints due to the Exclusive Economic Zones (EEZ), environmental, commercial and defense concerns. Section 3.2 identifies and describes several implementation scenarios for techno-economic evaluation by integrating electrolyzers with offshore wind farms by choosing the conditions according to the unique operational challenges to face in marine environments. Lastly, Section 3.3 describes these specific impacts and requirements that electrolyzers, specifically PEM, suffer in offshore environment due to the platform dynamics and tilt, intermittency and variable power supply, saline environment, and feedwater quality concerns when integrating with offshore wind.

3.1. Justification of implementation zone

To assess the most promising European locations for offshore green hydrogen production, it is necessary to consider a certain range of technical, economical, geopolitical factors and parameters. To determine and justify the most suitable implementation zone requires analysis of the regional hydrogen demand by considering the current major industrial off-takers and the outlook for this resource. Another important parameter to consider in the offshore environment is the proximity and readiness of port infrastructure for support in installation and maintenance for the whole lifetime of the project. Additionally, one of the main attractive potentials of offshore wind that must be considered is the availability and quality of the wind resource to generate greater energy production and more reliable power output compared to onshore, as well as the corresponding geographic conditions like water depth, waves, and area that may affect the costs and conditions of the project. This location must also be paired with the presence of future developments of hydrogen transport infrastructure and consider the constraints of areas given by the exclusion zones according to EEZ, environmental regulations, maritime commercial activity, human recreational activities, and national defense. These parameters help define viable scenarios and locations to justify the selection of strategic zones with strong potential for the deployment of offshore electrolysis systems.

The current and future market trends have been identified by the European Hydrogen Strategy, dividing it into three development phases of kick-start until 2025, ramp-up from until 2035 and market growth post 2035. Currently, the kick-start phase has seen the deployment of pilot and commercial electrolyzers with size currently increasing and expecting to advance into the ramp-up phase to expand the hydrogen use from local to national level. To achieve this, it must be supported by infrastructure like storage and transport networks like pipelines and regulatory tools and economic incentives. The final market growth phase will see a mature hydrogen market that can sustain itself by supply and demand with the potential to replace fossil fuels across various sectors while also ensuring fair competition and interoperability with the use of regulations [117].

Clean hydrogen is expected to play a vital role in decarbonizing the European industry, specifically in sectors that have a potential for high hydrogen consumption in its process. Hydrogen has been used previously as a feedstock in refineries and ammonia production, accounting for nearly 80% of Europe's 8.6 Mtons hydrogen demand in 2020 [118]. Refineries use hydrogen to remove impurities and reduce sulfur content to produce cleaner fuels, while ammonia needs hydrogen to be produced and used in fertilizers, plastics, or as maritime clean fuel. Methanol production is another example of a chemical process in need of hydrogen to be used as a synthetic fuel. Additionally, an industry with the most potential for its use of clean hydrogen is the steel industry, even though it currently is not a major hydrogen consumer. The plans to use hydrogen in the steel industry in processes like the direct reduction of iron or as a fuel for heating to significantly reduce emissions makes it one of the largest off-takers in the future [119]. By 2030, over half of the 6.1 Mtons H₂/yr of planned low-carbon hydrogen consumption in industrial projects being tracked by Hydrogen Europe corresponds to the steel sector's efforts alone [117].

According to the Clean Hydrogen Monitor reported in 2022 shown in Figure 3.1, the five biggest planned clean hydrogen consumers in the EU, EFTA, and UK by 2030 are Germany with 2,112 ktons H₂/yr, Sweden with 711 kt H₂/year, Netherlands with 571 kt H₂/year, France with 537 ktons of H₂/yr, and Spain with 523 ktons H₂/yr [120]. These figures represent the industrial decarbonization strategies being considered in Europe across the different sectors, being mainly concentrated around Western Europe with Germany in the lead. These countries are investing heavily in green hydrogen infrastructure and projects to be able to reach national decarbonization targets by reducing emissions coming from fossil-based hydrogen and shift industrial energy consumption.

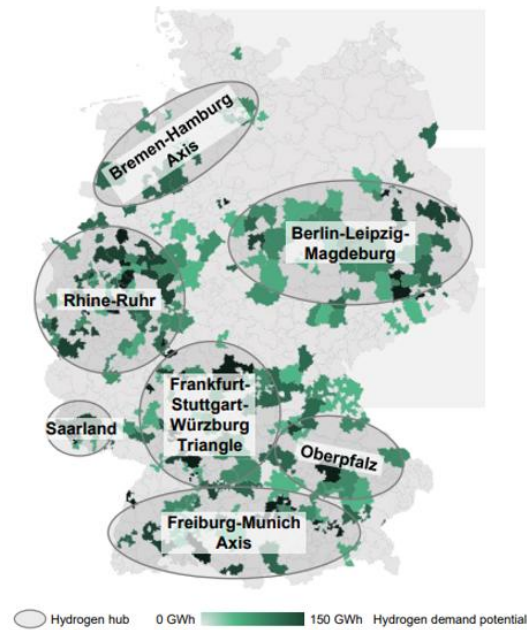


*Figure 3.2: Forecasted hydrogen demand clusters in Germany until 2030.
Source: [123].*

Sweden is becoming a significant player by incorporating green hydrogen with major industrial off-takers in steel, transport and chemical industries. The northern region has major flagship projects in Boden like H₂ Green Steel aiming to produce up to 5 million tons of steel annually using hydrogen by 2030 and HYBRIT Green Steel initiative in Luleå which already delivered the first green steel and is currently developing underground hydrogen storage [125]. In the central and southern region, the hydrogen infrastructure is expanding with projects like Lhyfe's 10 MW plant in Vaggeryd [126] and the Nordic Hydrogen Corridor's refueling network along the Scandinavian-Mediterranean [127]. Figure 3.3 shows the regional distribution of operational, planned and in development hydrogen projects in Sweden until December 2024. These regional hubs are laying the foundation for future connectivity, with the Swedish Energy Agency targeting 5 GW of electrolyser capacity by 2030 and 15 GW by 2045 with green hydrogen [125].



*Figure 3.3: The Hydrogen Map. Sweden and Finland 2025-02.
Source: [128].*

The Netherlands is advancing its strategy for green hydrogen by incorporating it into industrial decarbonization, port-based production, and international connectivity, by subsidizing over 1 GW in electrolyzers or nearly €800 million. The major players and projects in refining, chemical, steel, and transport are companies like Shell's 200 MW Holland Hydrogen I project supplied from offshore wind and Tata Steel Nederland plant to produce green steel [129]. The hydrogen activity is concentrated mainly into the Rotterdam Port Area with multiple electrolysis and import projects and Northern Netherlands as a hydrogen valley supported by offshore wind. Other regional hydrogen valleys can be seen in Figure 3.4, where hydrogen consumption and production will be concentrated in the country [130]. The Port of Amsterdam will also be a key location for the first green hydrogen import corridor, linking Oman's Port of Duqm to Amsterdam and key logistical hubs in Germany including the Port of Duisburg [131]. Infrastructure development in hydrogen pipelines is linked to HyWay27 initiative which repurposes existing gas pipelines and the North Sea Energy Infrastructure Plan to integrate offshore hydrogen with wind power and subsea pipelines to achieve the Dutch targets of 8 GW of electrolysis capacity by 2032 with fundings coming from the National Recovery and Resilience Plan [132].



*Figure 3.4: Hydrogen Valleys in Netherlands.
Source: [130].*

France is accelerating its green hydrogen strategy by focusing on the industrial and transport sectors including refineries, chemical plants, and heavy transport sectors. Some of the key off-takers consist of projects like Air Liquide-TotalEnergies collaboration at La Mède biorefinery which will produce 25,000 tons of green annually to reduce CO₂ emissions by 130,000 tons, as well as renewable hydrogen supply agreements in Grandpuits and Gonfreville refineries [133]. Hydrogen activity is being concentrated in industrial hubs with high potential capacity such as Fos-sur-Mer, Hauts-de-France, Normandy, and Grand Est, supported by regional hydrogen valleys and EU funding, as shown in Figure 3.5 [134]. It currently relies on short-distance hydrogen pipelines and preparing with broader integration with future onshore and offshore infrastructure and cross-border corridors passing across Germany, Spain, and the North Sea region through EU's Hydrogen and Decarbonized Gas Market Package [135].

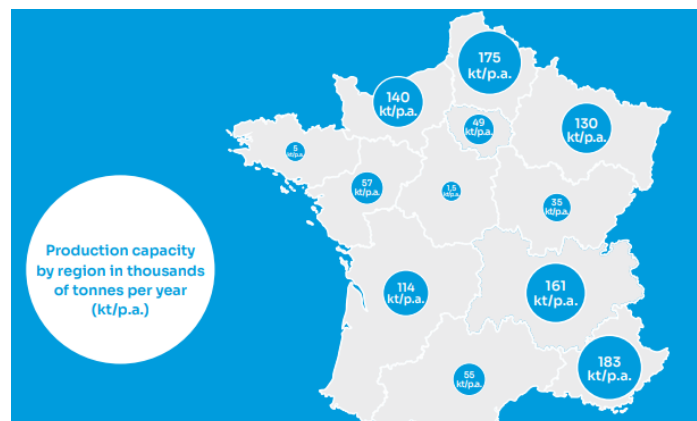


*Figure 3.5: Production capacity by region in France per year.
Source: [134].*

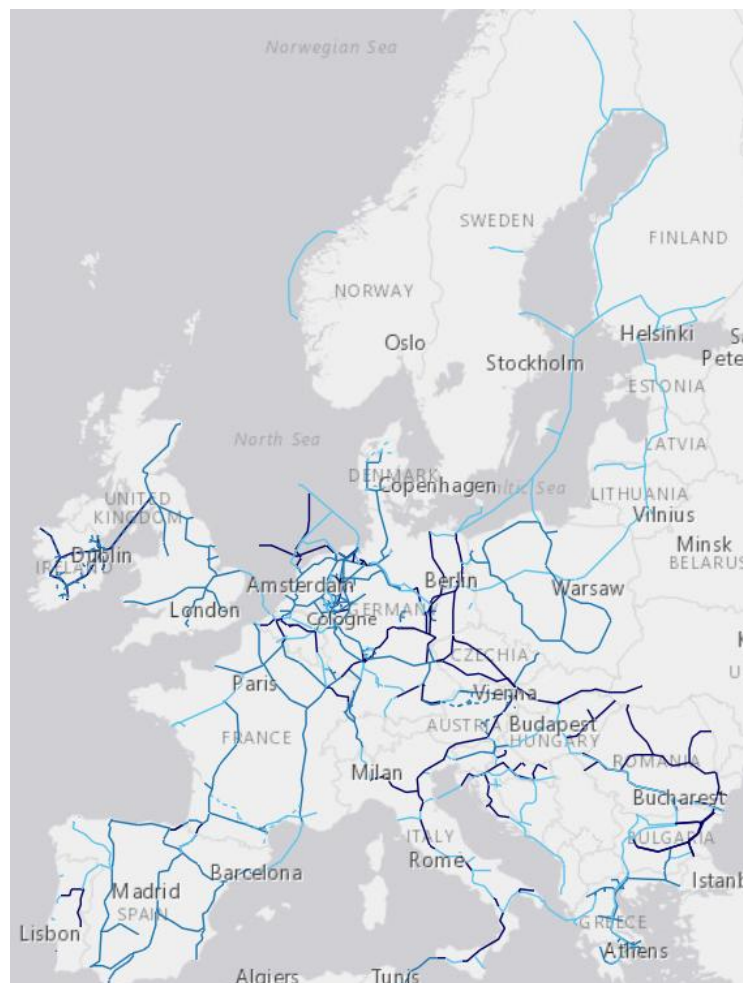
Spain is currently advancing and positioning itself as one of the European leaders in green hydrogen due to the strong industrial demand with major industrial off-takers in various sectors like chemical, refineries, steel, and transport by using its abundant renewable resources and strategic infrastructure. The Spanish government has chosen 16 key projects supported by €1.2 billion to be a part of Hydrogen Valleys program with major energy companies such as Respol, EDP, Moeve, BP, and Iberdrola across various regions such as Andalusia, Asturias, Valencian Community, Catalonia, and Galicia, as shown in Figure 3.6 [136]. Flagship projects like HyDeal España aim to deliver up to 330,000 tons of hydrogen annually to Asturias using solar power, pipelines, and storage [137]. Some key hydrogen infrastructure projects are H2Med, which connects Barcelona to Marseille via the BarMar interconnector through offshore pipelines with capacity of 2 million tons in transportation per year and CelZa as a part of a hydrogen corridor linking Portugal, Spain, France and Germany. Together with other projects like HyDeal's transmission routes, it reinforces Spain's potential as a hydrogen export hub in Europe [138].



Figure 3.6: Hydrogen Project Census in Spain.
Source: [139].

To be able to cover this potential hydrogen demand by importing and exporting across different borders to various end-users across Europe, infrastructure must be developed between production and consumption points. The European Hydrogen Backbone initiative plans to include both retrofitting natural gas pipelines and building new specific hydrogen pipelines to satisfy the future hydrogen demand. This plan determines the infrastructure needs of supply in demand in different regions by interconnecting different regions across regions of Europe in

28,000 km of both new and retrofit pipelines by forming five overlapping import corridors between North Africa & Central Europe, Southwest Europe, North Sea, Nordic and Baltic, and East and Southeast Europe, with all of them connecting with Germany, which possesses the most potential demand for hydrogen. Going into 2040, these pipelines are expected to develop into a total length of 53,000 km with a 60% being retrofitted pipelines, as seen in Figure 3.7 where all the different projects for infrastructure for hydrogen in Europe can be seen, depicting the future infrastructure map [140].



*Figure 3.7: Hydrogen Infrastructure Map for European Hydrogen Backbone in 2040.
Source: [141].*

A comparative overview of the five leading European countries previously discussed for clean hydrogen consumption by 2030 can be seen in Table 3.1. It includes the highlights for their industrial strategies, infrastructure developments, major projects, and the strategic initiatives to justify the key implementation zones for hydrogen production. Additionally, the planned infrastructure of the European Hydrogen Backbone links 3 of the 5 leading countries

in planned H₂ consumption by the Southwest import corridor that by 2030 plans to cover 10,000 km of large-scale pipelines across Portugal, Spain, France, Belgium, Luxembourg and Germany with a planned supply capacity of 164 TWh. Taking all of this into account, the Atlantic continental European coastline is considered as a potential site for offshore hydrogen production.

Table 3.1: Overview of Leading Countries according to Hydrogen Potential Consumption, Off-takers and Infrastructure.

Country	Planned H₂ Consumption [kt/year]	Key Industrial Off-takers	Strategic Justification
Germany	2,112	ArcelorMittal, RWE, Evonik (steel, chemical, refining)	Largest demand; central hub in EU; €4.6B federal funding; cross-border connectivity
Sweden	711	H ₂ Green Steel, HYBRIT (steel, chemical, transport)	Strong renewable base; early green steel production; underground H ₂ storage
Netherlands	571	Shell, Tata Steel, ENGIE (refining, chemical, steel)	Port-based production/import; €800M subsidies; key EU import/export hub
France	537	Air Liquide, TotalEnergies (refining, chemical, transport)	Regional hydrogen valleys; EU integration; industrial decarbonization
Spain	523	Repsol, Iberdrola, BP, EDP (chemical, steel, transport)	Renewable-rich; export potential; strategic corridors starting in Portugal through France & Germany

The GIS-based assessments for mapping of the wind resource and site selection in the Atlantic Coast of Europe has been studied previously by Díaz and Guedes [142], where 42 floating wind farms in Portugal, Spain and France were identified and evaluated according to the available wind resource, existing uses of maritime space and environmental constraints, and the operational needs of a floating wind farm. These previously identified potential sites are considered for the site selection of a 500MW offshore hydrogen production using offshore wind resource, taking into consideration the criteria mentioned in Table 3.2. The exclusion according to the constraints given reduced the decision matrix of potential sites to only 15, showing the location parameters for Wind Velocity (WV), Wind Potential (WP), Distance to Port (DP), Distance to Shore (DS), and Water Depth (WD) for 4 locations in Portugal, 3 in Spain, and 8 in France as shown in Table 3.3.

Table 3.2: Objective and Exclusion Criteria for MCDM.

Parameter	Objective	Exclusion Criteria
Wind Velocity (WV)	Maximize	-
Wind Potential (WP) [h/yr]	Maximize	-
Distance to Port (DP) [km]	Minimize	-
Distance to Shore (DS) [km]	Minimize	-
Water Depth (WD) [m]	Minimize	X ≤ 150 m
Delaunay's Triangulation Method WF Capacity [MW]	Exclusion Criteria Only	X ≥ 500 MW

Table 3.3: Site-Selection Decision Matrix for MCDM method in the European Atlantic Coast.

Source: [142], see Table 3.2 for abbreviations of parameters.

Region	Location	Option	WV [m/s]	WP [h/yr]	DP [km]	DS [km]	WD [m]
Portugal	Viana do Castelo (1)	1	7,4	3894	12,7	12	100
	Viana do Castelo (2)	2	7,4	3894	28,5	27,8	150
	Porto	3	7	3376	33,1	33,1	150
	Figueira da Foz	4	7,9	4131	62,1	51	150
Spain	A Guarda-Baiona (1)	5	7,4	3894	35,2	8	150
	Ribadeo	6	9,3	4923	89,5	17,6	150
	Navia	7	4,7	3521	48,7	10,3	150
France	Leon-Mimizan	8	6,2	2767	42,6	22,7	150
	Arcachan	9	7,5	3340	80,7	36,2	100
	Royan (1)	10	7,7	3654	44,5	30,9	75
	Royan (2)	11	8,7	4389	99	83,6	150
	La Rochelle	12	9	4660	136,7	112,5	150
	Pornic	13	9,5	5005	134	71,7	150
	Guilvinec	14	9,7	5123	124,5	68,5	150
	Brest	15	10,1	5464	82,3	35,4	100

A Multi-Criteria Decision Making (MCDM) Method will be used to validate the decision of the potential site-selection by using a Combined Weight Criteria W_j that is composed of a balanced combination of a subjective (AHP) and objective (Entropy) method and subsequently ranking the sites using the TOPSIS method. The Combined Weight Criteria is calculated by accounting a balanced factor $\alpha = 0.8$, that will be applied to the resulting weight criteria of both the subjective and objective methods, as shown in Equation (3.1).

$$W_j = \alpha \cdot AHP w_j + (1 - \alpha) \cdot Ent w_j \quad (3.1)$$

The AHP Method is a pairwise comparison method developed by Saaty, in which it is used to model subjective decision-making processes based on multiple criteria based on a hierarchical comparison. It pairs the different decision elements and approaches with a scaling method to assign values of relative importance among all the decision parameters. To quantify each parameter, it is required to have some experience and knowledge of the application to be able to assign the corresponding value, which can be classified according to Table 3.4, which denotes the relative importance between parameters. The methodology for the calculation of the AHP method will be made according to the work of Martínez [143] and Piantanakulchai and Saengkhao [144].

Table 3.4: Scales of Pairwise Comparisons.
Source: [143], [144].

Definition	Intensity of Importance
Equal Importance	1
Moderate Importance	3
Essential or Strong Importance	5
Very Strong or Demonstrated Importance	7
Extreme Importance	9
Intermediate Importance	2,4,6,8

The relative importance of two criteria is rated using this scale among the n criteria and arranged in a global matrix A of size $(n \times n)$, as shown in Equation (3.2), in which each of the pairwise comparisons are assigned, taking care of having reciprocal values when criteria j_{th} is compares with criteria i_{th} .

$$A = \begin{pmatrix} a_{11} & a_{12} & \dots & a_{1n} \\ a_{21} & a_{22} & \dots & a_{2n} \\ \vdots & \vdots & \ddots & \vdots \\ a_{n1} & a_{n2} & \dots & a_{nn} \end{pmatrix} \text{ with } a_{ii} = 1, a_{ij} = \frac{1}{a_{ji}}, a_{ij} \neq 0 \quad (3.2)$$

From this generalized matrix A , it is possible to determine the relative priority among the parameters. The analytical solution from Equation (3.3) provides the relative weight for each decision parameter, by having the normalized right eigenvector W is associated with the largest eigenvalue λ_{max} of the square matrix A , which can be computed according to Equation (3.4).

$$(A - \lambda_{max})W = 0 \quad (3.3)$$

$$\lambda_{max} = \sum_{i=1}^m \left[\left(\sum_{j=1}^n a_{ij} \right) \times AHP w_j \right] \quad (3.4)$$

To ensure consistency in between subjective perception and the accuracy of the results, a Consistency Index CI is used to measure the degree of inconsistency of the square matrix A and is calculated according to Equation (3.5). This value is compared with the same index derived from a randomly generated square matrix called the Random Consistency Index RCI as shown in Equation (3.6), which in this case the number of parameters $n = 5$, the corresponding $RCI = 1.12$.

$$CI = \frac{\lambda_{max} - n}{n - 1} \quad (3.5)$$

$$CR = \frac{CI}{RCI} \quad (3.6)$$

This ratio of CI to RCI for the same order matrix is the Consistency Relationship CR , which judges the given subjective importance in the pairwise matrix in the whole generalized matrix A and should be generally less than 0.1 in this case of 5 decision parameters to be considered acceptable.

The Entropy Method is a procedure proposed and developed by Zeleny in 1982, which is used to characterize the weight w of each criterion taken into consideration for the decision-making process between different alternatives. This procedure is used mainly for its objective characterization of the criteria, avoiding human intervention in the weighting of all the indicators. The methodology for the calculation of the Entropy method will be made according to the work of Gil-García et al. [145]. The first step of the method is given by the normalization of the decision matrix, which is given by Equation (3.7) to calculate the normalized value of the j_{th} criteria in i_{th} alternative.

$$P_{ij} = \frac{x_{ij}}{\sum_{i=1}^n x_{ij}} \quad (3.7)$$

Once having normalized the value of the whole site-selection decision matrix, it is possible to calculate the entropy of each criterion according to Equation (3.8), where m is the

number of alternatives in the decision matrix. This entropy is used to calculate the weight of the criteria according to the Entropy method by using Equation (3.9).

$$E_j = -\frac{1}{\ln(m)} \sum_{i=1}^m P_{ij} \ln(P_{ij}) \quad (3.8)$$

$$Ent w_j = \frac{d_j}{\sum_{j=1}^n d_j}, \text{ with } d_j = |1 - E_j| \quad (3.9)$$

Once having calculated the weights of each of the criteria by using a balanced combination of both an objective and subjective method, it is possible to proceed with a ranking and selection of alternatives by using MCDM. For this, the Technique for Order of Preference by Similarity to Ideal Solution or TOPSIS method will be used. This method is considered as a distance-based method, which calculated the distance between the alternative and the ideal best and worst solution. The methodology for the calculation of the TOPSIS method will be made according to the work of Gil-García et al. [145] and Shehab et al. [146]. The first step is to construct a normalized decision matrix to standardize the data and make the criteria comparable, which can be done according to Equation (3.10).

$$R_{ij} = \frac{a_{ij}}{\sqrt{\sum_{i=1}^m a_{ij}^2}} \quad (3.10)$$

This normalized decision matrix must then be transformed by applying the calculated combined weight for each of the criteria to find each of the weighted normalized matrix elements V_{ij} according to Equation (3.11).

$$V_{ij} = R_{ij} \times w_j \quad (3.11)$$

With this, it is possible to find the ideal solutions for this decision matrix. The positive-ideal solution represents the best performance from the alternatives in each criterion that its set objective in the decision matrix is to be maximized, while the negative-ideal solution represents the best performance from the alternatives in each criterion that its set objective in the decision matrix is to be minimized. These ideal best value V^+ and worst value V^- can be computed according to Equation (3.12) and Equation (3.13) respectively, taking into consideration what

the set objective for each criterion is either maximizing A^+ or minimizing A^- for best performance.

$$V_j^+ = \max(v_{ij}) \text{ for } A^+; \min(v_{ij}) \text{ for } A^- \quad (3.12)$$

$$V_j^- = \min(v_{ij}) \text{ for } A^+; \max(v_{ij}) \text{ for } A^- \quad (3.13)$$

Once having determined both ideal solutions, the Euclidean distance of every of the alternatives is calculated against both the ideal best and worst solutions, representing the distance of each alternative by trying to be closer to the best solution in each criterion as shown in Equation (3.14) and being as far as possible from the undesirable solution as shown in Equation (3.15).

$$S_i^+ = \sqrt{\sum_1^n (V_{ij} - V_j^+)^2} \quad (3.14)$$

$$S_i^- = \sqrt{\sum_1^n (V_{ij} - V_j^-)^2} \quad (3.15)$$

Finally, the alternatives can be ranked by calculating the proximity scored according to the distance to the ideal solution for both the positive and negative impact matrices, having the highest-ranked alternative the one with the closest distance to the from the ideal according to Equation (3.16).

$$P_i = \frac{S_i^-}{(S_i^+ - S_i^-)} \quad (3.16)$$

Table 3.5 illustrates the decision matrix generated for the AHP method which demonstrates the pairwise comparison and the selected subjective importance for each criterion. The comparison for subjective importance given is considered consistent due to the resulting value of $CI = 0.087$, resulting in a value of $CR = 0.078$, which is lower than the 0.1 limit established. Table 3.6 represents the normalized decision matrix used for the Entropy method that forms the objective part of the weight calculation for each criterion.

Table 3.5: Comparison among criteria for AHP Method.
See Table 3.2 for abbreviations of parameters.

	WV	WP	DP	DS	WD
WV	1	1/9	1/7	1/5	1/3
WP	9	1	3	5	7
DP	7	1/3	1	3	4
DS	5	1/5	1/3	1	2
WD	3	1/7	1/4	1/2	1

Table 3.6: Normalized decision matrix P_{ij} for Entropy Method.
See Table 3.2 for abbreviations of parameters and Table 3.3 for locations.

Location	WV	WP	DP	DS	WD
1	0,062	0,063	0,012	0,019	0,049
2	0,062	0,063	0,027	0,045	0,074
3	0,059	0,054	0,031	0,053	0,074
4	0,066	0,067	0,059	0,082	0,074
5	0,062	0,063	0,033	0,013	0,074
6	0,078	0,079	0,085	0,028	0,074
7	0,039	0,057	0,046	0,017	0,074
8	0,052	0,045	0,040	0,037	0,074
9	0,063	0,054	0,077	0,058	0,049
10	0,064	0,059	0,042	0,050	0,037
11	0,073	0,071	0,094	0,135	0,074
12	0,075	0,075	0,130	0,181	0,074
13	0,079	0,081	0,127	0,115	0,074
14	0,081	0,083	0,118	0,110	0,074
15	0,085	0,088	0,078	0,057	0,049

Table 3.7 presents the computed weights for both AHP and Entropy Method, as well as the final Combined Weight results by using a balance factor of $\alpha = 0.8$, for which it is possible to see that the 2 most important parameters to take into consideration is the wind potential, which influences directly the capacity factor and hydrogen produced, and distance to port, which influences directly the installation and logistics costs for maintenance due to the distance that the vessels will need to travel to access the windfarm.

Table 3.7: Criteria Weights for AHP, Entropy and Combined Methods with balancing factor $\alpha = 0.8$. See Table 3.2 for abbreviations of parameters.

Method	WV	WP	DP	DS	WD
AHP	3,53%	51,16%	25,33%	12,50%	7,48%
Entropy	3,62%	3,67%	35,16%	53,12%	4,42%
Combined	3,54%	44,04%	26,80%	18,59%	7,02%

Table 3.8 shows the weighted and normalized decision matrix using the Combined Weight calculated earlier, which shows the values for all alternatives regarding all criteria. From this, the ideal solution can be identified, for which both wind velocity and potential have a set objective to maximize, while distance to port, distance to shore, and water depth has a set objective to minimize. With the ideal best and worst solution, the Euclidean distance can be calculated for both best and worst solution and the proximity can be scored and ranked accordingly.

Table 3.8: Weighted and normalized decision matrix V_{ij} , ideal solutions and rank of TOPSIS Method. See Table 3.2 for abbreviations of parameters and Table 3.3 for locations.

Location	WV [max]	WP [max]	DP [min]	DS [min]	WD [min]	Si+	Si-	Pi	Rank
1	0.008	0.105	0.011	0.011	0.008	0.043	0.147	0.774	1
2	0.008	0.105	0.025	0.026	0.008	0.049	0.127	0.719	3
3	0.008	0.091	0.029	0.031	0.008	0.065	0.118	0.646	6
4	0.009	0.112	0.054	0.048	0.009	0.070	0.094	0.575	10
5	0.008	0.105	0.030	0.008	0.008	0.048	0.136	0.739	2
6	0.011	0.133	0.077	0.017	0.011	0.069	0.115	0.624	8
7	0.005	0.095	0.042	0.010	0.005	0.062	0.125	0.667	4
8	0.007	0.075	0.037	0.021	0.007	0.079	0.118	0.597	9
9	0.008	0.090	0.070	0.034	0.008	0.086	0.089	0.506	11
10	0.009	0.099	0.038	0.029	0.009	0.060	0.114	0.654	5
11	0.010	0.119	0.085	0.079	0.010	0.108	0.061	0.362	14
12	0.010	0.126	0.118	0.106	0.010	0.148	0.051	0.258	15
13	0.011	0.135	0.116	0.068	0.011	0.122	0.072	0.372	13
14	0.011	0.139	0.107	0.065	0.011	0.113	0.077	0.406	12
15	0.011	0.148	0.071	0.034	0.011	0.065	0.114	0.635	7
V ⁺	0.011	0.148	0.011	0.008	0.010				
V ⁻	0.005	0.075	0.118	0.106	0.020				

In this case, the best ranked is given to Viana do Castelo (1), second rank is given to A Guarda-Baiona and third rank is given to Viana do Castelo (2). It is notable to mention that these 3 locations have moderate amounts of wind potential but also have relatively close distances for port and shore. Additionally, these locations are relatively close to each other, giving this zone near the north of Portugal and close to Galicia in Spain a suitable location. For this reason, the considered location for the techno-economical evaluation that will be considered will be the best ranked according to the MCDM method used, which corresponds to Viana do Castelo (1), with the characteristics shown in Table 3.9 and at the location shown in Figure 3.8.

Table 3.9: Characteristics of the site selected for techno-economical evaluation.
Source: [142].

Location Chosen: Viana do Castelo (1)	
Wind Velocity (reference)	7.4 m/s
Wind Potential (reference)	3,894 h/yr
Distance to Port	12.7 km
Distance to Shore	12 km
Water Depth	100 m
Latitude	41.9°
Longitude	-9.1°



Figure 3.8: Site-selected location Viana do Castelo for case study.
Source: [147].

3.2. Implementation scenarios

To perform and assess the techno-economical evaluation case in the site-selected location of Viana do Castelo near the coasts of Portugal, it is essential to explore different implementation scenarios that can represent the different connection schemes possible. The three scenarios that will be considered are Centralized Onshore, Centralized Offshore, and Decentralized Offshore, with each one representing different transmission chains for hydrogen production and unique economical, technical, operational, and logistical challenges. The objective of analyzing these scenarios is to assess the respective impacts on system efficiencies, the constraints and

opportunities that influence performance, the overall techno-economic performance and reliability of offshore hydrogen production systems.

All three site-specific scenarios are planned for a coupling that integrates a 510 MW floating offshore wind farm using 34 x 15 MW wind turbines off Viana do Castelo to electrolyzers. For electrolyser technology, AWE currently is developing modules with high MW production and with pressurized output of hydrogen comparable to PEM but has the trade-off of having lower current densities, large physical footprint, limited dynamic operation and needing to use a highly corrosive KOH electrolyte. AEM is a promising technology looking to combine advantages of both AWE and PEM by being compact and pressurized output but has the trade-off of limited durability, low technological maturity, and chemical and mechanical stability issues. SOEC operates at high temperatures to allow very high efficiencies with the possibility of integrating with residual heat of other processes and working in reverse as fuel cell but has the trade-off of material degradation due to thermal cycling, slower startup times, and high temperatures needed for operation. Taking these into account, all scenarios will use PEM electrolyzers since they are the leading technology in offshore readiness due to their compact BoP and footprint, fast dynamic response against variability in the energy, their low minimum load of 5-10% and its built pressurization, with their major drawback being its use of PGM-based metals, fluorinated polymers, and water quality for electrolysis.

In the case of hydrogen transport, subsea hydrogen pipelines will deliver continuous export of compressed hydrogen to shore due to being preferable to tankers or FPSOs for distances below ~1000 km. Considering that the water depth in the specified site is equal to 100 meter depth, floating foundations are the most suitable platforms to be used for both wind turbines and offshore platforms for substation and electrolysis plant. Semi-submersible platforms will be considered due to their proven technological maturity for deep waters, self-stability through ballast, large deck space for heavy BoP and being cost-effective below 150 meters depth, having minimal tilt under waves to protect PEM electrolyzers durability and being able to survive mooring cable failures, even though the large footprint of the structure means higher wave loading and lateral excursions which affect cables and wind farm spacing design.

For the Centralized Onshore scenario, the generated power from the wind turbines is gathered by dynamic medium-voltage inter-array cables by using a string-based layout and connected into an HVAC offshore substation. From there, power travels through static submarine HVAC export lines to an onshore power substation. In here, the voltage is converted and adjusted for the electrolyser production plant which are distributed by using multiple 100 MW PEM modules alongside their cooling systems, water-treatment and buffer tanks for

intermediate storage. Having electrolysis onshore limits, the offshore footprint and reduces structural and maintenance complexity at sea. The trade-off with this involves the cost-effectiveness of long-distance subsea cabling and associated transmission losses, needing robust coastal grid connections.

For the Centralized Offshore scenario, it also uses dynamic medium-voltage inter-array cabling in a string-based layout as with the Onshore scenario and connected to an electrolysis plant offshore through a power converter. This creates a floating hydrogen production facility, which is fed desalinated seawater and exports the produced H_2 by submarine rigid pipelines installed at the seabed. This layout eliminates the long-distance losses of HVAC and HVDC export cables and the associated transmission losses, making it a cost-effective option for high-capacity production and long-range transport. The offshore electrolysis plant must accommodate multiple 100 MW electrolysis modules, desalinators, cooling systems, hydrogen buffer tanks and backup power while still maintaining constraints with space and weight limits. The centralization of electrolysis generates a production risk since some plant failures may halt hydrogen production, which demand on-site personnel and to manage the centralized brine discharge from the desalination. Although logistics are simpler compared to a decentralized scheme and pipeline export avoids losses, it needs a substantial investment for the large floating platform and has complex O&M due to wave motion, which makes it best suitable for deep-water sites or locations where onshore electrolysis is not possible.

For the Decentralized Offshore scenario, every one of the 34 turbines is integrated into its own compact hydrogen production, consisting of a 15 MW PEM electrolyser, desalinators, cooling system, hydrogen buffer tank, battery backup and power converter. This whole system is mounted directly in each of the semi-submersible foundations having all power generated from the wind turbine straight into the electrolyser, avoiding any extra conversion or transmission losses from both inter-array and export cables. Pressurized H_2 is transported using a radial-based layout by stages, connecting a maximum of five turbines with flexible pipes into a subsea manifold, and subsequently connecting these manifolds until a single static export pipeline to shore using rigid pipes in the seabed. This modular layout delivers redundancy in the system, as any unit can fail without halting the complete production of the wind farm. It also eliminates the need for a central platform, enabling phased deployment and easy scale up of the project and spreading out the brine discharge related to the desalinated seawater fed into the electrolyzers. The trade-off lies in having 34 different BoPs for the electrolysis system that must be installed in the same platform as the wind turbine, which raises installation footprint, and adds complexity to the O&M across the turbine array.

Each of these scenarios diverge mostly in where hydrogen is being produced and how it gets transported to shore. In the Centralized Onshore scenario, the electrolyser plant is on land with power being carried to shore via high-voltage cables which simplify the offshore platforms but has high subsea cable investment and transmission losses. The Centralized Offshore scenario collects all power and places the electrolysis plant on a centralized floating platform and exports H₂ through subsea pipeline, eliminating transmission losses but demanding expensive offshore construction and concentrated O&M risks. The Decentralized Offshore scenario installs compact PEM electrolyzers in each turbine and routes pressurized hydrogen through a network of flexible and rigid pipelines to shore, adding system redundancy, dispersing brine discharge, and removing transmission losses but needing multiple equipment, space and weight on turbine platform, and added maintenance complexity. Each approach trades off infrastructure complexity, CAPEX and OPEX, scalability and environmental footprint in different ways. In Chapter 4, these scenarios will be fed into a techno-economic model to identify the most suitable configuration for this site-specific location for green hydrogen production.

3.3. Impact and specific requirements of electrolyzers in offshore environments

Considering the scenarios discussed previously, integrating the PEM electrolyzers into floating foundations can present certain challenges that may impact the system design and operation in marine environments and add certain specific technical requirements for safe, durable and efficient operation. Firstly, the dynamic motions and maximum tilt of the semi-submersible foundation for both Centralized and Decentralized Offshore scenarios impose tilt limits, response-amplification and structural loads that must not compromise the stack integrity. Second, the inherently intermittent and variable behavior of the energy supplied by wind turbines due to rapid ramp rates, partial load operation and frequent start-stop cycles impacts into the efficiency and durability of the electrolyzers, needing robust dynamic models, buffering strategies and minimum load constraints. Thirdly, saline conditions that exist in the marine environment offshore expose the electrolysis systems and equipment to high corrosion and salt deposition, requiring protection against salt spray, corrosion-resistant materials and protective coatings. Lastly, the water quality to be fed into the electrolyser must be high purity with a very low conductivity due to the membrane's sensitivity to ionic and organic contaminants, achieved through advanced pretreatment, recycling and monitoring systems.

3.3.1. Dynamics and maximum tilt of platform

The stability of the floating platforms used for electrolyzers in the offshore scenarios are a key challenge in the system design and performance. The dynamic behavior of these platforms can affect the efficiency and durability of the electrolyser stacks and equipment offshore due to waves and wind loading that the platform is subjected to. Special care needs to be taken into consideration during design for stability criteria in certain azimuth directions to ensure safe and efficient deployment in marine conditions. Certain studies have discovered that floating platforms with hydrogen systems present larger pitch movements compared to wind turbines under certain load cases like DLC 1.6 with max aerodynamic thrust and severe wave conditions and DLC 6.1 with a 50-year storm. These pitch differences can be up to 40% in extreme conditions, which can impact negatively the lifetime and efficiency of the electrolyser. However, natural periods are slightly longer by 1.5 seconds in roll, pitch, and yaw, which may reduce resonance effects from wave dynamics and with RAOs for pitch and longitudinal acceleration shifting toward higher wave periods and a reduction in amplitude, making it more stable under dynamic response in certain sea states [148].

PEM electrolyzers are normally considered as the most suitable for offshore hydrogen production, but it must also be considered that they are sensitive to mechanical stress. This makes it important to have stable mounting and to add protection from the dynamic loads to avoid any performance degradation. A way to do this is by using structural strategies such as mooring systems and counterweights to diminish the effects of the waves and wind dynamic loads and the response on the platform to ensure the durability and efficiency of the PEM systems and equipment in offshore environments [149]. The marine environment presents challenges due to its hostile nature due to its constant multi-directional movement and high corrosion levels, imposing extra stress on electrolyser components. While some studies acknowledge the influence of these dynamic loads, they often do not experimentally assess the direct impact on the electrolyser performance, highlighting a gap in the current research [150], [151].

Some real-world measurements have been taken from floating platforms used in-situ direct seawater electrolysis in Xinghua Bay using finite element motion simulation under a force 8 wind and 1 m significant wave height to provide insight into the motion tolerances of the electrolyser. These motions measured for the floating platform stabilized by mooring ropes were observed to be between 5.5 to 7.9 m in surge, -0.55 to 0.56 m in sway, and 0.54-0.9 m in heave and rotating from -2.5° to 2.0° in roll, -8.5° to 7.2° in pitch, and -12.4° to 10.2° in yaw.

These values were within a controllable range and can be referenced for an acceptable motion limit in offshore electrolyser applications [149].

Additionally, experimental testing has been performed in Navantia to simulate the conditions for a PEM electrolyser under offshore static and dynamic conditions to verify the operational performance and motion limitations using a hexapod platform. A total of 10 tests aim to simulate any possible mechanical failures, reduced efficiencies, or safety concerns from hydrogen and oxygen crossover in the stack due to the conditions in marine environments. Initially, a baseline test was performed in static condition to establish reference performance under nominal conditions. Subsequently, the PEM electrolyser was subjected to static tests with defined tilt impact tests with configurations along X and Y axes to evaluate the sensitivity to inclination without any dynamic acceleration. The following tests performed were dynamic sinusoidal acceleration tests along the X, Y, and Z axes defining a maximum linear acceleration in the horizontal vertical axes. Finally, two dynamic motion profiles were executed based on a realistic marine scenario and a severe synthetic profile to assess system limits. These tests provided valuable insights into the behavior of electrolysers under realistic motion conditions, contributing to the definition of acceptable operational envelopes for future developments.

This experimental campaign concluded that the PEM electrolyser maintained correct operational behavior across all static, dynamic and simulated profiles. However, several interruptions were recorded due to communication failures rather than system malfunctions. The cause of this was due to mounting deficiencies in the inadequate securing of the BoP components like pumps, sensors, and separators that were originally designed for stationary environments, which were mitigated once the most vulnerable components were reinforced. The system also demonstrates a non-linear behavior that improved energy efficiency at higher current densities with the peak being at a partial load around 80%, indicating favorable performance under increased load. Lastly, enhanced measurements techniques are advised to better understand separator behavior and its impact on overall system performance, especially regarding the severe synthetic profile that deals with the extremes of the electrolyser.

Considering the limits tested experimentally with the hexapod, the first iteration of an offshore platform for a centralized electrolysis plant will be simulated to determine a first approximation on the impact on offshore dynamic and tilt conditions. For this first iteration, the equipment list for a 500 MW centralized electrolysis platform was defined according to the methodology described by Ekhar [152], by scaling down to 500 MW and considering 100 MW PEM modules instead of 20 MW with characteristics estimated from the compiled electrolysers

commercial database, as well as considering high-power transformers, diesel generators, PSA units, and other BoP components as shown in Table 3.10.

Table 3.10: Equipment weight and quantity assumptions for a 500 MW centralized electrolysis plant. Sources: [152] and own assumptions.

Equipment	Capacity	Number [#]	Total Weight [tons]
100 MW Module	20,000 Nm ³ /h	5	4,000
High power transformer	125 MVA (33/1 kV)	4	542
High power transformer	250 MVA (66/33 kV)	2	456
Diesel Generator	5 MW	10	300
PSA Units (dryers)	15,500 Nm ³ /h	7	114
Battery backup	2.5 MWh	5	98
LennRO - seawater	100 m ³ /h	2	68
LennRO - brackish	70 m ³ /h	2	48
HV switchgear bays - block 1	66kV	12	54
Grounding transformer	3.75 MVA (33KV)	4	39
Grounding transformer	7.5 MVA (66KV)	2	33
MV switchgear bays - block 2	33 kV	10	14
Seawater pump	850 m ³ /h	1	1
Re-circulation pump	300 m ³ /h	1	1
PHE	270 m ³ /h	1	1

Using the total equipment weight that was estimated to be 5,768 tons, design estimations were done according to the semi-submersible platform design described [152] according to Equations (3.17) to (3.19), resulting in a total of 13,355 tons for the topside mass considering the supporting steelwork and the assumed auxiliary, cladding and grating mass. With this new weight, it is possible to estimate the hull mass at 11,625 tons and estimating the operational ballast water total weight at 13,092 tons placed at the bottom of the platform to lower the center of gravity (CoG) for a grand total estimated mass of 38,072 tons as shown in Table 3.11.

$$\text{Supporting steelwork mass} = 1.035 \times \text{Equipment mass [tons]} \quad (3.17)$$

$$\text{Auxiliary, cladding and grating mass} = 0.17 \times \text{Equipment mass [tons]} \quad (3.18)$$

$$\text{Hull mass} = 0.5276 \times \text{Topside mass} + 4578.38 \text{ [tons]} \quad (3.19)$$

Table 3.11: Estimated total weights for a 500 MW centralized electrolysis plant mounted on a semi-submersible platform.

Section	Weight [tons]
Total Equipment Mass	5,768
Assumed Auxiliary Equipment	288
Supporting Steelwork Mass	6,269
Auxiliary, cladding and grating mass	1,030
Total topside mass	13,355
Hull mass	11,625
Operational Ballast Water	13,092
Total Mass	38,072

To define the semi-submersible platform's geometry, the design from the ECOFOSS semi-submersible project led by Navantia Seanergies was used as a reference [153], with the platform formed by two pontoons that contain mainly the ballast water tanks, four vertical columns that connect the pontoons with the first deck, and two braces that join and support the pontoons and columns. The topside consists of a multi deck design with a total of 4 principal decks consisting of the Cable deck which deals with the reception of the inter-array cables through J-tubes and auxiliary machines and export equipment for the hydrogen pipeline. The second deck consists of the Main deck, which contains the electrical equipment rooms with all the necessary power electronics that are needed to receive and transform the voltage and distribute it along the electrolyser modules. The third and fourth decks deal with the electrolysis plant that consists of 3x100 MW PEM modules and 2x100 PEM modules respectively, which are placed at the top due to safety reasons and explosive atmosphere risks. With proposed geometry and estimated total weights, it is possible to design and establish key dimensions for the semi-submersible platform as shown in Table 3.12.

Table 3.12: Semi-submersible Design Parameters for a 500 MW Centralized Electrolysis Plant. Source: [153] and own assumptions.

Design Parameter	Dimension [m]
Length Overall	85
Breadth (Maximum)	62.5
Breadth (Pontoons)	18
Depth (Pontoons)	10
Draught (Operational)	17.5
Deck #1 Height (Cable Deck)	23
Deck #2 Height (Main Deck)	28
Deck #3 Height (PEM Deck #1)	38
Deck #4 Height (PEM Deck #2)	45.5

Having defined the main dimensions and geometry of the platform, the hull mesh up to the waterline at 17.5 m was modeled as seen in Figure 3.9, containing the node and panel definitions that serve as the input mesh model for hydrodynamics to be analyzed with the use of the Hydrostar software. Additionally, the wave forcing conditions were specified by generating the wave frequencies to be studied, ranging from 0.05 to 1.99 rad/s in steps of 0.02 rad/s, the headings from the waves, ranging from 0 to 180° in steps of 22.5°, and assuming a uniform water depth same as the case study selected of 100 meters. The four-deck 2D layout assumption was drafted and positioned the equipment list and PEM modules atop the topside structure for both safety and service access, which greatly influence the platform's linear acceleration response and tilt as shown in Appendix 8.4. With this, it is possible to compare the limits tested during the PEM electrolyzers hexapod tests according to the maximum tilt and linear acceleration in the principal axes and determine an initial insight in the response for the electrolyzers placed at a semi-submersible platform.

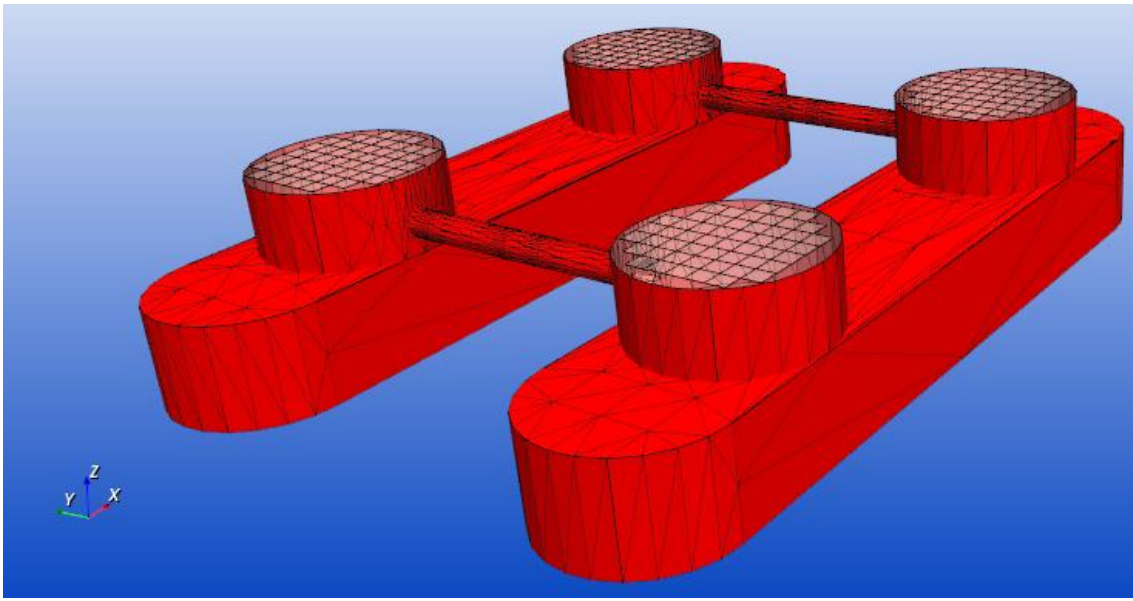


Figure 3.9: Semi-submersible Hull Mesh for Centralized Electrolysis Platform at Waterline.

To calculate the mass and inertia properties needed for the hydrodynamic analysis, the individual weights for the specified equipment and its placement in the 2D layout as well as the platform and topside weight were considered to calculate the CoG of the whole semi-submersible electrolysis plant. Additionally, the inertia of the whole platform was calculated by calculating the local inertia I_{local} (tons·m²) of each of the items in the equipment list by assuming a geometry of a solid rectangular cuboid of width, length and height as the one stated in the 2D layout in Equation (3.20) and using the parallel axis (Steiner) theorem to relate the moment of inertia of each axis to the CoG of the whole platform, as

shown in Equation (3.21) for the inertias in the diagonal of the matrix $I_{global,diag}$ (tons·m²) and Equation (3.22) for the products of inertia off the diagonal $I_{global,prod}$ (tons·m²). Finally, the global radii of gyration of the platform R_{global} (m) can be calculated using Equation (3.23).

$$I_{local} = \begin{bmatrix} \frac{1}{12}m(y^2 + z^2) & 0 & 0 \\ 0 & \frac{1}{12}m(x^2 + z^2) & 0 \\ 0 & 0 & \frac{1}{12}m(x^2 + y^2) \end{bmatrix} [tons \cdot m^2] \quad (3.20)$$

$$I_{global,diag} = \begin{cases} I_{xx} = \sum I_{xx,i} + m_i(y_i^2 + z_i^2) \\ I_{yy} = \sum I_{yy,i} + m_i(x_i^2 + z_i^2) \\ I_{zz} = \sum I_{zz,i} + m_i(x_i^2 + y_i^2) \end{cases} [tons \cdot m^2] \quad (3.21)$$

$$I_{global,prod} = \begin{cases} I_{xy} = \sum -m_i x_i y_i \\ I_{xz} = \sum -m_i x_i z_i \\ I_{yz} = \sum -m_i y_i z_i \end{cases} [tons \cdot m^2] \quad (3.22)$$

$$R_{global} = \sqrt{\frac{I}{M}} [m] \quad (3.23)$$

Once obtained the total mass and inertia properties, it is possible to consolidate and input the total mass of 38.1 Mkg and the CoG which resulted in a height of 17.192 meters above from the bottom of the platform and 0.308 meters below the waterline. Additionally, a linear viscous damping of 3% was also assumed to generate a more realistic motion response as shown in the input parameters from Table 3.13. Finally, a static stability check was performed as shown in Table 3.14 and returned a positive metacentric height in both longitudinal with $GM_l = 1.817 \text{ m}$ and in transversal with $GM_t = 3.672 \text{ m}$, which reflects a good initial stability of the semi-submersible platform and may help the PEM modules remain within the safe operating angles.

Table 3.13: Semi-submersible Mass and Inertia Properties.

Properties	Resulting Values
Total Mass [kg]	3.81E+07
CoG in X axis from Bottom [m]	0
CoG in Y axis from Bottom [m]	0
CoG in Z axis from Bottom [m]	17.192
CoG in Z axis from WL [m]	-0.308
Radii of Gyration in XX [m]	28.216
Radii of Gyration in YY [m]	26.329
Radii of Gyration in ZZ [m]	28.822
Radii of Gyration in XY [m]	0.016
Radii of Gyration in XZ [m]	0.007
Radii of Gyration in YZ [m]	0.027
Linear Viscous Damping [%]	3

Table 3.14: Semi-submersible Parameters for Static Stability Check.

Parameter	Dimension [m]
KB	6.85
BM _l	12.159
BM _t	14.014
KG	17.192
GM _l	1.817
GM _t	3.672

The last input for Hydrostar corresponds to the selection of the computation of the Response Amplitude Operators (RAOs), which were defined at the platform's CoG for both motion and acceleration at all six degrees of freedom (DoF) as shown in Appendix 8.5. Additionally, a JONSWAP spectrum was generated by taking ten years of historical buoy data of waves at Costera de Silleiro [154] near the selected location with a significant wave height $H_s = 6.56 \text{ m}$, a peak period $T_p = 13.83 \text{ s}$, a wave heading of 292.5° , and a peak enhancement factor $\gamma = 3.3$ as shown in Table 3.15.

Table 3.15: Historical waves of buoy at Costera de Silleiro from 1996-2006.

Wave Parameters	Values
Longitude [°]	-8.93
Latitude [°]	42.1
Water Depth [m]	70
Number of Waves	133
1/3 Highest Waves	45
Significant Wave Height H_s [m]	6.56
Peak Period T_p [s]	13.83
Wave Heading [°]	292.5

Having calculated both the RAOs corresponding to the wave heading of 292.5° in motion and acceleration and generated the JONSWAP wave spectrum, it is now possible to calculate the response of the platform and translate it into the maximum linear acceleration and tilt that the PEM modules at the different locations of the platform will experience. For the maximum tilt, the RAO of the motion for Roll and Pitch of the platform are used directly into the calculation of the response, while for the maximum linear acceleration for the 3 axes, a RAOs must be computed by combining the magnitudes for the translational and rotational effects from different DoF by using Equation (3.24) for X-axis, Equation (3.25) for Y-axis, and Equation (3.26) for Z-axis towards the local CoG of the 5x100 MW PEM modules shown in Table 3.16.

$$RAO_{axi} = RAO_{asurge} + (RAO_{apitch} \cdot \bar{z}) \left[\frac{m}{s^2} / m \right] \quad (3.24)$$

$$RAO_{ayi} = RAO_{asway} + (RAO_{aroll} \cdot \bar{z}) \left[\frac{m}{s^2} / m \right] \quad (3.25)$$

$$RAO_{azi} = RAO_{aheave} + (RAO_{apitch} \cdot \bar{x} + RAO_{aroll} \cdot \bar{y}) \left[\frac{m}{s^2} / m \right] \quad (3.26)$$

Table 3.16: PEM Modules Relative distance to CoG of platform.

EQUIPMENT	X REL	Y REL	Z REL
PEM MODULE #1 (D3)	0	17,25	22,808
PEM MODULE #2 (D3)	0	-17,25	22,808
PEM MODULE #3 (D4)	0	20,5	30,308
PEM MODULE #4 (D4)	0	0	30,308
PEM MODULE #5 (D4)	0	-20,5	30,308

Once having defined the RAOs for the different cases of the different locations of PEM modules, the response can be calculated with the JONSWAP spectrum obtained previously according to Equation (3.27) for a typical sea state for the considered significant wave height, peak period and heading. With these responses, the 3σ peak response method was used to estimate a moderate peak value for each of the cases and be able to compare the responses of the PEM modules against the experimental tests by calculating the variance of the response spectrum with Equation (3.28), the standard deviation of the response with Equation (3.29), and the peak response value of the response with Equation (3.30) and shown the results of each of these cases in Table 3.17.

$$S(\omega) = RAO^2 \cdot S_{JONSWAP} \quad (3.27)$$

$$VAR = \int_{\omega_{min}}^{\omega_{max}} S(\omega) d\omega \quad (3.28)$$

$$\sigma = \sqrt{VAR} \quad (3.29)$$

$$Peak = 3\sigma \quad (3.30)$$

Table 3.17: Peak Response Check for Maximum Tilt and Linear Accelerations in PEM Modules.

Section	DoF Parameter	Peak Response	Limit Check
Platform Maximum Tilt [°]	Roll	2,478	Pass
	Pitch	1,048	Pass
Linear Horizontal Accelerations PEM Modules [m/s ²]	A _x D3	0,412	Pass
	A _y D3	0,876	Pass
	A _x D4	0,460	Pass
	A _y D4	0,985	Pass
Linear Vertical Accelerations PEM Modules [m/s ²]	A _z PEM #1	0,772	Exceed*
	A _z PEM #2	0,415	Pass
	A _z PEM #3	0,816	Exceed*
	A _z PEM #4	0,556	Pass
	A _z PEM #5	0,403	Pass

*Exceeded values from experimental limits were compared against confidential experimental limit states and were considered within an acceptable range

The computed peak response values for the maximum tilt, as well as the linear accelerations in the horizontal and vertical axes were compared against the experimental limit states tested in the hexapod. The exact values for the experimental limit states for the testing are confidential and only providing if it is below or above those limits. The only responses that exceeded the experimental testing correspond to the linear vertical acceleration for the PEM modules #1 and #3, which are positioned in both decks and are placed at the port side, due to the added acceleration of the rolling of the platform into the heave acceleration. These exceeded values only mean that they are above the values proven by experimental tests which do not affect the operational behavior of the PEM electrolyser or significantly impact the operational performance and not corresponding to the safety or critical values of the electrolyser. The obtained responses were considered as acceptable, since this behavior may also be mitigated in the hydrodynamic simulation with the addition of a higher linear viscous damping that can better represent the real conditions, since the considered 3% may not be a realistic value, as well as adding the mooring system into the calculation, since it may significantly lower the platform's response and diminish the heave, roll, and pitch response to lower the vertical accelerations. In the case of exceedance while in operation, mitigation control strategies may

be implemented by partial operation or deactivating certain parts of the module to not compromise the stacks functioning. Additionally, as this is a first design, a detailed layout with a rearrangement of the CoG of the platform and the position of the PEM modules may be performed to modify the effects of the obtained motions in roll and heave to reduce the peak response acting on the electrolyser stacks.

3.3.2. Intermittency and variability of energy

The variable nature of offshore wind resources due to fluctuating wind speeds, changing sea states and seasonal weather patterns create a highly intermittent power supply that can create some challenges when paired directly with electrolyzers. Unlike systems plugged into stable grids, offshore electrolyzers must deal with rapid swings in input power, higher number of start-stop cycles and dynamically adjust hydrogen production rates to match with the available energy without compromising the efficiency or durability of the electrolyser stack. In centralized configurations, the challenges are concentrated into a few large-scale units which demand power management strategies and buffering solutions to smooth out peaks and troughs. On the other hand, decentralized configurations offer greater flexibility but increase complexity in this coordination and control due to integrating a smaller electrolyser into each of the wind turbines. It is important to understand how this intermittency and variability can translate into necessary specific technical requirements. Some techniques used to control this are ramp-rate limits, energy storage integration and advanced power electronics, which ensure a reliable, safe and cost-effective operation for green hydrogen production.

Full system dynamic models are essential when coupling PEM electrolyzers directly with the variable energy output from wind turbines to capture transient behavior. Some of the behaviors that static models often overlook are hydrogen crossover risks at low current densities and efficiency losses during rapid power swings. Integrating the cell-level performance with other systems like heat management and controls ensures having a safer and more efficient operation when dealing with fluctuating inputs. These dynamic simulations also help predict impacts due to start-stop cycles and mitigate any safety hazards that may arise when dealing with irregular power supply. These modeling frameworks are crucial for the design of electrolysis systems in offshore conditions to maintain their performance and durability throughout the project's lifetime [27], [155].

The attractiveness of PEM electrolyzers and their suitability to offshore hydrogen production comes from their operative flexibility, operating down to 5-10% of the nominal capacity and being able to handle extreme power ramps of 80% to 100% within one second.

This partial load capability permits continued hydrogen production even during low wind periods and rapid ramp responses enable the system to track the wind turbine's output closely. However, one thing to take into consideration is that these transient operations can generate lower efficiencies and may accelerate the stack degradation if not managed correctly. This makes ramp-rate control strategies a key part of operation to balance the responses to ensure the durability and efficiency of the system [24], [156].

Recent research on PEM electrolyzers under fluctuating wind conditions study the need for tailored degradation testing and operational strategies for offshore environments. A study performed by analyzing wind farm data in Northwest China developed a degradation test spectrum that can mirror real life conditions in power variability revealed that rapid load changes of up to 9.6% per minute and frequent start-stop cycles significantly reduce the stack's lifetime. It also highlights that having long periods of low load operation in between 5% to 30% of the rated power and the start-stop cycles accelerate membrane and catalyst degradation through mechanisms like increase hydrogen peroxide formation and ionic polymer loss. Moreover, the study's dynamic modeling approach may offer a robust framework to simulate offshore wind intermittency by dividing into five typical operation scenarios of low load, normal operation, overload, start-stop, and variable load. This model enables the capture of the effects of fluctuating input power and permits the design of control systems and buffering strategies that can mitigate degradation of the stacks while still maintaining high efficiency operation [157].

Intermittent operation also presents safety constraints that require minimum loads from the electrolyser. Studies on water recovery tanks have identified a power threshold of 10% to 15% of the nominal capacity to avoid accumulation of hydrogen in the explosive range due to crossover at part load conditions. Additionally, the 5% load is similarly required to ensure that the stack temperature and pressure control are within safe limits during variable power input [148], [158]. Integrating buffering and storage strategies are indispensable to smooth out power fluctuations and maintain a continuous hydrogen output. An option for this is using battery-assisted systems that can absorb any short-term variabilities to reduce the stress on the electrolyser and improve efficiency. Another option would be to pair uninterruptible power supplies with energy storage that can stabilize the system and ensure hydrogen production is stable despite the wind variability [149], [156].

Variable wind power profiles that reach fluctuation rates of 100%/s impact the electrical current, thermal and pressure dynamics, gas purity, and output consistency of the electrolyser. Empirical tests were conducted on a 60 kW PEM system under variable loads to demonstrate

stable pressure and temperature control that present efficiency losses below 0.6 A/cm^2 , which highlight the need for an optimized PSA regeneration at low loads. Comprehensive reviews link designing thermally robust stacks, deploying advanced control systems, and incorporating buffer storage are vital to sustain high efficiencies throughout the life of the PEM electrolyser and prolonging component life in offshore deployments [159], [160], [161], [162], [163].

3.3.3. Marine environment

Marine environments expose PEM electrolysers to harsh conditions of corrosion and material degradation due to humidity and salt spray, which can cause an accelerated degradation of components and systems. These environmental conditions can cause a punctured membrane, which can result in dangerous explosive concentrations of hydrogen within the stack. Because of this, protective measures must be considered to mitigate these risks by using anticorrosion coatings, zinc cathodic protection, and dehumidification modules [149], [156]. That is why design adaptations are necessary to be considered, for example platforms often include seawater lift systems to supply water for both treatment and cooling. Additionally, electrolysis units are commonly placed on top of structural columns of the platform to isolate potential explosive zones and protect against wave impacts and slamming [148].

Experimental testing under simulated marine conditions have shown promising results for PEM electrolyser components. These components were tested in a Dry Corrosion Test Cabinet that simulated the conditions of humidity and salinity in offshore conditions. The results of the material testing indicated no significant structural degradation or contamination from sodium or chlorine, which suggested that with proper treatment and material selection PEM electrolysers may be able to withstand marine exposure [150].

3.3.4. Water quality

The water quality and purity of the feedwater is another challenge present in PEM electrolysers in both onshore and offshore conditions. They require deionized water that presents a conductivity below $1 \mu\text{S/cm}$ and organic contaminants with levels under 0.05 mg/L [162]. To meet these strict requirements using seawater, offshore systems must use advanced treatment technologies to remove any contaminants to avoid membrane degradation. A suitable option would be to use reverse osmosis, since it has a relatively low impact on the overall cost of hydrogen production and has shown significant results in removing the impurities and contaminants while reducing the conductivity to acceptable levels. Some desalination systems have a process which consists in first pre-treatment to remove dissolved solid content to prevent

scaling as accumulation of insoluble salts in the RO membrane and having additional desalination steps like a reverse osmosis with low brackish water to further lower the total dissolved solids and a post-treatment to de-ionize using an ion-exchange and ensure the water quality reaches an acceptable conductivity below 1 $\mu\text{S}/\text{cm}$. [27], [152], [155], [164].

Water recovery and recycling are also critical in offshore systems due to not having easy access to freshwater. Deionized water that exits with the hydrogen output must be captured and reused, while anodic water must be purified before reintroducing in the system to avoid any parasitic current and ensure safety of the stack. This makes real-time monitoring of conductivity essential to maintain the water quality inside acceptable ranges [158].

3.3.5. Summary of requirements

The integration of PEM electrolyzers into offshore conditions generates significant impacts and requirements to be considered and solved. When subjected to the motion generated by the waves and wind impacting the offshore platform can affect the structural integrity and performance of the electrolyser stacks. Experimental testing using a hexapod platform confirmed some operational limits in PEM systems to operate under various static and dynamic conditions without impacting the performance or generating any safety risks due to hydrogen to oxygen crossover, by using improved mounting strategies to ensure a correct operation and mitigate effects to the sensing and measuring of the BoP due to the motions of the platform.

The hydrodynamic modeling of a 500 MW centralized electrolysis platform revealed that the position of the PEM electrolyzers modules in the top part of the platform generated acceptable dynamic responses in most of the cases analyzed. The calculated motion and acceleration responses showed that the PEM modules remained inside the tested limits of the experimental results, although some exceeded thresholds in vertical accelerations. These results were determined that were not critical to the performance and could be further reduced by refining damping assumption and including mooring effects in future simulations to ensure a more realistic scenario and ensure operational performance and long-term durability.

The intermittent and variable nature of the offshore wind power resource also introduces operational challenges for the electrolyzers when considering the rapid ramp rates that change with the variability of the wind speed, the frequent stop-cycles when the wind speed is near the cut-in speed of the wind turbine and the minimal load of the electrolyser, as well as the fluctuating load conditions presented. These dynamic loads need a robust control strategy, buffering systems, and dynamic modeling to ensure safe and efficient hydrogen production. Centralized configurations require a coordinated power management system according to the

available power, while decentralized systems offer more flexibility but increase complexity due to only being connected into one wind turbine. PEM electrolyzers are well-suited to these conditions due to their fast response and partial load capabilities but must have dynamic control to prevent any efficiency losses or accelerated degradation due to intermittency and variability.

Marine environmental conditions such as salt spray and humidity can pose corrosion risks and degradation to both electrolyser components and other BoP components, which require to assess protective coatings, cathodic protection, enclosed locations, and elevated placement of equipment. Additionally, PEM electrolyzers demand ultra-pure water with very low conductivity, which require having to use advanced desalination techniques, de-ionization, and water recycling systems of seawater to be able to ensure membrane integrity and safe operation in offshore environments.

4. TECHNO-ECONOMIC EVALUATION FOR INTEGRATION OF HYDROGEN PRODUCTION WITH FLOATING OFFSHORE WIND

The aim of this chapter is to present a comprehensive techno-economic evaluation by integrating green hydrogen production with floating offshore wind systems. It is built up from the strategic site selection outlined previously in Viana do Castelo and uses key parameters corresponding to the specific location for its wind resource potential, proximity to both port infrastructure and shore, and water depth. It compares the 3 implementation scenarios established previously for the Centralized Onshore, Centralized Offshore and Decentralized Offshore scenarios. Section 4.1 introduces the methodology used to develop both technical and economic models derived from literature. Section 4.2 presents the detailed case analysis and results of the proposed offshore hydrogen production configurations from the established case study. Lastly, Section 4.3 presents a sensitivity analysis that explores the influence of key location parameters in the system performance and cost-effectiveness to identify the behavior for each of the configurations for green hydrogen in floating offshore environments. This evaluation aims to provide an approach to critical insights into the operational, financial, and logistical trade-offs of centralized and decentralized offshore electrolysis systems to contribute to the broader goal of decarbonizing the marine industry through renewable energy integration.

4.1. Methodology for Techno-Economic Model

The methodology used to design the techno economic model to evaluate the different scenarios considered for integration of green hydrogen production with floating offshore wind systems is an adaptation of the framework presented by Rogeau et al. [12]. The general methodology, key parameters, equations and assumptions from the original model are preserved where applicable, while in others they are modified to better reflect the key site-specific characteristics of the selected site at Viana do Castelo and to reference the unique configurations of the three implementation scenarios chosen. The main objective of the model focuses on the calculation of the Levelized Cost of Hydrogen (LCOH) as the primary economic indicator that incorporates certain project specific parameters such as the lifetime, rate of return and the total lifetime costs along the years. Additionally, location dependent parameters such as water depth, wind potential, distance to shore and distance to port consist of the key parameters that influence the behavior of the model and reflect the influence in both technical feasibility and economic performance.

The LCOH (€/kg) is a metric that is normally used to evaluate and compare the profitability of hydrogen production projects and represents the average cost along the lifespan of the project to produce one kilogram of hydrogen. This considers all lifetime expenditures along the project's life and compares it along the years with energy production, as shown below in Equation (4.1).

$$LCOH = \frac{\sum_{t=0}^L \frac{CAPEX_t + OPEX_t + DECEX_t}{(1+r)^t}}{\sum_{t=0}^L \frac{E_t}{(1+r)^t}} \quad [€/kg] \quad (4.1)$$

The numerator of Equation (4.1) consists of the total lifetime costs of the project over the years, divided into different types of costs for the project, with *CAPEX* corresponding to the capital expenditures, *OPEX* corresponding to the operational expenditures, and *DECEX* corresponding to the decommission expenditures (€). The denominator of Equation (4.1) *E* (kgH₂) represents the total amount of hydrogen produced over the years coming from the energy generated using the wind resource. Both components must be discounted over time to reflect the actual value of money according to the Net Present Value (NPV). Discounting to transform into the NPV ensures that any future costs and energy outputs are converted into present-day equivalents and allows a realistic economic comparison across the project's lifetime.

In this model, a rate of return *r* of 6% is applied, representing the minimum acceptable yield to justify the capital investment of the project's lifetime *L* assumed to be 25 years of service, which aligns with the typical duration for offshore wind and hydrogen infrastructure. Additionally, the installed capacity of the wind farms was set according to the defined earlier in the implementation scenarios with an installed capacity of 34 x 15 MW wind turbines for a total of 510 MW and considering a capacity density of 4.54 MW/km² according to observed values for floating offshore wind projects for the site-specific locations in the Atlantic Coast [27].

By discounting both the total costs and the hydrogen output over the lifetime of the project, the LCOH calculation captures the economic efficiency of the system in present-value terms. This approach enables a more accurate assessment of the viability and competitiveness of the project and the different implementation scenarios considered during the long term and ensures that both the investment and production are evaluated within a consistent financial framework.

4.1.1. Economic Model Estimation

The first step in the calculation of the LCOH for each of the implementation scenarios corresponds to the calculation of the total lifetime costs for the project. This will be done by modelling an estimation of *CAPEX*, *OPEX*, and *DECEX* for each of the main equipment necessary for the integration of wind turbines and hydrogen production via electrolysis. The bottom-up breakdown will be done by introducing key adjustments to *CAPEX* in the equipment and installation costs, *OPEX* in the material and logistics costs, and *DECEX* for the decommissioning costs to better reflect the site-specific conditions and some key data.

4.1.1.1. CAPEX

As mentioned earlier, CAPEX corresponds to all the initial investments regarding the project, normally considered as the upfront expenditure coming from the design, construction, and commission of all the elements of the project before starting to produce energy. These expenditures correspond to the equipment and installation cost of the different elements or systems in the project, which will be grouped as wind turbines and their floating foundations, inter-array cables or pipelines, offshore floating foundation platform, conversion systems consisting of the electrolysis plant with their balance of plant, and the export transmission system used accordingly. The CAPEX typically represents the largest financial commitment in the early stages of projects and is often financed through a combination of equity and loans that are repaid over the years and considering investors getting returns on their capital. However, the financing structure for this techno-economic evaluation is not explicitly modeled and *CAPEX* is instead treated as a distributed cost over the project's lifetime to mimic the effect of repaying a loan through annual payments.

The total equipment cost of the wind turbines $CAPEX_{WT_{EQ}}$ (€) can be seen in Equation (4.2), in which it is divided into two elements by considering the turbine equipment and the turbine foundation.

$$CAPEX_{WT_{EQ}} = N_{WT} \cdot P_{WT} \cdot (RC_{TE} + RC_{TF}(WD_{WF}) \cdot (1 + 0.2 \cdot c_D)) \text{ [€]} \quad (4.2)$$

The total aggregate upfront cost of all the wind turbines is computed by multiplying the number of wind turbines N_{WT} by the rated power P_{WT} (kW) and the rated cost of each of the turbine's equipment and floating platform. The rated cost of the wind turbine equipment RC_{TE} covers the baseline cost per kilowatt of the turbine, which will be considered as 1,200 €/kW for

a 15 MW wind turbine, equivalent to the expected cost in 2030. For the rated cost of the turbine foundation $RC_{TF}(WD_{WF})$ (€/kW), it is defined as the cost of a floating platform support for each of the turbines that depends linearly on the water depth WD_{WF} (m) as shown in Equation (4.3) and corresponds to the expected cost coefficients for 2030. Additionally, in the case of a decentralized offshore electrolysis, the foundation of the wind turbines must accommodate the electrolyzers and balance of plant in-turbine, which is represented by an additional cost of 20% of the total cost of the foundation, which is represented by considering $c_D = 1$ when considering a decentralized configuration and $c_D = 0$ when centralized [12].

$$RC_{TF}(h) = 697 \cdot WD_{WF} + 1.223 \cdot 10^6 \text{ [€/kW]} \quad (4.3)$$

For the installation of floating wind turbines, the construction and assembly of the equipment and platform are made onshore at port and then towed to the farm site by using Anchor Handling Tug Supply Vessels (AHTS). This tow-out operation is usually completed by using three AHTSs and subsequently moored using special vessels which are Anchor Handling Vessels (AHVs). This anchoring operation may be done with the same vessels as the tow-out operations, and the main AHV needs the support of two smaller AHVs to support the operations [165]. The installation of the wind turbines follows a simplified model is used to estimate the total installation costs $CAPEX_{WTIC}$ (€) using Equation (4.4), for which the characteristics of the vessels needed and the time and equipment required to install the turbines on-site for the main operations are described in Table 4.1.

$$CAPEX_{WTIC} = \left(\frac{N_{u,WT}}{VC} \cdot \left(\frac{2 \cdot DP_{WF}}{v} + t_{load} \right) + t_{inst} \cdot N_{WT} \right) \cdot \frac{DR}{24} \text{ [€]} \quad (4.4)$$

In this case, the number of times an operation needs to be carried out depends on the number of units N_u and the vessel capacity VC (units/lift), for which the anchoring needs a total of 9 anchors per wind turbine when considering a 3x3 mooring configuration. It also depends on the distance to port DP_{WF} (km), the speed of the vessel v (km/h) and the loading time for each lift t_{load} (h) and the installation time t_{inst} (h) of each wind turbine N_{WT} to determine the amount of time needed to charter the ship for the operations and the day rate DR (€/d) is considered.

Table 4.1: Wind Turbine Installation Parameters.
Sources: [12], [165], [166], [167].

Operation	Tow-out	Anchoring (3x3 mooring configuration)
Vessel	AHTS w/ 2 support vessels	AHV w/ 2 support vessels
Number of units	34	306
Capacity [units/lift]	1	5
Speed [km/h]	6.5	18.5
Loading Time [h]	5	30
Installation Time [h]	0	90
Day rate [k€/d]	169	130

In the case of the centralized configurations, both offshore power substation and offshore electrolysis plant require a central floating platform in which the energy is collected. The equipment cost for this floating platform $CAPEX_{PFEQ}$ (€) is calculated according to Equation (4.5), which depends on the water depth in a linear function and is based on the cost modeling of turbine foundations. The coefficient used to estimate are the rated costs $RC_{PF}(WD_{WF})$ (€/kW) and the unit costs $UC_{PF}(WD_{WF})$ (€) of the foundations as shown in Equation (4.6) and Equation (4.7) respectively. Additionally, the rated costs depend on an equivalent electrical power P_{WF}^* (kW), depending on the type of substation or electrolysis plant, considering the difference in power density of the substations and the electrolysis plants according to Equation (4.8) [12].

$$CAPEX_{PFEQ} = RC_{PF}(WD_{WF}) \cdot P_{WF}^* + UC_{PF}(WD_{WF}) \quad [€] \quad (4.5)$$

$$RC_{PF}(WD_{WF}) = 87 \cdot WD_{WF} + 68 \cdot 10^3 \quad [€/kW] \quad (4.6)$$

$$UC_{PF}(WD_{WF}) = 116 \cdot WD_{WF} + 91 \cdot 10^3 \quad [€] \quad (4.7)$$

$$P_{WF}^* = \begin{cases} P_{WF} & \text{if HVDC substation} \\ 0.5 \cdot P_{WF} & \text{if HVAC substation} \\ 2 \cdot P_{WF} & \text{if electrolysis plant} \end{cases} \quad [kW] \quad (4.8)$$

The installation operations needed for the floating offshore platform $CAPEX_{PFIC}$ (€) are similar to the required for wind turbines, as shown in Equation (4.9). In this case, the tow-out of the offshore platform is performed using a heavy-lift cargo vessel (HLCV) [168] and the anchoring is made for a 4x2 mooring configuration to maintain the semi-submersible platform in position, with the vessel parameters shown in Table 4.2.

$$CAPEX_{PFIC} = \left(\frac{N_{u,PF}}{VC} \cdot \left(\frac{2 \cdot DP_{WF}}{v} + t_{load} \right) + t_{inst} \right) \cdot \frac{DR}{24} \quad [€] \quad (4.9)$$

Table 4.2: Installation parameters for offshore floating platform foundations.
Sources: [12], [165], [166], [168].

Operation	Tow-out	Anchoring (4x2 mooring configuration)
Vessel	HLCV	AHV w/ 2 support vessels
Number of units	1	8
Capacity [units/lift]	1	3
Speed [km/h]	13	18.5
Loading Time [h]	10	30
Installation Time [h]	0	90
Dayrate [k€/d]	300	130

For the Centralized Onshore configuration scenario, the power collected from the wind turbines must be directed into a power substation to transform the medium-voltage of 66 kV for inter-array into a high-voltage export cable to send to shore and arrive at an onshore HVDC substation that transforms the voltage into the required voltage for the electrolysis plant onshore. For this, the equipment cost of the power substation will depend on the capacity of the wind farm P_{WF} (kW) and the type of substation used, either HVAC or HVDC depending on the distance to shore. The equipment cost for substations $CAPEX_{HVAC,SS_{EQ}}$ (€) and $CAPEX_{HVDC,SS_{EQ}}$ (€) substations is shown in Equation (4.10) and Equation (4.11) respectively.

$$CAPEX_{HVAC,SS_{EQ}} = 22.87 \cdot P_{WF} + 7.06 \cdot 10^6 \quad [€] \quad (4.10)$$

$$CAPEX_{HVDC,SS_{EQ}} = 102.93 \cdot P_{WF} + 31.75 \cdot 10^6 \quad [€] \quad (4.11)$$

For the electrolysis plant, PEM electrolyzers were chosen, as discussed earlier, due to their pressurized production capability, its compact size, and its performance with variability and intermittent energy and offshore conditions. The equipment cost for electrolyzers $CAPEX_{EL_{EQ}}$ (€) is calculated according to Equation (4.12), which depends on the scaling effect and learning rate as shown in Figure 4.1. For the centralized configurations, the rated power of the equipment will be considered as a 100 MW PEM module, which results in a rated cost $RC_{EL} = 793.75$ (€/kW). In the case of a decentralized configuration, the rated power of the equipment corresponds to a 15 MW PEM electrolyser, which uses the full energy produced from a single 15 MW wind turbine, which results in a rated cost $RC_{EL} = 881.25$ (€/kW) [169].

Additionally, when the electrolyser equipment is at sea, the cost of the electrolyser installation doubles, which is included as a factor of 33% of the total equipment cost [170]. For this, $c_{OFF} = 1$, when considering an offshore configuration and $c_{OFF} = 0$ when considering an onshore configuration.

$$CAPEX_{ELEQ} = RC_{EL} \cdot P_{WF} \cdot (1 + 0.33 \cdot c_{OFF}) \quad [€] \quad (4.12)$$

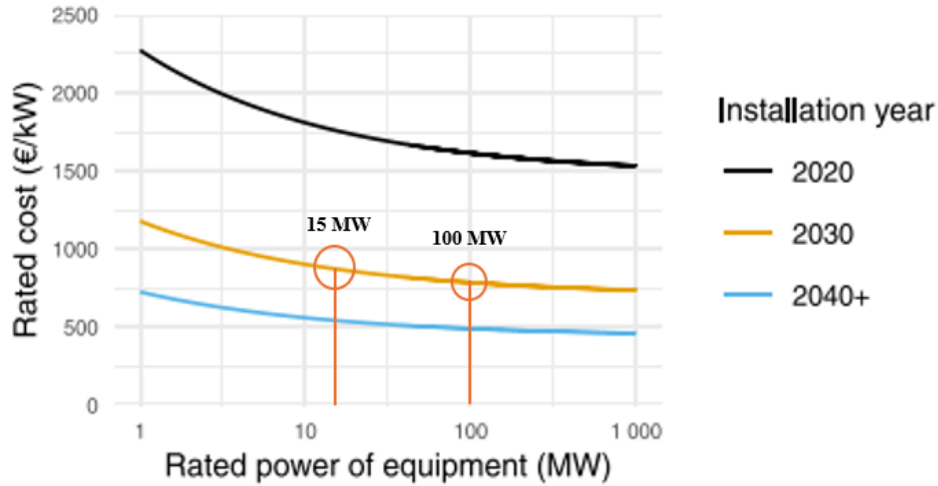


Figure 4.1: Evolution of electrolyser rated costs with scaling effect and learning rates.
Source: Adapted from [12].

In the case of the offshore configurations, an important element that needs to be added into BoP of the electrolysis plant corresponds to the power converters. This is required as the wind turbines supply AC power, and the electrolysis systems require DC power. In the case of centralized operation, a centralized power converter operation is done, while in decentralized operation each turbine has its own power converter. The equipment cost of the power converters $CAPEX_{PC_{EQ}}$ (€) is estimated using Equation (4.13) with the rated cost and depends on the total wind farm capacity P_{WF} (kW) [12].

$$CAPEX_{PC_{EQ}} = 104.13 \cdot P_{WF} \quad [€] \quad (4.13)$$

Additionally, PEM electrolyzers require specific water quality and purity in their feedwater. To meet the strict requirements by using seawater, a desalination system must also be added into the BoP to remove any contaminants and reduce conductivity to avoid any significant membrane degradation. Just as with the case of power converters, centralized have

one component for the centralized platform and in decentralized contain one per each wind turbine. The cost of the desalination system $CAPEX_{DSEQ}$ (€) is estimated using Equation (4.14) which depends on the nominal flow rate of water V_{H2O} (m³/h). The desalination system is sized to be equal to 80% of the rated power of the electrolyzers, which in this case is considered as the whole capacity of the wind farm P_{WF} (kW) as seen in Equation (4.15), since all energy generated is converted into hydrogen [12].

$$CAPEX_{DSEQ} = 30.56 \cdot V_{H2O} \quad [€] \quad (4.14)$$

$$V_{H2O} = 263 \cdot (0.8 \cdot P_{WF}) \quad [m^3/h] \quad (4.15)$$

Inter-array cables are needed to be able to collect the energy produced from the wind turbines in the centralized configurations. They are used to inter-connect the 34 wind turbines in a string-based layout with 7 arrays, as shown in Figure 4.2, by using 66 kV AC dynamic cables of increasing section sizes as more turbines are connected into the array. The total equipment cost for the inter-array cables $CAPEX_{IAEQ}$ (€) is estimated by using Equation (4.16), which calculates the total length in each of the arrays as a function depending on the length of the different cable sections L_{Si} (m) and their corresponding linear cost LC_{Si} (€/m) and multiplies it by the total number of arrays N_A .

$$CAPEX_{IAEQ} = N_A \cdot \left(\sum_{i=1}^7 (LC_{Si} \cdot L_{Si}) + LC_{Smax} \cdot D_{WT} \right) \quad [€] \quad (4.16)$$

The total length of each of the arrays is calculated by considering the possible 66kV inter-array cable sections depending on the amount of wind turbines and the power being transported by the inter-array cables. The 7 cable sections considered are given in Table 4.3, in which each of the dynamic linear costs corresponds to an extra 75% costs compared to the static linear cost [171]. Each of the length of the sections L_{Si} is calculated by Equation (4.17) depend on the number of wind turbines per section N_{Si} , the water depth WD_{WF} (m), and the mean distance between two turbines D_{WT} (m) as calculated in Equation (4.18), considering a capacity density $CD_{WF} = 4.54$ (MW/km²) [142]. Additionally, an extra cable length D_{WT} (m) must be considered at the end of the string to connect each array into the substation, which is given by considering the linear cost for the largest cable section LC_{Smax} (€/m)

$$L_{Si} = N_{Si} \cdot (2 \cdot 2.6 \cdot W D_{WF} + D_{WT}) \quad [m] \quad (4.17)$$

$$D_{WT} = \sqrt{\frac{P_{WT} \cdot 10^3}{C D_{WF}}} \quad [m] \quad (4.18)$$

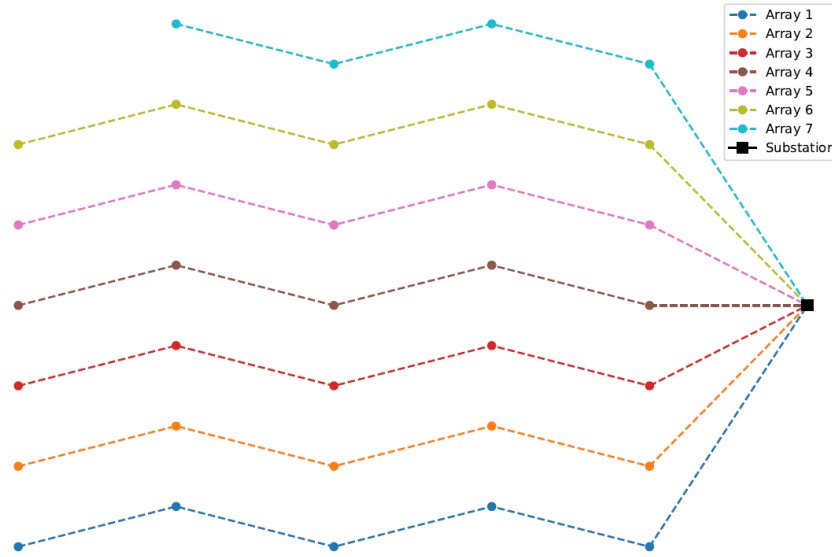


Figure 4.2: String-based wind farm layout with inter-array cables for centralized configurations.

The installation costs of the inter-array cables $CAPEX_{IAC_{IC}}$ (€) follows the same methodology as the total equipment costs, as seen in Equation (4.19). In this case, the linear installation cost LIC_{Si} (€/m) for each of the 7 cable sections is indicated in Table 4.3, which corresponds to the laying and burial operation costs at the seabed for the inter-array cables.

$$CAPEX_{IAC_{IC}} = N_A \cdot \left(\sum_{i=1}^7 (LIC_{Si} \cdot L_{Si}) + LIC_{Smax} \cdot D_{WT} \right) \quad [€] \quad (4.19)$$

Table 4.3: Techno-economic costs for 66 kV inter-array cables.
Sources: [12], [171] and own assumptions.

Si	Section [mm ²]	Resistance [ohm/km]	Capacity [MW]	Cost dynamic [€/m]	Cost static [€/m]	Installation cost [€/m]
1	95	0,25	24	198	113	113
2	150	0,16	30	235	134	121
3	300	0,08	42	326	186	149
4	400	0,06	49	390	223	156
5	630	0,04	59	499	285	171
6	800	0,03	69	632	361	180
7	1000	0,024	88	970	554	198

In the case of having a decentralized configuration, each in-turbine electrolyser produces hydrogen that must be collected and sent to shore. This can be done by considering flexible pipelines that go from each of the electrolysers to the seabed and collected into manifolds. Since the manifolds count with a limited number of connections slots, these manifolds must then be further connected into stages to other intermediate manifolds with the help of rigid pipelines at the seabed to join all production into a single export pipe that goes to shore. In this case, a radial configuration will be considered for the wind farm, as shown in Figure 4.3, and divided into 3 stages of manifolds that collects the hydrogen produced from each wind turbine, with the number of manifolds and their connection slots as shown in Table 4.4, for which the output is considered as one of the slots, for which the first stage of manifolds have a maximum of 5 turbines each, second stage has 2 intermediate manifolds, and lastly stage 3 consists of the export manifold that collects the total hydrogen produced and has as output the export pipe to shore.

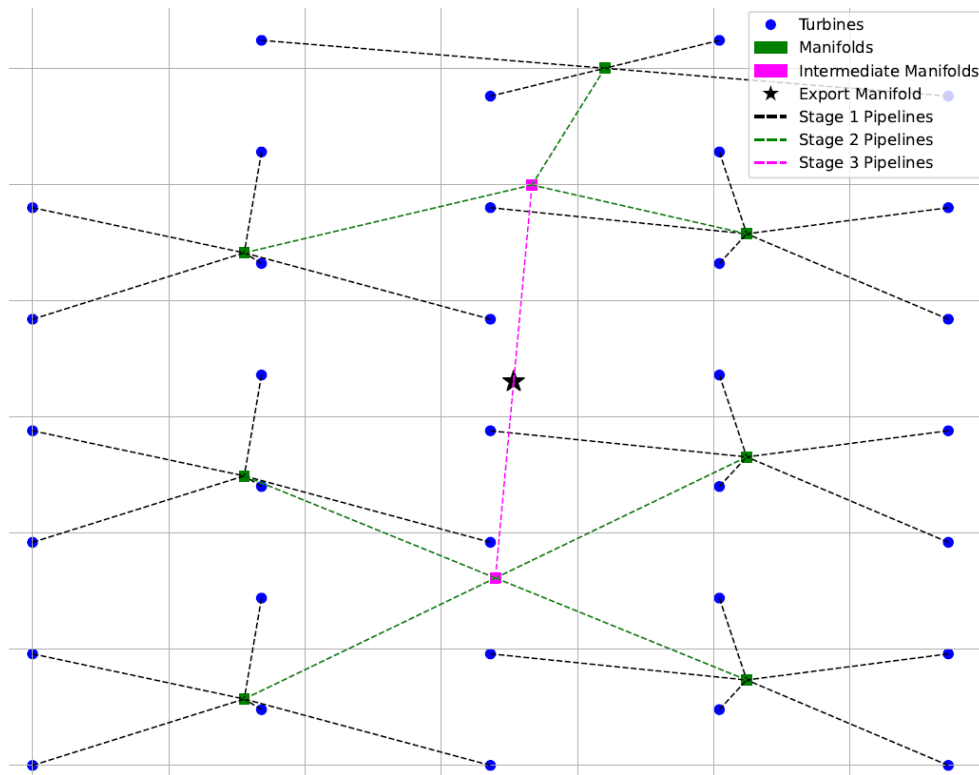


Figure 4.3: Radial-based wind farm layout with inter-array pipelines for decentralized configurations.

Table 4.4: Pipeline Inter-array radial configuration.

Stage i	Number of Slots (w/ OUT)	Number of Manifolds
S1	6	7
S2	5	2
S3	3	1

Considering the proposed radial-based layout, the equipment cost of the inter-array pipeline $CAPEX_{IAP_{EQ}}$ (€) is estimated with Equation (4.20) and consists in considering the total length of the pipelines at each of the stages L_i and applying a linear base cost $LC_{BA} = 1,736.73$ (€/m) for flexible pipes and $LC_{BA} = 173.67$ (€/m) for rigid pipes with adjusting factors corresponding to the size factor $a_{sp}(d_i)$ and the miscellaneous cost $LC_{misc}(d_i)$ (€/m) according to the diameter of the pipeline at each stage [172]. These size and miscellaneous cost factors for both flexible and rigid pipe sizes can be seen in Table 4.5.

$$CAPEX_{IAP_{EQ}} = \sum_{i=1}^3 (CF_{sp}(d_i) \cdot LC_{BA,i} + LC_{misc}(d_i)) \cdot L_i \quad [€] \quad (4.20)$$

Table 4.5: Pipe size and miscellaneous cost factors for pipelines.
Source: [172].

Cost Factor: Pipe Size $CF_{s,p}(d_i)$					
Rigid Size in (cm)	4 (10.16)	10 (25.40)	12 (30.48)	16 (40.64)	20 (50.80)
P50	0.25	1	1.3	1.8	2.6
Flexible Size in (cm)	4	5.625	8	10	-
P50	0.65	1	1.25	1.9	-
Cost Factor: Miscellaneous (€/m) $LC_{misc}(d_i)$					
Coating Pipe Size	4 (10.16)	10 (25.40)	12 (30.48)	16 (40.64)	20 (50.80)
P50	155.34	396.98	431.50	517.80	621.36

The length L_i (m) can be estimated using Equation (4.21) which depends on the stage, having the first flexible pipes be equal to the number of wind turbines N_{WT} , and that each individual pipelines lengths depends on the total area covered by the downstream turbines at each stage $A_i(\text{km}^2)$ and the water depth WD_{WF} (m), since the manifolds are placed in the radial center at the seabed from the connected turbines. For any subsequent stages, the length of the rigid pipelines depends on the number of connections $(N_s - 1)$ from each of the manifolds into the subsequent stage manifolds N_{MFi} and must also cover the area of the downstream turbines A_i in the current stage.

$$L_i = \begin{cases} N_{WT} \cdot \left(\frac{\sqrt{A_i}}{\sqrt{2}} \cdot 10^3 + WD_{WF} \right), & \text{if } i = 1 \\ (N_{si} - 1) \cdot N_{MFi} \cdot \frac{\sqrt{A_i}}{\sqrt{2}} \cdot 10^3, & \text{if } i \neq 1 \end{cases} \quad [m] \quad (4.21)$$

To calculate the diameter of the pipeline d_i at each of the stages, it is recursively estimated with Equation (4.22) from the subsequent stages until reaching the size of the export pipe that supports the maximum normal volumetric flow rate of the hydrogen from the total produced hydrogen, considering a minimum pipeline diameter of 5 cm for all stages.

$$d_i = \max\left(0.05, \frac{d_{i+1}}{\sqrt{(N_{si} - 1)}}\right) \quad [m] \quad (4.22)$$

The equipment cost estimation for the manifolds $CAPEX_{MF_{EQ}}$ (€) at each stage follows the same methodology as with the calculation and depends on the amount of manifolds at each stage N_{MFi} , miscellaneous costs, and a base cost that has some cost factors applied depending on the pipe size $a_{sMF}(d_i)$ and the number of connection slots $a_N(N_s)$ in the manifolds, with values taken from Table 4.6.

$$CAPEX_{MF_{EQ}} = \sum_{i=1}^3 \left((CF_{spMF}(d_i) \cdot CF_N(N_s) \cdot 2.265 + 0.188) \cdot 10^6 \cdot N_{MFi} \right) \quad (4.23)$$

Table 4.6: Pipe size and number of connection slots factors for manifolds.
Source: [172].

Cost Factor: Number of Slots $CF_N(N_s)$					
# of Slots	2	4	6	8	10
P50	0.7	1	1.3	1.5	2
Cost Factor: Pipe Size $CF_{spMF}(d_i)$					
OD in (cm)	8 (20.32)	10 (25.40)	12 (30.48)	16 (40.64)	20 (50.80)
P50	0.93	1	1.05	1.15	1.25

For the inter-array pipeline installation, the vessel used is a Flex-lay vessel, which has a laying rate of 7 km/d and a day rate cost of 400 k€/d, for which the entire length of all the inter-array pipeline stages L_{IAP} (m) must be considered. The installation costs for the inter-array pipelines $CAPEX_{IAP_{IC}}$ (€) is estimated by using Equation (4.24).

$$CAPEX_{IAP_{IC}} = \frac{L_{IAP}}{7,000} \cdot 400 \cdot 10^3 \quad [€] \quad (4.24)$$

An initial estimation for the total length of the export cable or pipeline L_{TR} (km) for transmission of energy or hydrogen produced to the shore is calculated by Equation (4.25). An extra 20% of distance is considered from the distance to shore DS_{WF} (km) to account for any necessary routing, slack of the lines, cable burial or approach to the onshore substation.

$$L_{TR} = 1.2 \cdot DS_{WF} \text{ [km]} \quad (4.25)$$

In the case of the onshore configuration, an export cable is needed for the transmission of energy collected at the offshore substation. Both HVAC and HVDC export cables may be considered, depending mainly on the distance to the shore due to the energy loss and reactive power experienced in HVAC cables in long distances, especially above 100 km of distance to shore [173]. To calculate the equipment costs for HVDC export cables $CAPEX_{HVDC,EC_{EQ}}$ (€), a linear cost of 1.95 €/kW/km is considered [174] in Equation (4.26), which depends on the total transmission length L_{TR} (m) and the total power capacity of the windfarm P_{WF} (kW). In the case of the installation costs, they are estimated to be equal to half of the equipment costs as shown in Equation (4.27)

$$CAPEX_{HVDC,EC_{EQ}} = 1.95 \cdot P_{WF} \cdot L_{TR} \text{ [€]} \quad (4.26)$$

$$CAPEX_{HVDC,EC_{IC}} = 0.5 \cdot CAPEX_{HVDC,EC_{EQ}} \text{ [€]} \quad (4.27)$$

Now in the case of HVAC export cables, it is necessary to consider the energy losses and the decrease in power capacity of the cable in terms of the length. For this, the power capacity for each of the cable sections was calculated for this site-specific case and the number of HVAC cables N_{EC} needed for each of the cables was calculated as shown in Table 4.7 [12]. For the estimation of the equipment cost of HVAC export cables $CAPEX_{HVAC,EC_{EQ}}$ (€) by Equation (4.28), the cable section chosen and must be given by considering the minimum number of cables needed to transport the total wind farm capacity with the least amount of tension to reduce its linear cost LC_{HVAC} (€/m). Additionally, the installation cost for the HVAC export cables $CAPEX_{HVAC,EC_{IC}}$ (€) is calculated with Equation (4.29) using the same methodology by considering the linear installation cost for the chosen cable section and tension LIC_{HVAC} (€/m)

$$CAPEX_{HVAC,EC_{EQ}} = N_{EC} \cdot L_{TR} \cdot LC_{HVAC} \cdot 10^3 \text{ [€]} \quad (4.28)$$

$$CAPEX_{HVAC,EC_{IC}} = N_{EC} \cdot L_{TR} \cdot LIC_{HVAC} \cdot 10^3 \text{ [€]} \quad (4.29)$$

Table 4.7: Techno-economic assumptions for site-specific HVAC export cables.

Sources: Calculation and assumptions from [12].

Tension [kV]	Section [mm ²]	Resistance [mohm/km]	Cost [€/m]	Installation Cost [€/m]	Capacity [MW]	# Cables needed
132	630	39.5	406	335	187	3
	800	32.4	560	340	203	3
	1,000	27.5	727	350	217	3
220	500	48.9	362	350	279	2
	630	39.1	503	360	308	2
	800	31.9	691	370	335	2
	1,000	27	920	380	359	2
400	800	31.4	860	540	601	1
	1,000	26.5	995	555	644	1
	1,200	22.1	1,130	570	681	1
	1,400	18.9	1,265	580	701	1
	1,600	16.6	1,400	600	715	1
	2,000	13.2	1,535	615	744	1

In the case of the offshore configurations, an export pipeline is considered to transport all the hydrogen produced offshore into the shore. This export pipeline is a rigid pipeline and the estimation of the equipment cost of the export pipeline $CAPEX_{EP_{EQ}}$ (€) is similar to the estimation for the inter-array pipeline that depends on the diameter of the pipe to calculate the pipeline size cost factor $a_{sp}(d_{EP})$ and miscellaneous cost $LC_{misc}(d_{EP})$ (€/m) from

Table 4.5, as shown in Equation (4.30). The estimation of the diameter of the export pipeline d_{EP} (mm) is interpolated according to the recommended pipeline diameters for the maximum volumetric flow rate present in the pipeline by considering an inlet pressure of 30 bar [175], as shown in Table 4.8.

$$CAPEX_{EP_{EQ}} = L_{TR} \cdot 10^3 \cdot \left(173.67 \cdot a_{sp}(d_{EP}) + LC_{misc}(d_{EP}) \right) \text{ [€]} \quad (4.30)$$

The estimation for the maximum volumetric flow rate Q_{EP} (Nm³/h) is given by considering the total wind farm capacity P_{WF} to calculate the maximum total hydrogen produced by considering a specific H₂ production equal to 0.0192 kgH₂/kWh [169] as shown in Equation (4.31).

$$Q_{EP} = 0.0192 \cdot \frac{P_{WF}}{0.0899} \quad [Nm^3/h] \quad (4.31)$$

The installation cost for the export pipelines $CAPEX_{EPIC}$ estimated by Equation (4.32) follows the same methodology as with the inter-array pipelines by considering an S-lay vessel that has a lay rate of 4 km/d and a day rate of 700 k€/d that must be installed along the whole length of transmission to shore L_{TR} (km).

$$CAPEX_{EPIC} = \frac{L_{TR}}{4} \cdot 700 \cdot 10^3 \quad [€] \quad (4.32)$$

Table 4.8: Recommended Pipeline Diameters for pure hydrogen (IN: 30 bar, OUT: 24 bar).
Source: [175].

Volume Flow Rate [Nm ³ /h]	Pipe Diameter [mm]
12,000	150
40,000	250
80,000	330
120,000	390

4.1.1.2. OPEX

OPEX corresponds to the operations and maintenance (O&M) of a project and refers to all the ongoing costs associated with running a project on a day-to-day basis and ensuring a continuous operation. It typically encompasses costs regarding the labor and administrative overheads, any utilities or consumables needed to run the equipment like lubricants, filters or chemicals, any insurance and site fees, as well as any routine repairs, preventive maintenance, spare parts and small or major equipment replacements. In this case, the OPEX costs will be split into two major categories, which are the repair costs and the logistics costs.

The repair costs RC account for the annual spare parts, consumables, and any preventive maintenance that must be done to each of the equipment to maintain a safe and efficient operation. These yearly O&M costs (€/yr) are typically modeled as a percentage of each of the component's equipment costs according to the model from Rogeau et al. [12]. This can be seen in Equation (4.33), in which the repair costs for wind turbines $OPEX_{WT_{RC}}$ (€/yr) amount to a 2.5% of the equipment costs and Equation (4.34) corresponds to the desalinators' repair costs $OPEX_{DS_{RC}}$ (€/yr) for a 3% of the equipment costs.

$$OPEX_{WT_{RC}} = 2.5\% \cdot CAPEX_{WT_{EQ}} \quad [€/yr] \quad (4.33)$$

$$OPEX_{DS_{RC}} = 3\% \cdot CAPEX_{DS_{EQ}} \quad [€/yr] \quad (4.34)$$

For the conversion elements, both HVAC and HVDC substations have repair costs of 1.5% of the equipment costs as seen in Equations (4.35) and (4.36) respectively, electrolyzers having 2% of the equipment costs as seen in Equation (4.37) and power converters 1% of the equipment costs as seen in Equation (4.38). These repairs costs for the conversion elements are doubled when at sea, having the coefficient $c_{OFF} = 1$ when in an offshore configuration and $c_{OFF} = 0$ when in an onshore configuration.

$$OPEX_{HVAC,SS_{RC}} = 1.5\% \cdot (1 + c_{OFF}) \cdot CAPEX_{HVAC_{EQ}} \quad [€/yr] \quad (4.35)$$

$$OPEX_{HVDC,SS_{RC}} = 1.5\% \cdot (1 + c_{OFF}) \cdot CAPEX_{HVDC_{EQ}} \quad [€/yr] \quad (4.36)$$

$$OPEX_{EL_{RC}} = 2\% \cdot (1 + c_{OFF}) \cdot CAPEX_{EL_{EQ}} \quad [€/yr] \quad (4.37)$$

$$OPEX_{PC_{RC}} = 1\% \cdot (1 + c_{OFF}) \cdot CAPEX_{PC_{EQ}} \quad [€/yr] \quad (4.38)$$

In the case of the power cables for both export and inter-array connections, the overall repair costs per year comes to a 0.2% of the equipment cost as shown in Equations (4.39), (4.40), and (4.41) and for both inter-array and export pipelines the repair costs equal to a 2% of the equipment costs as shown in Equations (4.42) and (4.43).

$$OPEX_{HVAC,EC_{RC}} = 0.2\% CAPEX_{HVAC,EC_{EQ}} \quad [€/yr] \quad (4.39)$$

$$OPEX_{HVDC,EC_{RC}} = 0.2\% CAPEX_{HVDC,EC_{EQ}} \quad [€/yr] \quad (4.40)$$

$$OPEX_{IAC_{RC}} = 0.2\% CAPEX_{IAC_{EQ}} \quad [€/yr] \quad (4.41)$$

$$OPEX_{IAP_{RC}} = 2\% CAPEX_{IAP_{EQ}} \quad [€/yr] \quad (4.42)$$

$$OPEX_{EP_{RC}} = 2\% CAPEX_{EP_{EQ}} \quad [€/yr] \quad (4.43)$$

Lastly, considering that the total lifetime of an electrolyser stack amounts to a total of 80,000 hours of operation, it will be lower than the total production time of the project's lifetime [169]. Additionally, this value does not account for the possible impacts in the reduction of the lifetime due to the increased start-stop cycles, the variability and the intermittency of the energy, as well as the marine environment and possible corrosion of the elements. Due to this, a one-time stack replacement will be considered as a repair cost as shown in Equation (4.44) that

amounts to 45% of the equipment cost of the electrolyzers for each scenario, placing it in the year that 60,000 hours of operation is reached, which equals the 75% of the reported lifetime of the stack to also reduce the degradation and the possible decrease in electrical efficiency.

$$OPEX_{SRRC} = 45\% CAPEX_{ELEQ} \quad [€] \quad (4.44)$$

The logistic costs cover the annual vessel chartering for all maintenance and repair operations like routine inspections, preventive maintenance, minor and major repairs, as well as failure response. In the case of minor repairs, the logistic costs are estimated by considering the daily chartering costs of crew transfer vessels (CTVs) as a scaling as a linear function with the distance to the nearest port. As the wind farm gets further from the port, all operations take more time to reach, which increases the cost to a certain distance of around 150 km from the port when the model switches into the use of a mothership-based service operation vessel (SOV). This type of ship works as an offshore support vessel that is specifically designed for the maintenance and servicing of installations offshore, offering hotel, warehouse and workshop capabilities with safe, easy, and fast access to the turbines.

The logistics costs for minor repairs LoC_{min} (€/yr) is calculated according to Equation (4.45), for which the turning point between changing from CTV into an SOV charter strategy is done at a distance from port DP_{WF} above 150 km. The daily charter rate of the SOV considered is 75 k€/d with all additional expenses like fuel and wages for a total of 27.5 M€/yr [168]. This maintenance strategy guarantees 94% of availability of the wind farm [12]. These costs are distributed across the subsystems equally for all scenarios.

$$LoC_{min} = \begin{cases} 0.1833 \cdot 10^6 \cdot DP_{WF}, & \text{if } DP_{WF} \leq 150 \text{ km} \\ 27.5 \cdot 10^6, & \text{if } DP_{WF} > 150 \text{ km} \end{cases} \quad [€/yr] \quad (4.45)$$

In the case of major repairs, the floating wind turbines must be towed all the way to port for the repairs the same way is considered when installed by using AHTS with 2 support vessels. The estimation for the annual cost for major repairs LoC_{maj} (€/yr) depend on the wind turbine's failure rate $\lambda_{maj} = 0.08 \text{ f/year}$, which multiplied by the number of wind turbines N_{WT} gives the amount of times the tow-out operation must be performed to address the failures. The total cost for chartering the vessels depends on the distance to port DP_{WF} (km), the amount of time

it takes to make the trips, the reparation time t_{rep} (h) and the daily rate of the vessels as mentioned in the vessel parameters shown in Table 4.9.

$$LoC_{maj} = N_{WT} \cdot \lambda_{maj} \cdot \left(\frac{2n \cdot DP_{WF}}{v} + t_{rep} \right) \cdot \frac{DR}{24} \quad [\text{€/yr}] \quad (4.46)$$

Table 4.9: Major wind turbine repair vessel parameters.
Sources: [12].

Operation	Tow-out
Vessel	AHTS with 2 support vessels
Speed [km/h]	6.5
Repair time [h]	50
Day rate [k€/d]	130
Round trips	2

These O&M costs expenses will be considered as an evenly annualized cost over the whole project's lifetime, except for the PEM stack replacement done at the about half of the lifetime to account for the durability and lifetime of the stack, as well as the restoration of the stack efficiency due to the degradation of the caused by normal operation time and the impacts due to the marine conditions offshore and the variability of the energy produced.

4.1.1.3. DECEX

Lastly for the lifetime costs of the project, DECEX covers all expected costs at the end of a project's lifetime corresponding to all operations needed to dismantle, remove, and dispose of all elements of the wind farms like offshore wind turbines, platforms, cables, pipeline, and the restoration of the site to acceptable environmental and navigational conditions. These operations are mandatory to comply with regulatory and environmental compliance and are an obligation to clear all related infrastructure once the whole service period of the project is completed. In this case, since decommissioning operations have significant similarities with the installation methodology, the cost estimation will also be similar. In the case of the wind turbine and floating platform, the tow-out for both stays the same and only reduces the decommissioning time for anchors $t_{decom} = 30$ hours for Equations (4.47) and (4.48) respectively.

$$DECEX_{WT} = \left(\frac{N_{u,WT}}{V_C} \cdot \left(\frac{2 \cdot DP_{WF}}{v} + t_{load} \right) + t_{decom} \cdot N_{WT} \right) \cdot \frac{DR}{24} \quad [€] \quad (4.47)$$

$$DECEX_{PF} = \left(\frac{N_{u,PF}}{V_C} \cdot \left(\frac{2 \cdot DP_{WF}}{v} + t_{load} \right) + t_{decom} \right) \cdot \frac{DR}{24} \quad [€] \quad (4.48)$$

In the case of the inter-array and export pipelines, the removal rate increases, reducing the total time for decommissioning compared to the installation, with a removal rate of 10 km/d for inter-array as shown in Equation (4.49) and 5 km/d as shown in Equation (4.50).

$$DECEX_{IAP} = \frac{L_{IAP}}{10,000} \cdot 400 \cdot 10^3 \quad [€] \quad (4.49)$$

$$DECEX_{EP} = \frac{L_{TR}}{5} \cdot 700 \cdot 10^3 \quad [€] \quad (4.50)$$

Lastly, in the case for the decommissioning costs for the inter-array cables and export cables for both HVAC and HVDC, they are considered to be equal to half of the installation costs as shown in Equations (4.51), (4.52), and (4.53) respectively.

$$DECEX_{IAC} = 0.5 \cdot CAPEX_{IAC_{IC}} \quad [€] \quad (4.51)$$

$$DECEX_{HVAC,EC} = 0.5 \cdot CAPEX_{HVAC,EC_{IC}} \quad [€] \quad (4.52)$$

$$DECEX_{HVDC,EC} = 0.5 \cdot CAPEX_{HVDC,EC_{IC}} \quad [€] \quad (4.53)$$

These decommissioning costs are placed as a total amount in the final year of the project in year 25. Applying the DECEX costs at the end of the life simulated a one-time payment for the removal and site restoration when the money is being spent in its proper timing, as mentioned similarly with the CAPEX and OPEX previously to discount the money according to the rate of return and year to establish the NPV of the project and calculate the lifetime costs along the years for the final project LCOH.

4.1.2. Technical Model Estimation

The second step in the calculation of the LCOH for each of the implementation scenarios corresponds to the calculation of the total energy production for the project determined by the amount of hydrogen produced along the years. This will be done by modelling an estimation of the power generated from the wind turbine by considering the MERRA-2 (global) hourly wind speed dataset recorded during the whole year in the location of the case study of Viana do

Castelo [147]. To determine the power curve used for energy production coming from wind resources, the 15 MW wind turbine Vestas V236-15.0 was considered as described in Table 4.10 is used along Equation (4.54) that describes the power generated per hour as shown in Figure 4.4.

$$P_{prod}(t) = \begin{cases} 0, & \text{if } v(t) < v_{cut-in} \text{ or } v(t) \geq v_{cut-out} \\ P_{WT} \cdot \left(\frac{v(t)^3 - v_{cut-in}^3}{v_{rated}^3 - v_{cut-in}^3} \right), & \text{if } v_{cut-in} \leq v(t) < v_{rated} \\ P_{rated}, & \text{if } v_{rated} \leq v(t) < v_{cut-out} \end{cases} \quad [kWh] \quad (4.54)$$

Table 4.10: Vestas V235-15.0 main parameters for power generation.
Source: [176].

Parameter	Value
Rated Capacity [kW]	15,000
Cut-in Wind Speed [m/s]	3
Rated Wind Speed [m/s]	11.1
Cut-out Wind Speed [m/s]	31

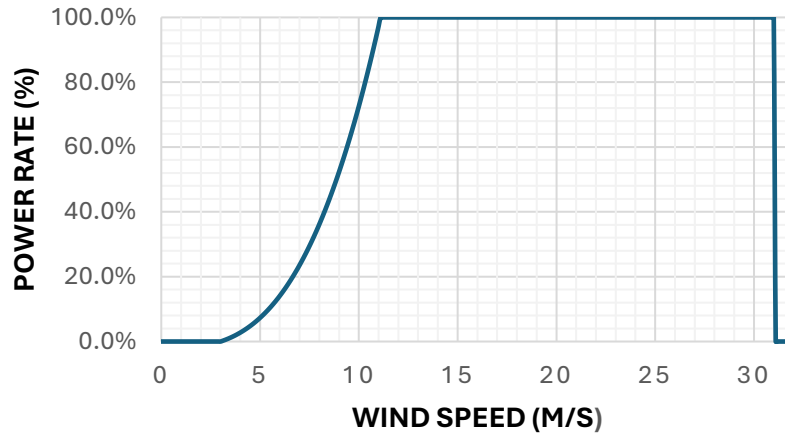


Figure 4.4: Power Curve approximation through Equation (4.54). Parameters adjusted for Vestas V236-15.0.

Source: See

Table 4.10.

The power generated by the wind turbines have energy losses when going in the transmission and conversion phase, which reduces the energy generated. For the conversion phase, the PEM electrolyser and its balance of plant have a certain efficiency when producing hydrogen from the electrolysis process. The characteristics of the PEM electrolyzers considered in this case correspond to Siemens Silyzer 300, as shown in Table 4.11.

Table 4.11: PEM Electrolyser Parameters: Siemens Silyzer 300.
Source: [169], [177].

Parameter	Value
Centralized PEM Electrolysis Module Capacity [MW]	100
Decentralized PEM electrolyser Capacity [MW]	15
Efficiency (LHV) [%]	63.80
Stack Lifetime [h]	80,000
Minimum Load [%]	5
Stack Degradation [%/1,000 h]	0.12

PEM electrolyzers require a minimum load for safe and efficient operation of 5% of the total rated power. This implies that when reaching the minimum load threshold of the electrolyser, a start-stop cycle occurs and can induce an acceleration of degradation and shortening the operating life. In the centralized configuration, constant production can be managed by redirecting the total collected energy from the wind farm to a certain number of electrolyzers to not have to completely stop production and to try and avoid entering a restart from cold conditions. However, in the decentralized configuration, the electrolyser only has access to the wind turbine it is connected to, which means that any wind turbine production below this threshold must enter into a start-stop cycle and not produce any energy, as calculated in Equation (4.55).

$$P_{prod,D}(t) = \begin{cases} P_{prod}(t), & \text{if } P_{prod}(t) \geq 5\% \cdot P_{Elec,D} \\ 0, & \text{if } P_{prod}(t) < 5\% \cdot P_{Elec,D} \end{cases} \quad [kWh] \quad (4.55)$$

Additional energy losses occur in the transmission of the energy from the inter- array and export of both cables and pipelines. In the case of HVDC export cables and pipelines, the percentage value of the transmission losses depends on the total length of each of the elements, as shown in Table 4.12. Equation (4.56) is used to calculate the efficiency for each of the transmission elements in the considered configuration.

$$\eta_{loss,TR} = 1 - \frac{P_{loss,TR}}{1,000 \text{ km}} \cdot L \quad [\%] \quad (4.56)$$

In the case of the HVAC cables, the energy losses $P_{loss,HVAC}(t)$ (kWh) produced throughout the year depend on the amount of power flowing through the cable at a certain time

$P_{prod}(t)$ (kWh) as shown in Equation (4.57). The power energy losses at each time step of an hour can be estimated using Equation (4.58) according to the characteristics of each of the cables by considering the cable tension U (kV), the cable resistance R (ohm/km) and the total HVAC cable length L_{HVAC} (km).

$$\eta_{HVAC} = 1 - \sum_t \frac{P_{loss,HVAC}(t)}{P_{prod}(t)} \quad [\%] \quad (4.57)$$

$$P_{loss,HVAC}(t) = \left(\frac{P_{prod}(t)}{U} \right)^2 \cdot R \cdot L_{HVAC} \cdot 10^3 \quad [kWh] \quad (4.58)$$

Besides the energy lost due to the transmission of the energy, losses can also come from not being able to transmit any of the produced energy due to failures in the transmission chain. To be able to quantify and estimate the impact of these failures, efficiency will be considered according to Equation (4.59), for which the failure rates λ_{fail} (f/yr/km) and the subsequent repair time t_{rep} (d) is shown in Table 4.12. For this, the number of affected wind turbines F_{WT} from the transmission element failure is considered, compared with the total number of wind turbines N_{WT} to determine the amount of time not working in the year and consider the efficiency. The affected wind turbines correspond to the whole wind farm for export cable and pipelines, half of an array for inter-array cables, and failure per stage in the inter-array pipelines.

$$\eta_{fail} = 1 - \frac{\lambda_{fail} \cdot t_{rep} \cdot F_{WT}}{365 \cdot N_{WT}} \quad [\%] \quad (4.59)$$

Table 4.12: Failure rates and repair times for transmission components.
Source: [12].

Element	Losses [%/1000km]	Failure rate [f/yr/km]	Repair time [d]
HVAC IA Cable	Equation (4.58)	0.003	40
HVAC Export Cable	Equation (4.58)	0.003	60
HVDC Export Cable	3.0	0.0015	60
Flexible Pipe	0.03	0.001	40
Rigid Pipe	0.03	0.0001	60

Additional efficiencies must be considered along the hydrogen production chain for the other elements involved in the conversion of energy. The efficiency values for each of the conversion elements are shown in Table 4.13, in which it also included the global availability of the wind farm of 94% with the O&M strategy considered.

Table 4.13: Efficiency values along the hydrogen production chain for conversion.
Source:[12], [169].

Element	Efficiency
Global Availability [%]	94
HVDC substation [%]	99
Power converters [%]	99.5
Desalinators [%]	99.9
PEM Electrolyser (LHV) [%]	63.80

Once calculated all resulting efficiencies from the energy losses from both transmission and conversion elements, the total power generated P_{Gen} (kWh) can be computed according with Equation (4.60) to the total produced energy from wind turbines and applying the total efficiency η_{total} (%) for each of the configurations accordingly. From this generated power, it is possible to finally compute the total hydrogen produced per year E_t (kgH₂) with Equation (4.61) using the LHV of hydrogen which is equal to 33.33 kWh/kg.

$$P_{Gen} = \left(\sum_{t=1}^{8760} P_{prod}(t) \right) \cdot \eta_{total} \quad [kWh] \quad (4.60)$$

$$E_t = \frac{P_{Gen}}{33.33} \quad [kWh] \quad (4.61)$$

Lastly, additional efficiency is considered for the performance of the electrolyser stack, which corresponds to the degradation of the stack. This efficiency changes throughout the hours operated during lifetime of the electrolyser, with an estimated linear degradation rate of 0.12% per 1000 h of operation [177]. This turns into an additional discount to the total hydrogen produced E_t (kgH₂) with a linear decrease in efficiency depending on the amount of operational lifetime t_{life} (h) considered over the years. This operational lifetime gets restarted once performing the stack replacement, which will be done in the year 15 as shown in Equation (4.62).

$$\eta_{SD}(t) = 1 - \frac{0.12\%}{1000 \text{ h}} \cdot t_{life} \quad [\%] \quad (4.62)$$

4.2. Case Analysis and Results

Building from the techno-economic model developed previously in Section 4.1 and the implementation scenarios established in Section 3.2, this section applies the costs, performance, and technical evaluation framework to the Viana do Castelo case study chosen previously in Section 3.1. The following analysis interprets the model outputs for each of the implementation scenarios configurations and highlights how the capital, operational, and decommissioning expenditures combine to form the total lifetime costs and how these coupled with the technical performance for the hydrogen generation influence the LCOH. These results will firstly be structured by considering a cost breakdown in 5 sub-systems, as shown in Table 4.14. These subsystems are divided into wind turbines, corresponding to the turbine equipment and foundations, inter-array, corresponding to the cables or pipelines needed to inter-connect the turbines, central platform, corresponding to the foundation needed in the centralized configurations, conversion, corresponding to the electrical substations, power converters, and the electrolysis plant, and finally the transmission, corresponding to the export cable or pipeline to shore.

Table 4.14: Cost breakdown of sub-systems for each implementation scenario.

Implementation Scenario	Sub-System	CAPEX [M€]	OPEX [M€]	DECEX [M€]	Lifetime Costs [%]
Centralized Onshore	Wind Turbines	1,300.52	827.49	18.19	65.58%
	Inter-Array	64.35	14.13	7.31	2.62%
	Central Platform	36.90	11.64	6.18	1.67%
	Conversion	507.78	441.85	-	29.02%
	Transmission	20.16	12.26	3.89	1.11%
Centralized Offshore	Wind Turbines	1,300.52	827.49	18.19	56.57%
	Inter-Array	64.35	14.13	7.31	2.26%
	Central Platform	95.57	11.64	6.18	2.99%
	Conversion	594.79	821.34	-	37.32%
	Transmission	13.46	17.11	2.02	0.86%
Decentralized Offshore	Wind Turbines	1,432.38	830.40	18.19	57.05%
	Inter-Array	68.07	46.48	2.96	2.94%
	Central Platform	-	-	-	0.00%
	Conversion	654.14	910.30	-	39.13%
	Transmission	13.46	20.02	2.02	0.89%

When looking at the subsystem level costs coming from the techno-economic model across all scenarios, the dominance of the lifetime costs comes from wind turbines due to their linear dependence of the 510 MW installed capacity of the wind farm. The Off,D has higher costs due to the model allocating additional foundation costs to integrate the electrolyzers and its BoP at each turbine, increasing both procurement and installation expenses. Inter-Array costs are less for the AC cables in centralized scenarios while higher in pipelines due to higher OPEX costs. Central platform costs vary across the scenarios, having minimal impact on On,C, a substantial impact on Off,D due to the larger footprint of electrolysis plant, and none for Off,D due to not requiring a central platform. Conversion costs are also dominant behind wind turbines and scale up when having to do installation and reparation offshore, as well as considering extra BoP in-turbines for the Off,D case. Lastly, transmission costs are modest in the case of pipeline export for offshore scenarios and slightly higher when considering HVAC export for onshore. CAPEX and OPEX drivers are mainly from wind turbines followed by conversion, which are particularly higher in offshore cases. DECEX remains a small fraction of the total costs since they are proportional to a fixed percentage of the installation costs.

The lifetime cost composition reinforces the cost drivers identified above, as shown in Table 4.15 and Figure 4.5, for which the total amounts through the life of the project are considered according to the techno-economic framework without applying any discount rates. On,C benefits from the absence of the large offshore platforms and the reduced O&M burden of electrolysis onshore, which yields the lowest lifetime cost across all implementation scenarios. This techno-economic model assigns various multipliers for maintenance and installation offshore, which means that shifting electrolysis to offshore for both centralized and decentralized scenarios increase both the CAPEX and OPEX significantly. Off,D scenario pushes it even further by distributing and multiplying the number of electrolyzers and BoP needed with its own maintenance and spare parts but eliminates the use of a centralized platform and adds more flexibility and robustness to the system. In all scenarios, DECEX accounts for a small percentage of around 1% of the lifetime costs which is consistent with the model's proportional estimation method based on installation costs which are dependent on the distance to port, which in this case is relatively close. This balance between CAPEX and OPEX shifts subtly offshore, with CAPEX share dropping and OPEX increasing due to higher operational intensity of the maritized assets offshore.

Table 4.15: Lifetime cost overview without NPV correction for each implementation scenario.

Implementation Scenario	Lifetime Costs [M€]	CAPEX [M€ / %]		OPEX [M€ / %]		DECEX [M€ / %]	
Onshore Centralized (On,C)	3,272.64	1,929.71	59.0	1,307.36	39.9	35.57	1.1
Offshore Centralized (Off,C)	3,794.10	2,068.69	54.5	1,691.70	44.6	33.70	0.9
Offshore Decentralized (Off,D)	3,998.42	2,168.05	54.2	1,807.20	45.2	23.16	0.6

From a performance point of view, the differences between each of the implementation scenarios are relatively small in the case study as shown in Table 4.16. The techno-economic framework calculates the total efficiency as the product of the wind-to-hydrogen transmission chain, the electrolyser efficiency and the wind farm availability for production. Offshore scenarios achieve slightly higher total efficiency when compared against onshore scenarios due to the near lossless hydrogen pipeline export compared to the HVAC transmission losses. This translates into about 1% more lifetime hydrogen output. Off,D gains a further minimal advantage by avoiding inter-array electrical losses. Annual and lifetime hydrogen outputs track these efficiencies since wind farm availability and electrolyser efficiency are held constant across the scenarios in this model. Key takeaway for this location is that while offshore configurations can achieve an extra 1-1.2% in hydrogen yield, the absolute gain is small compared to the cost penalties identified earlier, making LCOH increase for offshore.

Table 4.16: Technical Performance and Hydrogen Output across implementation scenarios.

Implementation Scenario	Onshore Centralized (On,C)	Offshore Centralized (Off,C)	Offshore Decentralized (Off,D)
WF Availability [%]	94.00	94.00	94.00
PEM Efficiency (LHV) [%]	63.80	63.80	63.80
Transmission Chain Loss and Failure [%]	97.65	98.82	99.34
Total Efficiency [%]	58.56	59.27	59.58
Total Power Produced [MWh]	1.17E+06	1.18E+06	1.18E+06
Annual H ₂ output [kgH ₂]	3.51E+07	3.55E+07	3.55E+07
Lifetime H ₂ output [kgH ₂]	8.77E+08	8.88E+08	8.87E+08

The LCOH results are where the lifetime costs and technical performance come together, as shown in Table 4.17, while the detailed calculations and considerations for LCOH across the project's lifetime is shown in Appendix 8.6. These results were separated into 2 cases across all implementation scenarios in which stack degradation of 0.12% every 1000 hours is

considered in the calculation of the LCOH, by considering an extra linear efficiency term across the years accounting for the lifetime of the stack and changing at the 15-year mark. Without degradation, On,C delivers the lowest LCOH by reflecting its significant lower lifetime costs despite the lower technical efficiency compared to offshore configurations. Introducing degradation into the hydrogen output calculation as a gradual decline in efficiency, the LCOH increases on all implementation scenarios by roughly 0.10 to 0.13 €/kg, or around a total efficiency of ~97.45%. This is because the same annual costs are spread over a smaller output along the years before the replacement restores the electrolyser performance.

Table 4.17: LCOH results comparison with and without stack degradation across implementation scenarios.

Implementation Scenario	LCOH w/o degradation [€/kg]	LCOH with degradation [€/kg]
Onshore Centralized (On,C)	3.90	4.00
Offshore Centralized (Off,C)	4.45	4.57
Offshore Decentralized (Off,D)	4.69	4.82

The Viana do Castelo case study confirms that for a deep-water Atlantic site with strong wind resources and a relatively close port and shore distances, Centralized Onshore electrolysis offers the most economical pathway at 4.00 €/kg considering stack degradation. Its cost advantages come from having to avoid any large offshore platforms containing the electrolysis plant and minimizing the marine O&M while also having a short HVAC export distance that keeps transmission losses low due to its short distance to port and shore respectively.

Centralized Offshore scenario gains modest efficiency and hydrogen output benefits coming from avoiding electrical transmission losses by using export pipeline but are outweighed by the CAPEX of a large floating platform and a higher offshore O&, resulting in a 14% higher LCOH than On,C at 4.57 €/kg. For Decentralized Offshore, it achieves the highest technical efficiency across all implementation scenarios and eliminates the central platform and any electrical losses, but the need for a distributed conversion units and extra BoP for each electrolysis system per turbine drives both the CAPEX and OPEX up, resulting in the highest LCOH at 4.82 €/kg for a 20% increase against On,C.

Across all scenarios, DECEX is considered as a minor cost component, while the difference in the lifetime hydrogen output remains small. The choice between the different configurations established for this framework relies on the trade-off between CAPEX and OPEX and the minimum efficiency gains for sites with similar characteristics to Viana do Castelo/ This suggests that keeping electrolysis onshore is the most cost-effective strategy for

sites near shore, while offshore options may be justified where export distances or grid constraints make electrical transmission less viable.

Bringing it all together, the techno-economic model makes it clear that for a site like Viana do Castelo that presents a deep water site with strong winds and close to the port and shore, the marginal efficiency gains of offshore electrolysis do not offset the substantial increase in CAPEX and OPEX, as shown in Figure 4.5 where the results for LCOH and lifetime costs are summarized across all implementation scenarios. Onshore Centralized electrolysis remains as the most cost-effective with lowest LCOH over both the Offshore Centralized and Decentralized cases that have increased costs due to offshore O&M and multiple BoP respectively. The model's sensitivity to OPEX multipliers and platform CAPEX suggests that these conclusions could shift in contexts where offshore servicing costs are lower, export distances are much greater, or grid connection is constrained. However, for this case the optimal balance of cost and performance lies firmly onshore, due mainly to the proximity to port and shore and the strong wind resource available at site.

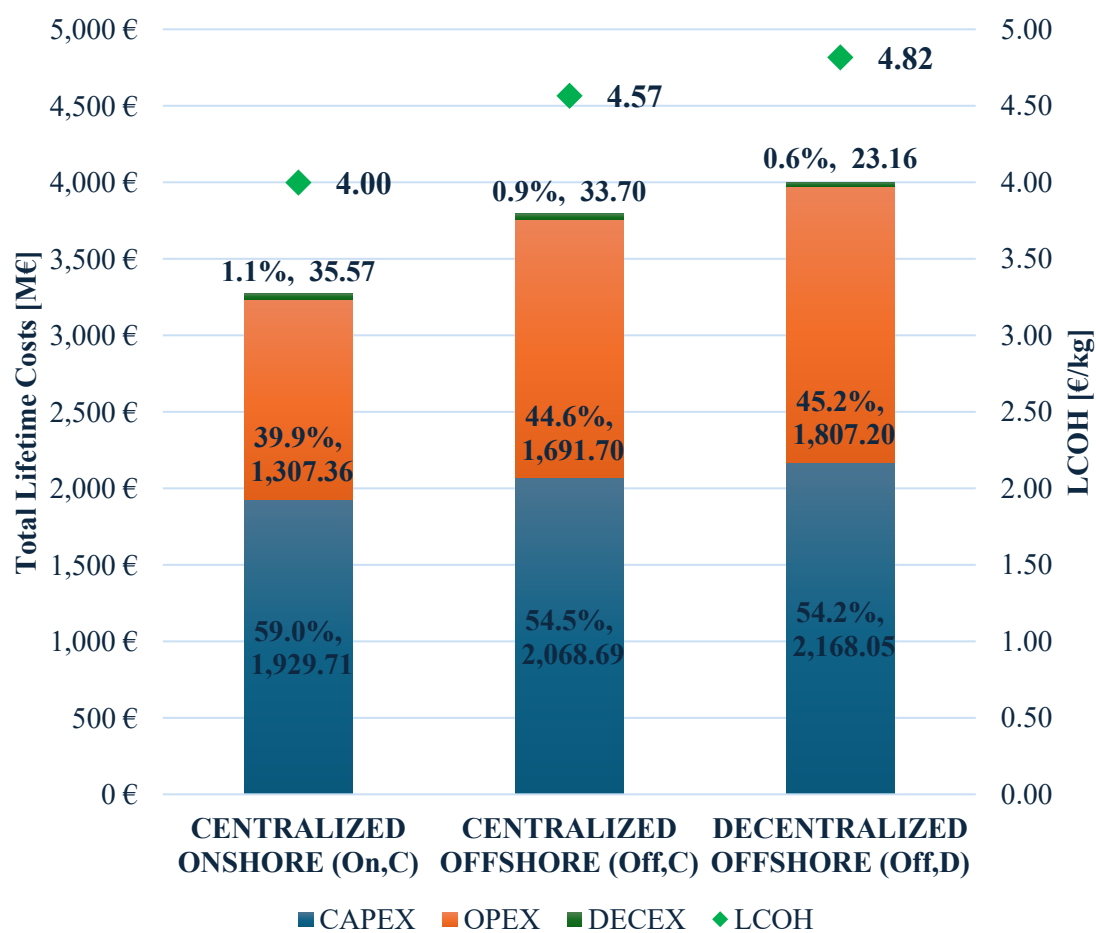


Figure 4.5: Lifetime cost structure and LCOH overview across all implementation scenarios in Viana do Castelo Case Study.

The comparative results presented underscore how the interplay between the capital intensity, operational demands, and efficiency gains shape the economic viability across each of the implementation scenarios and configurations. While the study case model offers a clear ranking for the Viana do Castelo site, these outcomes are inherently sensitive to the shifts in key parameters corresponding to the specific site location which influence the equipment costs, offshore O&M multipliers and electrolyser performance. To fully understand the robustness of the conclusions and to explore under what conditions alternative configurations might become competitive, the following section conducts a targeted sensitivity analysis. This next step tests the resilience of the preferred option and maps the boundaries within the techno-economic advantages identified to determine the influence of each of the key parameters that are related to a site-specific location.

4.3. Sensitivity Analysis

A sensitivity study was conducted to assess robustness and the impact of the location selection on the LCOH results from the techno-economic model for floating offshore hydrogen production. This study consisted in changing 4 key site-specific parameters, which correspond to water depth (m), distance to shore (km), distance to port (km), and wind potential (h/yr). The sensitivity methodology was done by considering the base case values as the LCOH results coming from the case study carried out in the site-specific location chosen in Viana do Castelo. Each of the analyzed parameters will be changing in a series of 20 steps in the whole range chosen, while the rest of the parameters will remain fixed according to the base case, as shown in Table 4.18. For each of the steps, the LCOH was recomputed for the three configurations to isolate the parameter's influence in the techno-economic performance and plotted each of these values as a function of the varied parameter.

Table 4.18: Sensitivity methodology for site-specific parameters.

Parameter	Min Range	Max Range	Step	Base Case
Water Depth [m]	55	150	5	100
Distance to Shore [km]	10	200	10	12
Distance to Port [km]	10	200	10	12.7
Wind Potential [h/yr]	2,650	5,500	150	3,915

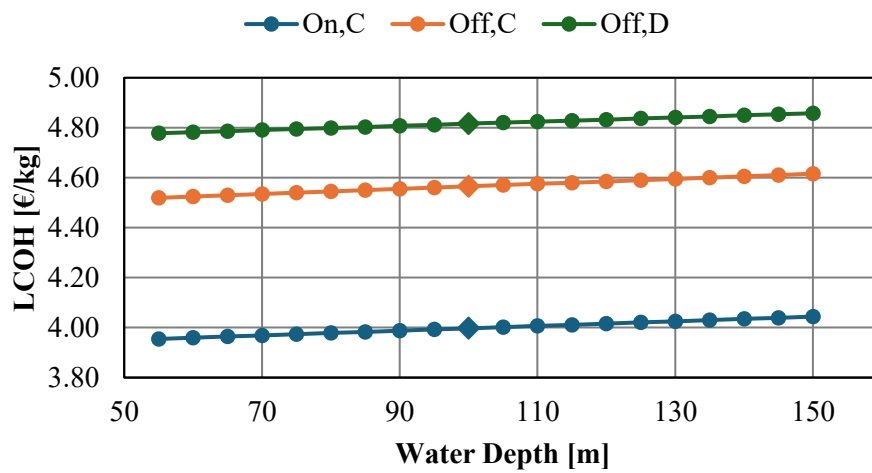


Figure 4.6: LCOH sensitivity analysis with Water Depth parameter for implementation scenarios.

As the water depth increases from the defined range of 55 to 150 meters, corresponding to the cost-effective range of semi-submersible platforms, the LCOH of the three scenarios rises linearly at similar rates due to the equipment cost of floating foundations and inter-array

connections depending on water depth. Figure 4.6 presents the LCOH results for each of the implementation scenarios, in which the On,C ranges from 3.95 to 4.04 €/kg with a $\pm 1.2\%$ change, Off,C ranges from 4.52 to 4.62 €/kg with a $\pm 1.1\%$ change, and the lowest slope coming from Off,D with a range from 4.78 to 4.86 €/kg with a $\pm 0.9\%$ change from base case. This difference in the behavior from both centralized configurations comes from the cost from the offshore platform dedicated to the substation or electrolysis plant and the decentralized not requiring one and having the inter-array pipeline be less costly according to water depth than inter-array cables.

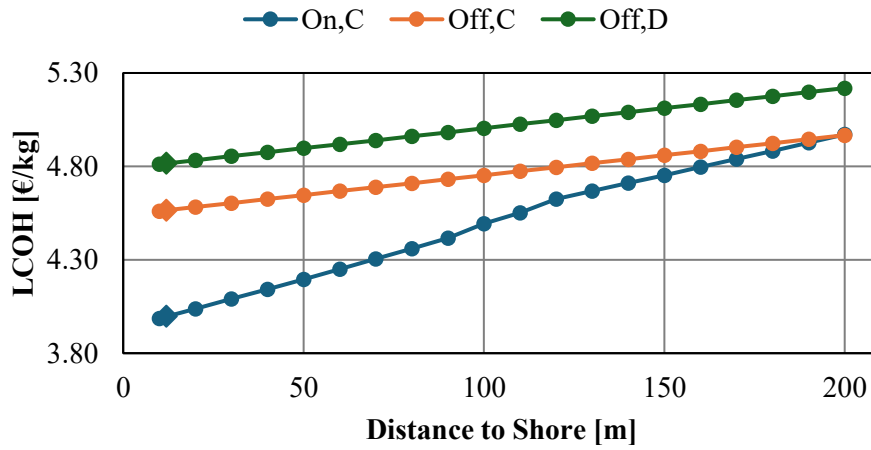


Figure 4.7: LCOH sensitivity analysis with Distance to Shore parameter for implementation scenarios.

Now looking at the distance to shore from the defined range of 10 to 200 km, the transmission length for both cables and pipelines increases. This export length strongly penalizes onshore electrolysis due to the subsea cable length and the associated transmission losses presented. Figure 4.7 presents the LCOH results for each of the implementation scenarios, in which the On,C ranges from 3.99 to 4.97 €/kg for a significant increase of 24% due to the cumulative cable losses in the export cable and the increased failure rates due to the extra length, with a change in the trend at 120 km due to a change into HVDC export cable from then onwards. In the case of the offshore implementation scenarios, hydrogen transport via pipelines presents much less sensitivity due to the distance to shore, with Off,C ranges from 4.56 to 4.97 €/kg with an 8.8% increase and Off,D ranges from 4.81 to 5.22 €/kg with an 8.4% increase. It is possible to observe that as distance to shore grows, the onshore electrolysis has less advantage than the offshore configurations and that the base case was near the best-case scenario in the range considered for the parameter.

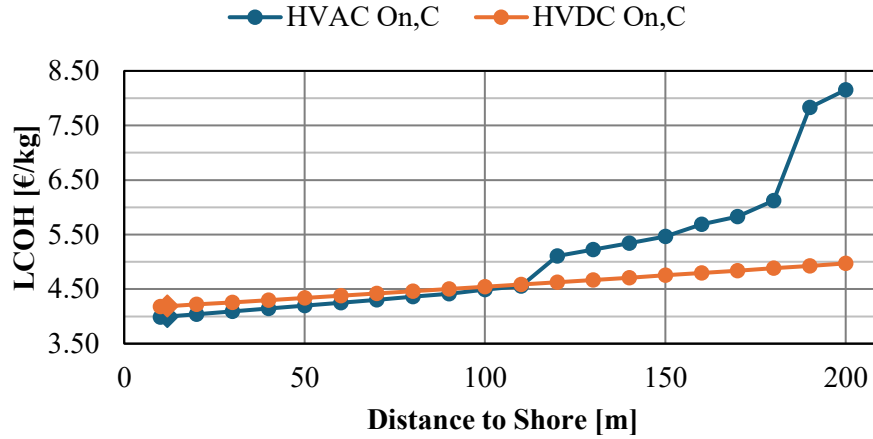


Figure 4.8: HVAC vs. HVDC comparison in Onshore Centralized Scenario.

The influence on the type of transmission system coming from distance to shore can be seen in Figure 4.8, for which the LCOH for both HVAC and HVDC are compared. This shows that HVAC export cables are optimal in this case for distances below 120 km but beyond HVDC become more feasible due to a higher substation CAPEX, but a lower linear losses and cost compared to HVAC systems. Additionally, the reason for the bumps in the linear trend for HVAC cables corresponds to the need for additional power cable lines to be able to transport the capacity of the wind farm. This makes HVDC a preferred option for very long transmission routes or for high-capacity projects.

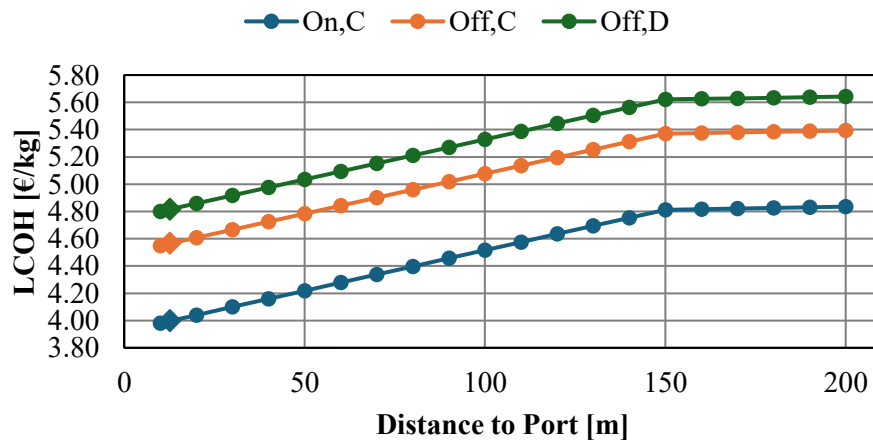


Figure 4.9: LCOH sensitivity analysis with Distance to Port parameter for implementation scenarios.

In the case of changing the distance to port parameter from the chosen range of 10 to 200 km raises the annual logistics OPEX due to the big influence coming from the linearized

cost for CTVs until it reaches a more stable trend once the chartering of an SOV becomes feasible at 150 km and a lower influence coming from the vessel costs due to installation and decommissioning costs. This same trend can be observed in the case for the LCOH of all 3 implementation scenarios, as On,C ranges from 3.98 to 4.83 €/kg for an increase of 20.9%, Off,C climbs from 4.55 to 5.39 €/kg for an increase of 18.1%, and Off,D from 4.80 to 5.64 €/kg with an increase of 17.2%. This makes the distance to port a significant parameter until 150 km, considering as a turning point when SOV becomes feasible and drives a step change in OPEX.

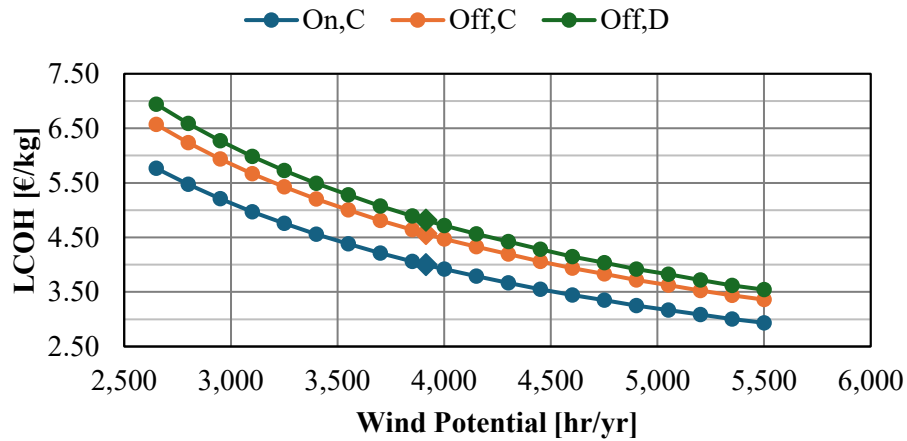


Figure 4.10: LCOH sensitivity analysis with Wind Potential parameter for implementation scenarios.

Lastly, the influence of the wind potential parameter in the range from 2,650 to 5,500 h/yr nearly halves all LCOH values for the implementation scenarios. For On,C it falls from 5.77 to 2.94 €/kg for a 49.1% change, Off,C ranges from 6.57 to 3.36 €/yr for a decrease of 48.9%, and Off,D from 6.94 to 3.54 €/yr for a decrease of 49.0%. All three implementation scenarios track almost in parallel in a decrease in LCOH due to having fixed costs of turbines, platforms and electrolyzers and spread over more hydrogen output due to an increased capacity factor coming from the wind resource.

This sensitivity study reinforces the multicriteria decision to choose Viana do Castelo as the option for hydrogen production using floating offshore wind due to its site-specific parameters at the Atlantic by being characterized by a moderately deep-water site with strong winds and short port and shore distances. Among the four location parameters, wind potential exerts the biggest influence and lever on the resulting LCOH, making it important to consider the capacity factor in the site selection. Additionally, distance to port induces significant cost escalations via the CAPEX and OPEX logistic equations below 150 km and tends to stabilize

above this turning point, while distance to shore increases the transmission distance which critically influences onshore power export from offshore hydrogen export, for which subsea pipelines outperform both HVAC and HVDC cables in long distances. Finally, water depth affects the least as a parameter in this techno-economic model when only considering the range where semi-submersibles are economically feasible.

5. CONCLUSIONS AND FUTURE WORK

The objective set for this work was to evaluate the coupling of floating offshore wind with electrolyzers for green hydrogen production, which demands careful alignment in between the technology choice, foundation design, configuration scheme, storage and transmission logistics, site selection and economic suitability. This chapter synthesizes the main conclusions to highlight how these findings address the original research objectives and summarizes the performance trade-offs, practical constraints, and strategic takeaways for the techno-economic design and framework for floating wind-to-hydrogen systems.

AWE remains the most mature technology with the lowest CAPEX for large scale hydrogen production. However, their reliance on corrosive KOH electrolyte, bulky cell stacks, and a limited dynamic flexibility with a high minimum load of 20%, slow start-up and ramp-up times render them not suitable for floating offshore wind due to the space constraints and the intermittency and variability of the wind resource. In contrast, PEM electrolysis offers a compact footprint, fast dynamic response, high current densities around 1 to 2.2 A/cm², low minimum load of 5%, and pressurized output of hydrogen around 30 bar makes it a current leading candidate for offshore readiness despite its reliance on PGM metals and fluorinated membranes. Emerging technologies like AEM and SOEC hold long term promise. AEM combines advantages from both AWE and PEM by using non-PGM catalysts with pressurized hydrogen output but faces challenges in membrane durability. SOEC has high electrical efficiencies reaching around 88 to 95% and can be paired with industrial heat waste or reversible SOFC operation but faces challenges with high-temperature material degradation due to its operation at 700-850 °C and thermal cycling, which limits its deployment for both technologies without any further advances in the technology.

On the foundation side, fixed structures excel in shallow water up to around 55 meters but are not economically suitable deeper, making floating foundations suitable for deeper depths. Semi-submersibles stand out for depths between 50 to 150 meters and offer a mature design suitable for high sea states and ample deck space to accommodate PEM electrolyser modules. Transmitting electricity or hydrogen onshore presents 3 different configuration schemes with some being more suitable depending on site-specific parameters. Centralized Onshore electrolysis via HVAC or HVDC cables leverages mature power export technologies but has electrical line losses which increase with the length of the export cable, making it suitable for near-shore. Centralized Offshore electrolysis collects the power from the wind farm through inter-array cables and concentrates it into a centralized offshore platform with an electrolysis plant and transmits the hydrogen produced to shore through subsea pipelines. For

Decentralized Offshore electrolysis, in-turbine electrolysis maximizes the network resilience by avoiding single point of failure and uses inter-array and export pipeline for collection and transmission but complicates O&M and raises CAPEX due to electrolyser BoP redundancy.

The combined multi-criteria decision analysis of AHP, Entropy, and TOPSIS identified Viana do Castelo as the best location in the Atlantic European coastline for floating offshore hydrogen production with a 500 MW capacity, with a strong wind resource of around 3,894 h/yr, a deep-water depth of 100 m, and a close distance of shore and port facilities of around 12 km. The integration of PEM electrolyzers into offshore platforms needs to consider mechanical, hydrodynamic, operational and environmental considerations. Hexapod experiments validated that with reinforced skid mounts, PEM electrolyzers maintained correct operational performance and hydrogen crossover risks across static, dynamic and simulated profiles. A hydrodynamic modeling of a 500 MW centralized platform confirmed that locating modules on the upper deck yields acceptable motion responses, with only occasional vertical acceleration exceeding that can be mitigated by refined damping assumptions, inclusion of mooring dynamics, adding partial operation control strategies when exceedance, or rearrangement of general platform, equipment, and PEM modules layout. The inherently intermittent nature of offshore wind requires further fast-ramping control strategies, transient buffering via batteries or water recovery tanks and coordinated power management to guard against membrane dehydration and efficiency losses. Additionally, the corrosive marine atmosphere and ultra-pure water demand of PEM electrolysis requires marine-grade enclosures, protective coatings, cathodic protection, and integrated water treatment with desalination and de-ionization systems to preserve stack integrity and ensure long term durability.

The three configuration schemes were modeled with a techno-economic framework to capture the influences in lifetime costs and technical operation at the chosen Viana do Castelo site. This techno-economic assessment yields LCOH ranges of 4.00 €/kg for Onshore, 4.57 €/kg for Centralized Offshore, and 4.82 €/kg for Decentralized Offshore electrolysis, assuming a 0.12% per 1000 hours stack degradation rate. Sensitivity to wind availability between 2,650 to 5,500 h/yr shifts LCOH around ~49%, identifying the capacity factor as the dominant lever. Export distances beyond ~120 km makes HVAC export cables economically and technically unfeasible due to electrical losses, tipping the balance towards HVDC transmission or hydrogen pipelines. Similarly, port distances escalating towards 150 km increase linearly O&M costs when considering CTV which represents around a ~20% change in LCOH until an SOV becomes economically suitable and stabilizes the LCOH increase. Conversely, water depths between 55 to 150 m where semi-submersible foundations are economically feasible only

influence around ~1%, indicating that floating foundation expenses are a minor driver in this techno-economic framework for the deep-water ranges considered.

Taken together, this comprehensive analysis confirms that PEM electrolysis integrated with semi-submersible platforms offers the most resilient, flexible, and low carbon route for floating offshore wind-to-hydrogen production. These findings confirm that centralized onshore electrolysis remains the most cost-effective pathway for Atlantic sites with a strong wind regime and short port and shore distances. Additionally, offshore electrolysis configurations become advantageous when grid or export constraints extend beyond approximately 120 km, or when onshore space is unavailable. With continuous advancements in catalyst loading, membrane durability, and integrated control, PEM electrolysis plants may be the optimal technology for integration with offshore wind resources and charting a path towards a decarbonized energy system.

5.1. Future Work and Recommendations

This study has established a techno-economic framework for integrating offshore wind with hydrogen production and the impact and specific requirements in offshore environments. To expand deeper towards this analysis, some future works and research streams are included.

Firstly, expanding hydrodynamic studies to capture detailed equipment layout, mooring line stiffness, and platform motions under extreme storm cases to determine operation and survivability for both centralized and in-turbine electrolyzers. This will pinpoint tilt and acceleration limits according to a more realistic case and will result in design guidance to optimize the component placement and mooring configurations that shield the BoP from damaging motions. The detailed equipment and mooring can also be used for cost assumptions.

Second, applying and refining the multi-criteria decision matrix for site-selection to consider other European regions and import corridors to consider and compare fixed foundations performance against floating foundation projects with various spectrum of water depths, wind climates, and grid distances. These comparative rankings will reveal region-specific priorities according to the ranges of site-specific key parameters.

Finally, combining the CAPEX and OPEX assumptions with real market data is essential for industry. Gathering market quotes or public tender figures for turbines, electrolyzers, foundations, and topsides can be fed into a simple cash-flow model that incorporates the loan schedules, subsidy regimes, and carbon-pricing scenarios. This outcome will be a more realistic LCOH result that can be adapted according to the local financing and incentive structures and be used as a decision maker tool by investors and policymakers.

6. ACKNOWLEDGEMENTS

Firstly, I would like to give special thanks to my supervisors that helped me along the way, Dr. Sara Oliveira da Costa (Navantia Seanergies) for consistent support throughout this work by thoughtful feedback, mentoring, and consideration. Dr. Rafael d'Amore (Universidad Politécnica de Madrid) for guiding me along the research at every turn and for the meticulous review of my report.

I also thank Navantia Seanergies for giving me the opportunity to learn directly from industry through an internship to gain insight about various topics related to my thesis and by taking me into a very welcoming atmosphere and making it a very pleasant experience. To all my colleagues, who have been very generous with their time, shared valuable data, and offered practical advice on academic, professional, and personal issues.

I am profoundly grateful to Professor Philippe Rigo (University of Liège), coordinator of the EMSHIP+ program, for giving me the opportunity to participate in this program. I would also like to acknowledge the faculty and staff of both University of Liège and Universidad Politécnica de Madrid through the foundational coursework and facilities provided that enriched my understanding and knowledge of the field.

I would like to also say thanks to my EMSHIP+ cohort for all the wonderful moments shared studying, working, and for all the parties and hanging out after school. I will always cherish these moments and will always keep them close to me.

Finally, I would like to thank my whole family, friends and girlfriend for all the patience, encouragement, and belief in me. Your moral support kept me going during this whole process. I would especially like to thank my parents, Sergio Aranda and Margarita Márquez, my grandparents, Manuel Márquez and Griselda López, and my brother, Sergio Aranda, for making me who I am today and giving me all their support along the way and kept me grounded and motivated during all the long nights away from home and celebrated every milestone along the way.

7. REFERENCES

- [1] World Meteorological Organization, “State of the Global Climate 2024.” Accessed: Mar. 25, 2025. [Online]. Available: <https://wmo.int/publication-series/state-of-global-climate-2024>
- [2] IEA, “Net Zero by 2050 - A Roadmap for the Global Energy Sector,” Oct. 2021, Accessed: Mar. 25, 2025. [Online]. Available: https://iea.blob.core.windows.net/assets/deebef5d-0c34-4539-9d0c-10b13d840027/NetZeroBy2050-ARoadmapfortheGlobalEnergySector_CORR.pdf
- [3] M. Momirlan and T. N. Veziroglu, “The properties of hydrogen as fuel tomorrow in sustainable energy system for a cleaner planet,” *Int J Hydrogen Energy*, vol. 30, no. 7, pp. 795–802, Jul. 2005, doi: 10.1016/J.IJHYDENE.2004.10.011.
- [4] T. Sun, E. Shrestha, S. P. Hamburg, R. Kupers, and I. B. Ocko, “Climate Impacts of Hydrogen and Methane Emissions Can Considerably Reduce the Climate Benefits across Key Hydrogen Use Cases and Time Scales,” *Environ Sci Technol*, vol. 58, no. 12, pp. 5299–5309, Mar. 2024, doi: 10.1021/ACS.EST.3C09030.
- [5] S. Satyapal, “Hydrogen: A Flexible Energy Carrier.” Accessed: Mar. 25, 2025. [Online]. Available: https://www.energy.gov/eere/articles/hydrogen-flexible-energy-carrier?nrg_redirect=473822
- [6] IEA, “Hydrogen production – Global Hydrogen Review 2024 – Analysis - IEA.” Accessed: Mar. 25, 2025. [Online]. Available: <https://www.iea.org/reports/global-hydrogen-review-2024/hydrogen-production>
- [7] Hydrogen Europe, “In a nutshell | Hydrogen Europe.” Accessed: Mar. 25, 2025. [Online]. Available: <https://hydrogeneurope.eu/in-a-nutshell/>
- [8] European Commission, “A Hydrogen Strategy for a climate neutral Europe,” Jul. 2020.
- [9] C. Martínez de León, P. Molina, C. Ríos, and J. J. Brey, “Green hydrogen production’s impact on sustainable development goals,” *Int J Hydrogen Energy*, vol. 142, pp. 642–653, Jun. 2025, doi: 10.1016/J.IJHYDENE.2024.12.355.
- [10] European Hydrogen Observatory, “REPowerEU.” Accessed: Mar. 26, 2025. [Online]. Available: <https://observatory.clean-hydrogen.europa.eu/eu-policy/repowereu>
- [11] Wind Europe, “Wind energy in Europe: 2024 Statistics and the outlook for 2025-2030 | WindEurope.” Accessed: Mar. 27, 2025. [Online]. Available: <https://windeurope.org/intelligence-platform/product/wind-energy-in-europe-2024-statistics-and-the-outlook-for-2025-2030/>
- [12] A. Rogeau, J. Vieubled, M. de Coatpont, P. Affonso Nobrega, G. Erbs, and R. Girard, “Techno-economic evaluation and resource assessment of hydrogen production through offshore wind farms: A European perspective,” *Renewable and Sustainable Energy Reviews*, vol. 187, p. 113699, Nov. 2023, doi: 10.1016/J.RSER.2023.113699.

- [13] A. Ursua, L. M. Gandía, and P. Sanchis, “Hydrogen Production From Water Electrolysis: Current Status and Future Trends,” *Proceedings of the IEEE*, vol. 100, pp. 410–426, Jun. 2012, doi: 10.1109/JPROC.2011.2156750.
- [14] IRENA, “Green Hydrogen Cost Reduction: Scaling up Electrolysers to Meet the 1.5°C Climate Goal,” Abu Dhabi, 2020.
- [15] D. Niblett, M. Delpisheh, S. Ramakrishnan, and M. Mamlouk, “Review of next generation hydrogen production from offshore wind using water electrolysis,” *J Power Sources*, vol. 592, p. 233904, Feb. 2024, doi: 10.1016/J.JPOWSOUR.2023.233904.
- [16] A. S. Emam, M. O. Hamdan, B. A. Abu-Nabah, and E. Elnajjar, “A review on recent trends, challenges, and innovations in alkaline water electrolysis,” *Int J Hydrogen Energy*, vol. 64, pp. 599–625, Apr. 2024, doi: 10.1016/J.IJHYDENE.2024.03.238.
- [17] C. Zhang *et al.*, “Technical and economic analysis of hydrogen production, storage and transportation by offshore wind power in different scenarios: A Guangdong case study,” *Int J Hydrogen Energy*, vol. 94, pp. 829–837, Dec. 2024, doi: 10.1016/J.IJHYDENE.2024.10.346.
- [18] S. Tasleem, C. S. Bongu, M. R. Krishnan, and E. H. Alsharaeh, “Navigating the hydrogen prospect: A comprehensive review of sustainable source-based production technologies, transport solutions, advanced storage mechanisms, and CCUS integration,” *Journal of Energy Chemistry*, vol. 97, pp. 166–215, Oct. 2024, doi: 10.1016/J.JECHEM.2024.05.022.
- [19] E. Schropp *et al.*, “Environmental and material criticality assessment of hydrogen production via anion exchange membrane electrolysis,” *Appl Energy*, vol. 356, p. 122247, Feb. 2024, doi: 10.1016/J.APENERGY.2023.122247.
- [20] N. Sezer, S. Bayhan, U. Fesli, and A. Sanfilippo, “A comprehensive review of the state-of-the-art of proton exchange membrane water electrolysis,” *Mater Sci Energy Technol*, vol. 8, pp. 44–65, Jan. 2025, doi: 10.1016/J.MSET.2024.07.006.
- [21] T. Smolinka, E. T. Ojong, and J. Garche, “Hydrogen Production from Renewable Energies—Electrolyzer Technologies,” *Electrochemical Energy Storage for Renewable Sources and Grid Balancing*, pp. 103–128, Jan. 2015, doi: 10.1016/B978-0-444-62616-5.00008-5.
- [22] V. A. Martinez, H. Ziar, J. W. Haverkort, M. Zeman, and O. Isabella, “Dynamic operation of water electrolyzers: A review for applications in photovoltaic systems integration,” *Renewable and Sustainable Energy Reviews*, vol. 182, p. 113407, Aug. 2023, doi: 10.1016/J.RSER.2023.113407.
- [23] M. Laborde and F. González, *La Energía del Hidrógeno*. CYTED, 2010.
- [24] T. Nguyen, Z. Abdin, T. Holm, and W. Mérida, “Grid-connected hydrogen production via large-scale water electrolysis,” *Energy Convers Manag*, vol. 200, p. 112108, Nov. 2019, doi: 10.1016/J.ENCONMAN.2019.112108.

- [25] S. G. Nnabuiife, A. K. Hamzat, J. Whidborne, B. Kuang, and K. W. Jenkins, "Integration of renewable energy sources in tandem with electrolysis: A technology review for green hydrogen production," *Int J Hydrogen Energy*, vol. 107, pp. 218–240, Mar. 2025, doi: 10.1016/J.IJHYDENE.2024.06.342.
- [26] H. Setyawan, "Teknologi elektroliser untuk hidrogen ramah lingkungan (Bag. 1)," Sep. 2020.
- [27] A. Benmehel, S. Chabab, A. L. Do Nascimento Rocha, M. Chepy, and T. Kousksou, "PEM water electrolyzer modeling: Issues and reflections," *Energy Conversion and Management: X*, vol. 24, p. 100738, Oct. 2024, doi: 10.1016/J.ECMX.2024.100738.
- [28] S. Giancola *et al.*, "Composite short side chain PFSA membranes for PEM water electrolysis," *J Memb Sci*, vol. 570–571, Jun. 2018, doi: 10.1016/j.memsci.2018.09.063.
- [29] S. Vattiata, "PRODUCTION OF GREEN HYDROGEN BY ELECTROLYSER FROM A LARGE-SCALE AGROVOLTAIC POWER PLANT.," 2023.
- [30] J. C. Maya, F. Chejne, C. A. Gómez, J. Montoya, H. Chaquea, and B. Pecha, "Analysys of the performance a PEM-type electrolyzer in variable energy supply conditions," *Chemical Engineering Research and Design*, vol. 196, pp. 526–541, Aug. 2023, doi: 10.1016/J.CHERD.2023.07.002.
- [31] I. Marouani *et al.*, "Integration of Renewable-Energy-Based Green Hydrogen into the Energy Future," *Processes*, vol. 11, no. 9, 2023, doi: 10.3390/pr11092685.
- [32] E. Eikeng, A. Makhsoos, and B. G. Pollet, "Critical and strategic raw materials for electrolyzers, fuel cells, metal hydrides and hydrogen separation technologies," *Int J Hydrogen Energy*, vol. 71, pp. 433–464, Jun. 2024, doi: 10.1016/J.IJHYDENE.2024.05.096.
- [33] D. Sampangi and H. Vurimindi, "Hydrogen production by PEM water electrolysis – A review," *Mater Sci Energy Technol*, vol. 2, pp. 442–454, Jun. 2019, doi: 10.1016/j.mset.2019.03.002.
- [34] S. Yuan, C. Zhao, H. Li, S. Shen, X. Yan, and J. Zhang, "Rational electrode design for low-cost proton exchange membrane water electrolyzers," *Cell Rep Phys Sci*, vol. 5, no. 3, p. 101880, Mar. 2024, doi: 10.1016/J.XCRP.2024.101880.
- [35] N. Jain, A. Roy, R. Jain, and N. Karmakar, "Polymer Electrolyte Membrane Fuel Cells : Alternative to fossil fuels for power supply to Heavy Earth Moving and Allied Machinery in Mining and Civil Engineering Industry," Jun. 2013. doi: 10.13140/RG.2.1.3482.6086.
- [36] M. El-Shafie, "Hydrogen production by water electrolysis technologies: A review," *Results in Engineering*, vol. 20, p. 101426, Dec. 2023, doi: 10.1016/J.RINENG.2023.101426.

- [37] S. Shiva Kumar and H. Lim, “An overview of water electrolysis technologies for green hydrogen production,” *Energy Reports*, vol. 8, pp. 13793–13813, Nov. 2022, doi: 10.1016/J.EGYR.2022.10.127.
- [38] C. Liu *et al.*, “Development of advanced anion exchange membrane from the view of the performance of water electrolysis cell,” *Journal of Energy Chemistry*, vol. 90, pp. 348–369, Mar. 2024, doi: 10.1016/J.JECHEM.2023.11.026.
- [39] C. Li and J. B. Baek, “The promise of hydrogen production from alkaline anion exchange membrane electrolyzers,” *Nano Energy*, vol. 87, p. 106162, Sep. 2021, doi: 10.1016/J.NANOEN.2021.106162.
- [40] A. H. Faqueh and M. D. Symes, “Zero-gap bipolar membrane water electrolyzers: Principles, challenges and practical insights,” *Electrochim Acta*, vol. 493, p. 144345, Jul. 2024, doi: 10.1016/J.ELECTACTA.2024.144345.
- [41] C. Santoro *et al.*, “What is Next in Anion-Exchange Membrane Water Electrolyzers? Bottlenecks, Benefits, and Future,” Apr. 2022, *John Wiley and Sons Inc.* doi: 10.1002/cssc.202200027.
- [42] K. Chand and O. Paladino, “Recent developments of membranes and electrocatalysts for the hydrogen production by anion exchange membrane water electrolyzers: A review,” *Arabian Journal of Chemistry*, vol. 16, no. 2, p. 104451, Feb. 2023, doi: 10.1016/J.ARABJC.2022.104451.
- [43] Q. Xu *et al.*, “Anion Exchange Membrane Water Electrolyzer: Electrode Design, Lab-Scaled Testing System and Performance Evaluation,” *EnergyChem*, vol. 4, no. 5, p. 100087, Sep. 2022, doi: 10.1016/J.ENCHEM.2022.100087.
- [44] C. Simari *et al.*, “Composite anion exchange membranes based on polysulfone and silica nanoscale ionic materials for water electrolyzers,” *Electrochim Acta*, vol. 462, p. 142788, Sep. 2023, doi: 10.1016/J.ELECTACTA.2023.142788.
- [45] L. Liu, H. Ma, M. Khan, and B. S. Hsiao, “Recent Advances and Challenges in Anion Exchange Membranes Development/Application for Water Electrolysis: A Review,” *Membranes (Basel)*, vol. 14, no. 4, 2024, doi: 10.3390/membranes14040085.
- [46] Y. Patcharavorachot, N. Chatrattanawet, A. Arpornwichanop, and D. Saebea, “Comparative energy, economic, and environmental analyses of power-to-gas systems integrating SOECs in steam-electrolysis and co-electrolysis and methanation,” *Thermal Science and Engineering Progress*, vol. 42, p. 101873, Jul. 2023, doi: 10.1016/J.TSEP.2023.101873.
- [47] E. Schropp, G. Naumann, and M. Gaderer, “Hydrogen production via solid oxide electrolysis: Balancing environmental issues and material criticality,” *Advances in Applied Energy*, vol. 16, p. 100194, Dec. 2024, doi: 10.1016/J.ADAPEN.2024.100194.

- [48] A. Nechache and S. Hody, "Alternative and innovative solid oxide electrolysis cell materials: A short review," *Renewable and Sustainable Energy Reviews*, vol. 149, p. 111322, Oct. 2021, doi: 10.1016/J.RSER.2021.111322.
- [49] X. Zhang, J. E. O'Brien, R. C. O'Brien, J. J. Hartvigsen, G. Tao, and G. K. Housley, "Improved durability of SOEC stacks for high temperature electrolysis," *Int J Hydrogen Energy*, vol. 38, no. 1, pp. 20–28, Jan. 2013, doi: 10.1016/J.IJHYDENE.2012.09.176.
- [50] Seagreen Wind Energy, "Scotland's largest offshore wind farm," <https://www.seagreenwindenergy.com/>.
- [51] S. Rehman, L. M. Alhems, M. M. Alam, L. Wang, and Z. Toor, "A review of energy extraction from wind and ocean: Technologies, merits, efficiencies, and cost," *Ocean Engineering*, vol. 267, p. 113192, Jan. 2023, doi: 10.1016/J.OCEANENG.2022.113192.
- [52] Equinor, "Hywind Tampen," <https://www.equinor.com/energy/hywind-tampen>.
- [53] Principle Power, "Projects: Kincardine Offshore Wind Farm - Principle Power, Inc.," <https://www.principlepower.com/projects/kincardine-offshore-wind-farm>.
- [54] WindFloat Atlantic, "WindFloat Atlantic celebrates 5 years of operation | Windfloat Atlantic," <https://www.windfloat-atlantic.com/windfloat-atlantic-celebra-5-anos-de-operacoes-com-sucesso/>.
- [55] DNV, "Floating Offshore Wind: The next five years," <https://www.dnv.com/focus-areas/floating-offshore-wind/floating-offshore-wind-the-next-five-years/>.
- [56] S. Hong, J. McMorland, H. Zhang, M. Collu, and K. H. Halse, "Floating offshore wind farm installation, challenges and opportunities: A comprehensive survey," *Ocean Engineering*, vol. 304, p. 117793, Jul. 2024, doi: 10.1016/J.OCEANENG.2024.117793.
- [57] P. D. Sclavounos, S. Lee, J. DiPietro, G. Potenza, P. Caramuscio, and G. De Michele, "FLOATING OFFSHORE WIND TURBINES: TENSION LEG PLATFORM AND TAUGHT LEG BUOY CONCEPTS SUPPOTING 3-5 MW WIND TURBINES," Warsaw, Apr. 2010. Accessed: Jun. 16, 2025. [Online]. Available: <https://web.mit.edu/flowlab/pdf/EWEC2010.pdf>
- [58] SBM Offshore, "Floating Offshore Wind - SBM Offshore," <https://www.sbmoffshore.com/what-we-do/floating-offshore-wind/>.
- [59] Bluenewables, "CT-bos - Bluenewables," <https://bluenewables.com/CT-bos/>.
- [60] Y. Wang, T. Yao, Y. Zhao, and Z. Jiang, "Review of tension leg platform floating wind turbines: Concepts, design methods, and future development trends," *Ocean Engineering*, vol. 324, p. 120587, Apr. 2025, doi: 10.1016/J.OCEANENG.2025.120587.
- [61] F. J. Madsen *et al.*, "Experimental analysis of the scaled DTU10MW TLP floating wind turbine with different control strategies," *Renew Energy*, vol. 155, pp. 330–346, Aug. 2020, doi: 10.1016/J.RENENE.2020.03.145.

- [62] J. Chen and M. H. Kim, “Review of Recent Offshore Wind Turbine Research and Optimization Methodologies in Their Design,” *J Mar Sci Eng*, vol. 10, Jan. 2022, doi: 10.3390/jmse10010028.
- [63] D. Li, W. Lu, X. Li, X. Guo, J. Li, and W. Duan, “Second-order resonant motions of a deep-draft semi-submersible under extreme irregular wave excitation,” *Ocean Engineering*, vol. 209, p. 107496, Aug. 2020, doi: 10.1016/J.OCEANENG.2020.107496.
- [64] A. Maximiano, G. Vaz, R. Torres, L. Voltá, and T. Lourenço, “D5.4 Benchmark of PivotBuoy Compared to Other Offshore Wind Floating Systems,” Jun. 2021. doi: 10.13140/RG.2.2.31161.65120.
- [65] D. Nie *et al.*, “Investigation of mooring breakage impact on dynamic responses of a 15 MW floating offshore wind turbine,” *Ocean Engineering*, vol. 311, p. 118996, Nov. 2024, doi: 10.1016/J.OCEANENG.2024.118996.
- [66] R. Chitteth, C. Desmond, F. Judge, J.-J. Serraris, and J. Murphy, “Floating wind turbines: marine operations challenges and opportunities,” *Wind Energy Science*, vol. 7, pp. 903–924, Apr. 2022, doi: 10.5194/wes-7-903-2022.
- [67] Centrale Nantes SEM-REV, “FLOATGEN - SEM-REV,” <https://sem-rev.ec-nantes.fr/english-version/devices-tested/floating-offshore-wind-turbine-flotagen>.
- [68] BW Ideol, “Hibiki,” <https://www.bw-ideol.com/en/japanese-demonstrator>.
- [69] EOLMED, “Pilot Wind Farm,” <https://eolmed.qair.energy/en/project/pilot-wind-farm/>.
- [70] 4C Offshore, “EolMed Floating Wind Farm,” <https://www.4coffshore.com/windfarms/france/eolmed-france-fr64.html>.
- [71] Z. Li, Q. Song, F. An, B. Zhao, Z. Yu, and R. Zeng, “Review on DC transmission systems for integrating large-scale offshore wind farms,” *Energy Conversion and Economics*, vol. 2, no. 1, pp. 1–14, 2021, doi: <https://doi.org/10.1049/enc2.12023>.
- [72] A. Singlitico, J. Østergaard, and S. Chatzivasileiadis, “Onshore, offshore or in-turbine electrolysis? Techno-economic overview of alternative integration designs for green hydrogen production into Offshore Wind Power Hubs,” *Renewable and Sustainable Energy Transition*, vol. 1, p. 100005, Aug. 2021, doi: 10.1016/J.RSET.2021.100005.
- [73] O. S. Ibrahim, A. Singlitico, R. Proskovics, S. McDonagh, C. Desmond, and J. D. Murphy, “Dedicated large-scale floating offshore wind to hydrogen: Assessing design variables in proposed typologies,” *Renewable and Sustainable Energy Reviews*, vol. 160, p. 112310, May 2022, doi: 10.1016/J.RSER.2022.112310.
- [74] M. Matošec, “Repurposing gas transmission pipelines for hydrogen,” 2023.
- [75] L. Wilcox, “Repurposing Legacy Oil and Gas Assets for Green Hydrogen Production,” Feb. 2024. Accessed: Jun. 16, 2025. [Online]. Available: https://www.sccs.org.uk/sites/default/files/inline-files/06_Lawrence_Wilcox_plenary.pdf

- [76] P. Rajeev and D. J. Robert, “Effect of Irregular Seabed Profile on Upheaval Buckling of Buried Offshore Pipelines,” *J Pipeline Syst Eng Pract*, vol. 8, no. 4, p. 4017017, 2017, doi: 10.1061/(ASCE)PS.1949-1204.0000281.
- [77] Q. Bai and Y. Bai, “Flexible Pipe,” *Subsea Pipeline Design, Analysis, and Installation*, pp. 559–578, Jan. 2014, doi: 10.1016/B978-0-12-386888-6.00024-9.
- [78] B. A. Oni, S. E. Sanni, and A. N. Misiani, “Green hydrogen production in offshore environments: A comprehensive review, current challenges, economics and future-prospects,” *Int J Hydrogen Energy*, vol. 125, pp. 277–309, May 2025, doi: 10.1016/J.IJHYDENE.2025.03.429.
- [79] V. Monsma, T. Illson, R. Thodla, and A. Hussain, “Repurposing onshore pipelines is essential to scaling hydrogen. How can it be done in practice? ,” Oslo, Apr. 2023.
- [80] Lhyfe, “Sealhyfe produces its first kilos of green hydrogen in the Atlantic,” <https://www.lhyfe.com/press/lhyfe-announces-that-sealhyfe-the-worlds-first-offshore-hydrogen-production-pilot-produces-its-first-kilos-of-green-hydrogen-in-the-atlantic-ocean/>.
- [81] ACCIONA, “OCEANH2, the industrial research project coordinated by ACCIONA, launches,” Mar. 2021.
- [82] PosHYdon, “About PosHYdon,” <https://poshydon.com/en/home-en/about-poshydon/>.
- [83] L. Collins, “World’s first offshore platform to produce green hydrogen, ammonia and methanol completed in China,” Apr. 2025.
- [84] A. Habibic, “‘World’s first’ hydrogen shore power demo presented at Port of Leith,” Mar. 2025.
- [85] CORDIS, “Offshore hydrogen from shoreside wind turbine integrated electrolyser,” 2025. doi: 10.3030/101007168.
- [86] Lhyfe, “Offshore Hydrogen Production on a New Scale: HOPE Project,” Jun. 2023.
- [87] Federal Ministry of Research, Technology and Space, “How the H2Mare project intends to produce hydrogen offshore,” <https://www.wasserstoff-leitprojekte.de/projects/h2mare>.
- [88] TechnipFMC, “Deep Purple™ Pilot - TechnipFMC plc,” <https://www.technipfmc.com/en/what-we-do/new-energy/hydrogen/deep-purple-pilot/>.
- [89] DEME, “HYPORT®: green hydrogen plant in Ostend,” <https://www.deme-group.com/news/hyportr-green-hydrogen-plant-ostend>.
- [90] RWE, “H₂ pilot plant in Lingen | Hydrogen project of RWE,” <https://www.rwe.com/en/research-and-development/hydrogen-projects/lingen-pilot-h2-electrolysis-plant/>.

- [91] Simply Blue Energy, “Salamander Project - Floating Offshore Wind Scotland - Simply Blue Energy,” <https://salamanderfloatingwind.com/>.
- [92] HØST PtX Esbjerg, “About us - HØST PtX Esbjerg,” <https://hoestptxesbjerg.dk/about-host/>.
- [93] RWE, “H2opZee – Demonstration project for green hydrogen in the Netherlands,” <https://www.rwe.com/en/research-and-development/hydrogen-projects/h2opzee/>.
- [94] RWE, “NorthH₂ | Hydrogen project of RWE,” <https://www.rwe.com/en/research-and-development/hydrogen-projects/north2/>.
- [95] Dolphyn Hydrogen, “Where We Are,” <https://www.dolphynhydrogen.com/where-we-are#large-scale-commercial-developments>.
- [96] AquaVentus Förderverein e.V., “AquaVentus,” <https://aquaventus.org/en/>.
- [97] RWE, “AquaVentus – Hydrogen production in the North Sea | RWE,” <https://www.rwe.com/en/research-and-development/hydrogen-projects/aquaventus/>.
- [98] Bureau Veritas, “Offshore certification,” <https://marine-offshore.bureauveritas.com/offshore/offshore-certification>.
- [99] European Commission, “Renewable Energy Directive,” https://energy.ec.europa.eu/topics/renewable-energy/renewable-energy-directive-targets-and-rules/renewable-energy-directive_en.
- [100] European Commission, “Commission sets out rules for renewable hydrogen,” Feb. 2023.
- [101] European Commission, “Trans-European Networks for Energy,” https://energy.ec.europa.eu/topics/infrastructure/trans-european-networks-energy_en.
- [102] European Hydrogen Backbone, “The European Hydrogen Backbone (EHB) initiative | EHB European Hydrogen Backbone,” <https://www.ehb.eu/>.
- [103] IEA, “Global Hydrogen Review 2024 – Analysis - IEA,” 2024.
- [104] International Organization for Standardization, “Hydrogen generators using water electrolysis — Industrial, commercial, and residential applications (ISO 22734:2019),” 2019.
- [105] TÜV SÜD, “Certification of Electrolysers against ISO 22734,” <https://www.tuvsud.com/en-gb/services/auditing-and-system-certification/certification-of-electrolysers-against-iso-22734>.
- [106] International Organization for Standardization, “Hydrogen generators using water electrolysis Part 2: Testing guidance for performing electricity grid service (ISO/AWI TS 22734-2),” 2025.
- [107] International Organization for Standardization, “Gaseous hydrogen — Fuelling stations Part 1: General requirements (ISO 19880-1:2020),” 2020.

- [108] International Electrotechnical Commission, “Fuel cell technologies - Part 2-100: Fuel cell modules - Safety (IEC 62282-2-100:2020),” 2020.
- [109] DNV, “DNV-ST-J301 Electrolyser systems,” 2024.
- [110] ASME, “Hydrogen Codes & Standards - ASME,” <https://www.asme.org/resources/clean-hydrogen#codes-and-standards>.
- [111] K. Xu, “Introduction to ASME Code Rules on Electrochemical Cell Stacks for Electrolysis,” <https://www.nationalboard.org/NationaBoardNews.aspx?NewsPageID=3276>.
- [112] A. Glover, J. T. Mohr, and A. Baird, “Codes and Standards Assessment for Hydrogen Blends into the Natural Gas Infrastructure,” Jun. 2021. doi: 10.2172/1871191.
- [113] CSA Group, “An overview of CSA Group standards, codes, and activities for the hydrogen ecosystem,” <https://www.csagroup.org/article/an-overview-of-csa-group-standards-codes-and-activities-for-the-hydrogen-ecosystem/>.
- [114] CSA Group, “Enclosed hydrogen equipment — Safety (CSA/ANSI B107:24),” 2024.
- [115] H2Tools, “What qualifications or certifications should be required for an electrolyzer?,” <https://h2tools.org/faq/electrolyzer-qualificationscertifications>.
- [116] H2Tools, “Best Practices Overview,” <https://h2tools.org/bestpractices/best-practices-overview>.
- [117] G. Pawelec, J. Fonseca, and M. Maron, “Hydrogen Outlook - Hydrogen x REVOLVE,” 2022.
- [118] Clean Hydrogen JU, “Chapter 2 2022 Hydrogen Supply Capacity and Demand,” 2022. Accessed: Aug. 05, 2025. [Online]. Available: <https://observatory.clean-hydrogen.europa.eu/sites/default/files/2023-05/Chapter-2-FCHO-Market-2022-Final.pdf>
- [119] W. Liu, H. Zuo, J. Wang, Q. Xue, B. Ren, and F. Yang, “The production and application of hydrogen in steel industry,” *Int J Hydrogen Energy*, vol. 46, no. 17, pp. 10548–10569, Mar. 2021, doi: 10.1016/J.IJHYDENE.2020.12.123.
- [120] J. Fonseca, “Clean Hydrogen Monitor 2022: Planned clean hydrogen consumption in industry,” 2022. Accessed: Jun. 21, 2025. [Online]. Available: https://usercontent.one/wp/hydrogeneurope.eu/wp-content/uploads/2022/10/Clean_Hydrogen_Monitor_10-2022_DIGITAL.pdf
- [121] A. Walstad, “Germany Begins Pipeline Conversions to Fulfill Lofty Hydrogen Ambitions,” <https://pgjonline.com/magazine/2025/march-2025-vol-252-no-3/features/germany-begins-pipeline-conversions-to-fulfill-lofty-hydrogen-ambitions>.

- [122] Strategy&, “H2 readiness of German industry,” 2023. Accessed: Jun. 23, 2025. [Online]. Available: <https://www.strategyand.pwc.com/de/en/industries/energy-utilities-resources/hydrogen-economy/strategyand-hydrogen-economy.pdf>
- [123] Messe Düsseldorf GmbH, “Germany’s seven largest hydrogen projects in the area of production and infrastructure,” https://www.wiretradefair.com/en/Media_News/News/Topics/Germany_s_seven_largest_hydrogen_projects_in_the_area_of_production_and_infrastructure.
- [124] Baker Mckenzie, “Global Hydrogen Policy Tracker - Germany - Hydrogen Developments,” <https://resourcehub.bakermckenzie.com/en/resources/hydrogen-heat-map/emea/germany/topics/hydrogen-developments>.
- [125] Green Hydrogen Organisation, “GH2 Country Portal - Sweden,” <https://gh2.org/countries/sweden>.
- [126] Green H2, “Lhyfe Secures €11M Funding to Build Green Hydrogen Production Facility in Sweden,” Feb. 2025.
- [127] A. Čučuk, “Nordic-Baltic Hydrogen Corridor project moves forward,” Dec. 2024.
- [128] LTU Lulea University of Technology and VTT Technical Research Centre of Finland, “The Hydrogen Map. Sweden and Finland 2025-02,” https://ltu.instante.se/V%C3%A4tgas/Hydrogen_map_English_112024.html.
- [129] R. Parkes, “H2 subsidies | The Netherlands grants €800m for over 1GW of green hydrogen projects for heavy industry,” Dec. 2022.
- [130] Roland Berger and INYCOM, “Hydrogen Valleys,” https://h2v.eu/hydrogen-valleys?populate=&field_ch_1_q_10_value=NL&field_value_chain_coverage_target_id=All&field_end_uses_target_id=All.
- [131] Hydrogen Europe, “Parties sign for world’s first green hydrogen import corridor,” <https://hydrogeneurope.eu/parties-sign-for-worlds-first-green-hydrogen-import-corridor/>.
- [132] G. Erbach, N. Dewulf, and V. Seppälä, “The Netherlands’ climate action strategy,” Dec. 2024.
- [133] R. Perkins, “Air Liquide to build green hydrogen plant for TotalEnergies’ La Mede biorefinery,” Nov. 2024.
- [134] France Hydrogène, “A road-map for an ambitious hydrogen strategy by 2030 Part 2,” Dec. 2022. Accessed: Jun. 25, 2025. [Online]. Available: <https://www.france-hydrogene.org/app/uploads/sites/4/2023/01/VF-Executive-summary-FH-2022-EN-Web.pdf>
- [135] M. Dulian, G. Erbach, and S. Chahri, “Renewable and low-carbon hydrogen: State of play and outlook,” Feb. 2025. Accessed: Jun. 25, 2025. [Online]. Available:

https://www.europarl.europa.eu/RegData/etudes/BRIE/2025/767227/EPRS_BRI%282025%29767227_EN.pdf

- [136] Fuel Cells Works, “Spain Advances Green Hydrogen with €1.2B H2 Hubs Program, Selecting Repsol, EDP, Moeve, BP, and Iberdrola for Key Projects,” <https://fuelcellsworks.com/2025/02/07/green-hydrogen/spain-advances-green-hydrogen-with-1-2b-h2-hubs-program-selecting-repsol-edp-moeve-bp-and-iberdrola-for-key-projects>.
- [137] Global Energy Monitor, “Spanish Hydrogen Backbone,” https://www.gem.wiki/Spanish_Hydrogen_Backbone.
- [138] Enagás, “H2med - Hydrogen Network - Enagás,” <https://www.enagas.es/en/energy-transition/hydrogen-network/h2med/>.
- [139] Asociación Española del Hidrógeno, “Hydrogen project census,” <https://aeh2.org/en/hydrogen-project-census/>.
- [140] M. Kuhn and I.-P. Yovchev, “Clean Hydrogen Monitor 2022: Hydrogen transport and storage infrastructure,” 2022. Accessed: Jun. 25, 2025. [Online]. Available: https://usercontent.one/wp/hydrogeneurope.eu/wp-content/uploads/2022/10/Clean_Hydrogen_Monitor_10-2022_DIGITAL.pdf
- [141] ENTSG, GIE, EUROGAS, CEDEC, GD4S, and GEODE, “H2 Infrastructure Map Europe,” <https://www.h2inframap.eu/>.
- [142] H. Díaz and C. Guedes Soares, “An integrated GIS approach for site selection of floating offshore wind farms in the Atlantic continental European coastline,” *Renewable and Sustainable Energy Reviews*, vol. 134, p. 110328, Dec. 2020, doi: 10.1016/J.RSER.2020.110328.
- [143] J. Martínez, “USO DE MÉTODOS MULTICRITERIO DE TOMA DE DECISIONES PARA LA SELECCIÓN DE BIOMASA EN REACTORES FISCHER TROPSCH,” *Ingenius*, p. 27, Jul. 2016, doi: 10.17163/ings.n15.2016.03.
- [144] M. Piantanakulchai and N. Seangkhao, “Evaluation of alternatives in transportation planning using multi-stakeholders multi-objectives AHP modeling,” https://www.researchgate.net/publication/228426663_Evaluation_of_alternatives_in_transportation_planning_using_multi-stakeholders_multi-objectives_AHP_modeling.
- [145] I. C. Gil-García, A. Ramos-Escudero, Á. Molina-García, and A. Fernández-Guillamón, “GIS-based MCDM dual optimization approach for territorial-scale offshore wind power plants,” *J Clean Prod*, vol. 428, p. 139484, Nov. 2023, doi: 10.1016/J.JCLEPRO.2023.139484.
- [146] Z. N. Shehab, R. M. Faisal, and S. W. Ahmed, “Multi-criteria decision making (MCDM) approach for identifying optimal solar farm locations: A multi-technique comparative analysis,” *Renew Energy*, vol. 237, p. 121787, Dec. 2024, doi: 10.1016/J.RENENE.2024.121787.

- [147] S. Pfenninger and I. Staffell, “Renewables.ninja.” Accessed: Jul. 28, 2025. [Online]. Available: <https://www.renewables.ninja/>
- [148] C. A. Rodríguez Castillo, M. Collu, and F. Brennan, “Design considerations and preliminary hydrodynamic analysis of an offshore decentralised floating wind-hydrogen system,” *Int J Hydrogen Energy*, vol. 89, pp. 496–506, Nov. 2024, doi: 10.1016/J.IJHYDENE.2024.09.340.
- [149] T. Liu *et al.*, “In-situ direct seawater electrolysis using floating platform in ocean with uncontrollable wave motion,” *Nat Commun*, vol. 15, Jul. 2024, doi: 10.1038/s41467-024-49639-6.
- [150] A. Di Blasi *et al.*, “Evaluation of materials and components degradation of a PEM electrolyzer for marine applications,” *Int J Hydrogen Energy*, vol. 38, no. 18, pp. 7612–7615, Jun. 2013, doi: 10.1016/J.IJHYDENE.2012.10.062.
- [151] E. Amores, M. Sánchez-Molina, and M. Sánchez, “Effects of the marine atmosphere on the components of an alkaline water electrolysis cell for hydrogen production,” *Results in Engineering*, vol. 10, p. 100235, Jun. 2021, doi: 10.1016/J.RINENG.2021.100235.
- [152] A. P. Ekhar, “Techno-economic analysis of offshore platforms for green hydrogen production,” 2021. Accessed: Jul. 28, 2025. [Online]. Available: <https://repository.tudelft.nl/record/uuid:240bc535-b869-4a67-b8e3-63454e7984ee>
- [153] Elewit, “Construyendo el futuro de la energía off-shore con el desarrollo de subestaciones eléctricas flotantes cero emisiones.” Accessed: Jul. 28, 2025. [Online]. Available: <https://www.elewit.ventures/es/actualidad/proyecto-ecofoss-construyendo-futuro-de-energia-offshore-con-desarrollo-subestaciones-electricas-flotantes-cero-emisiones>
- [154] PORTUS (Puertos del Estado), “Datos Históricos Oleaje: Boya Costera de Silleiro.” Accessed: Jul. 28, 2025. [Online]. Available: <https://portus.puertos.es/#/>
- [155] A. Z. Arsad *et al.*, “Hydrogen electrolyser technologies and their modelling for sustainable energy production: A comprehensive review and suggestions,” *Int J Hydrogen Energy*, vol. 48, no. 72, pp. 27841–27871, Aug. 2023, doi: 10.1016/J.IJHYDENE.2023.04.014.
- [156] V. A. Martinez Lopez, H. Ziar, J. W. Haverkort, M. Zeman, and O. Isabella, “Dynamic operation of water electrolyzers: A review for applications in photovoltaic systems integration,” *Renewable and Sustainable Energy Reviews*, vol. 182, p. 113407, Aug. 2023, doi: 10.1016/J.RSER.2023.113407.
- [157] Y. Xu, G. Li, Y. Gui, and Z. Li, “Generation of input spectrum for electrolysis stack degradation test applied to wind power PEM hydrogen production,” *Global Energy Interconnection*, vol. 7, no. 4, pp. 462–474, Aug. 2024, doi: 10.1016/J.GLOEI.2024.08.006.

- [158] T. Pettersen, E. Cossar, T. H. Bergström, Y. D. Raka, S. Lee, and F. Zenith, “Simulation study on preventing explosive mixture formation in PEM electrolyzers’ water recovery tanks,” *Int J Hydrogen Energy*, vol. 84, pp. 1021–1032, Sep. 2024, doi: 10.1016/J.IJHYDENE.2024.07.439.
- [159] T. Egeland-Eriksen, J. F. Jensen, Ø. Ulleberg, and S. Sartori, “Simulating offshore hydrogen production via PEM electrolysis using real power production data from a 2.3 MW floating offshore wind turbine,” *Int J Hydrogen Energy*, vol. 48, no. 74, pp. 28712–28732, Aug. 2023, doi: 10.1016/J.IJHYDENE.2023.03.471.
- [160] E. Summers, J. Race, D. Mignard, M. Tian, and M. A. Almoghayer, “Offshore wind-to-hydrogen: the impact of intermittency on hydrogen production and transport,” in *Proceedings of the International Conference on Offshore Mechanics and Arctic Engineering - OMAE*, American Society of Mechanical Engineers (ASME), 2024. doi: 10.1115/OMAE2024-131833.
- [161] E. Nguyen, P. Olivier, M. C. Pera, E. Pahon, and R. Roche, “Impacts of intermittency on low-temperature electrolysis technologies: A comprehensive review,” *Int J Hydrogen Energy*, vol. 70, pp. 474–492, Jun. 2024, doi: 10.1016/J.IJHYDENE.2024.05.217.
- [162] E. Crespi, G. Guandalini, L. Mastropasqua, S. Campanari, and J. Brouwer, “Experimental and theoretical evaluation of a 60 kW PEM electrolysis system for flexible dynamic operation,” *Energy Convers Manag*, vol. 277, p. 116622, Feb. 2023, doi: 10.1016/J.ENCONMAN.2022.116622.
- [163] H. Kojima, K. Nagasawa, N. Todoroki, Y. Ito, T. Matsui, and R. Nakajima, “Influence of renewable energy power fluctuations on water electrolysis for green hydrogen production,” *Int J Hydrogen Energy*, vol. 48, no. 12, pp. 4572–4593, Feb. 2023, doi: 10.1016/J.IJHYDENE.2022.11.018.
- [164] W. Zhao *et al.*, “Membrane distillation for producing ultra-pure water for PEM electrolysis,” *Int J Hydrogen Energy*, vol. 99, pp. 232–240, Jan. 2025, doi: 10.1016/J.IJHYDENE.2024.12.219.
- [165] BVG Associates, “I.4.1 Anchor-handling vessel | Guide to a floating offshore wind farm.” Accessed: Aug. 05, 2025. [Online]. Available: <https://guidetofloatingoffshorewind.com/guide/i-installation-and-commissioning/i-4-anchor-and-mooring-pre-installation/i-4-1-anchor-handling-vessel/>
- [166] BVG Associates, “I.6.1 Tow-out | Guide to a floating offshore wind farm.” Accessed: Aug. 05, 2025. [Online]. Available: <https://guidetofloatingoffshorewind.com/guide/i-installation-and-commissioning/i-6-floating-offshore-wind-turbine-installation/i-6-1-tow-out/>
- [167] C. A. Chen, D. Chen, K. H. Chen, K. T. Ma, Y. Igarashi, and Z. Y. Lai, “DESIGN OF MOORING SYSTEM FOR A 15MW SEMI-SUBMERSIBLE, TAIDAFLOAT, IN TAIWAN STRAIT,” *Proceedings of the International Conference on Offshore*

- Mechanics and Arctic Engineering - OMAE*, vol. 5, 2023, doi: 10.1115/OMAE2023-104394.
- [168] ShipUniverse, “The Offshore Wind Boom: What Shipowners Need to Know – Ship Universe.” Accessed: Aug. 05, 2025. [Online]. Available: <https://www.shipuniverse.com/the-offshore-wind-boom-what-shipowners-need-to-know/>
- [169] Siemens Energy Global GmbH & Co. KG, “Hydrogen and Power-to-X solutions Versatile and scalable technology to make a difference in the energy transition,” 2024, Accessed: Aug. 05, 2025. [Online]. Available: https://p3.aprimocdn.net/siemensenergy/973beb1b-97e0-4150-9c2e-b29800761a8c/Electrolyzer_Brochure_Hydrogen_PowertoX-pdf_Original%20file.pdf
- [170] A. Singlitico, J. Østergaard, and S. Chatzivasileiadis, “Onshore, offshore or in-turbine electrolysis? Techno-economic overview of alternative integration designs for green hydrogen production into Offshore Wind Power Hubs,” *Renewable and Sustainable Energy Transition*, vol. 1, p. 100005, Aug. 2021, doi: 10.1016/J.RSET.2021.100005.
- [171] A. J. Collin *et al.*, “Electrical Components for Marine Renewable Energy Arrays: A Techno-Economic Review,” *Energies* 2017, Vol. 10, Page 1973, vol. 10, no. 12, p. 1973, Nov. 2017, doi: 10.3390/EN10121973.
- [172] Y. Bai and Q. Bai, “Subsea Cost Estimation,” *Subsea Engineering Handbook*, pp. 159–192, Jan. 2010, doi: 10.1016/B978-1-85617-689-7.10006-8.
- [173] Z. Li, Q. Song, F. An, B. Zhao, Z. Yu, and R. Zeng, “Review on DC transmission systems for integrating large-scale offshore wind farms,” *Energy Conversion and Economics*, vol. 2, no. 1, pp. 1–14, Mar. 2021, doi: 10.1049/ENC2.12023.
- [174] S. Lauria, M. Schembari, F. Palone, and M. Maccioni, “Very long distance connection of gigawattsize offshore wind farms: Extra high-voltage AC versus high-voltage DC cost comparison,” *IET Renewable Power Generation*, vol. 10, no. 5, pp. 713–720, May 2016, doi: 10.1049/IET-RPG.2015.0348.
- [175] S. Kuczynski, M. Łaciak, A. Olijnyk, A. Szurlej, and T. Włodek, “Thermodynamic and technical issues of hydrogen and methane-hydrogen mixtures pipeline transmission,” *Energies (Basel)*, vol. 12, no. 3, Feb. 2019, doi: 10.3390/EN12030569.
- [176] L. Bauer and S. Matysik, “Vestas V236-15.0 - 15,00 MW - Aerogenerator.” Accessed: Aug. 05, 2025. [Online]. Available: <https://es.wind-turbine-models.com/turbines/2317-vestas-v236-15.0>
- [177] G. Pawelec, “Clean Hydrogen Monitor 2022: Levelized costs of hydrogen production.” Accessed: Aug. 05, 2025. [Online]. Available: https://usercontent.one/wp/hydrogeneurope.eu/wp-content/uploads/2022/10/Clean_Hydrogen_Monitor_10-2022_DIGITAL.pdf

8. APPENDICES

8.1. Electrolyser Commercial Database

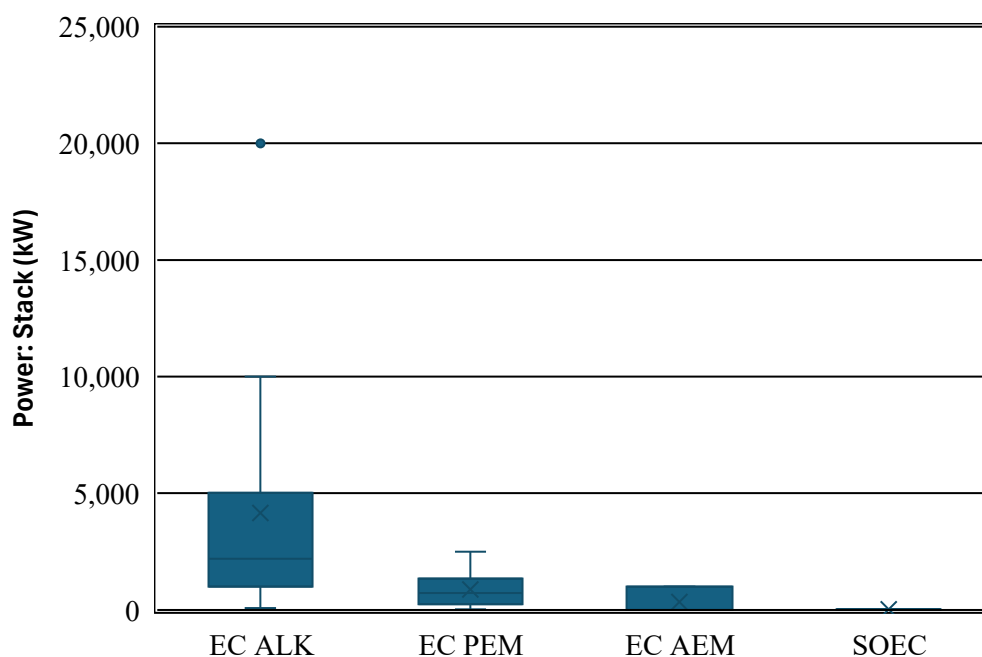


Figure 8.1: Commercial Database: Stack Power Boxplot.

Sources: All references for the Commercial Database sources are available upon request.

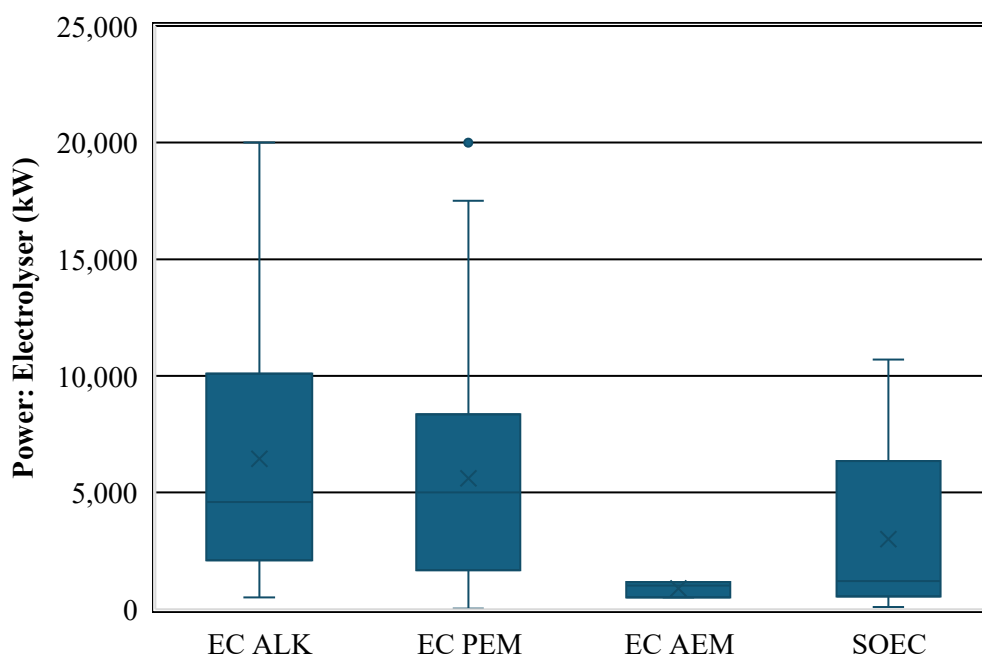


Figure 8.2: Commercial Database: Electrolyser Power Boxplot.

Sources: All references for the Commercial Database sources are available upon request.

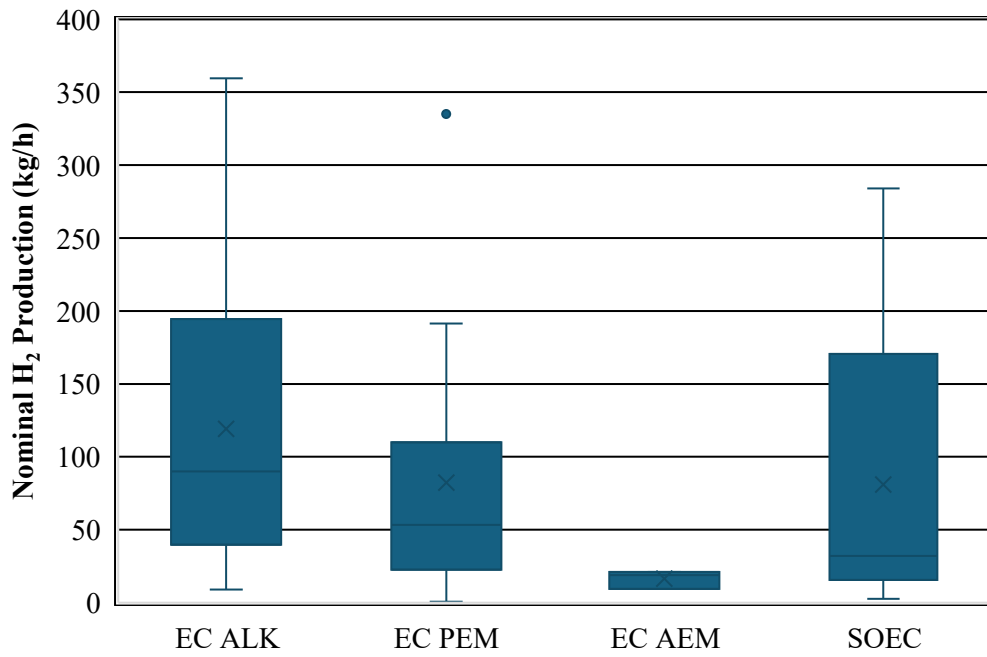


Figure 8.3: Commercial Database: Nominal H_2 Production Boxplot.
 Sources: All references for the Commercial Database sources are available upon request.

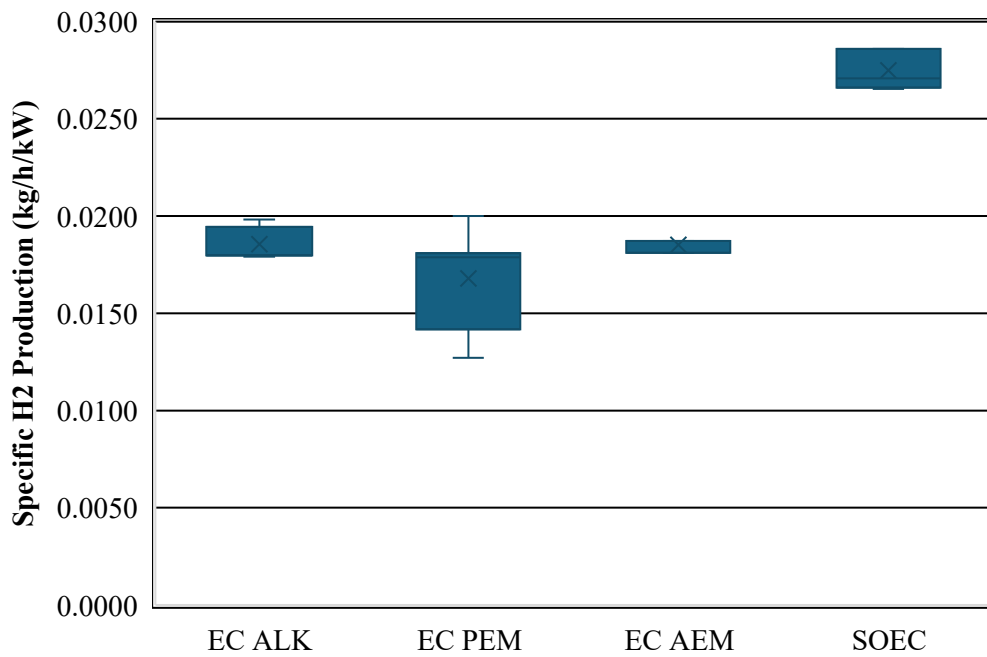


Figure 8.4: Commercial Database: Specific H_2 Production Boxplot.
 Sources: All references for the Commercial Database sources are available upon request.

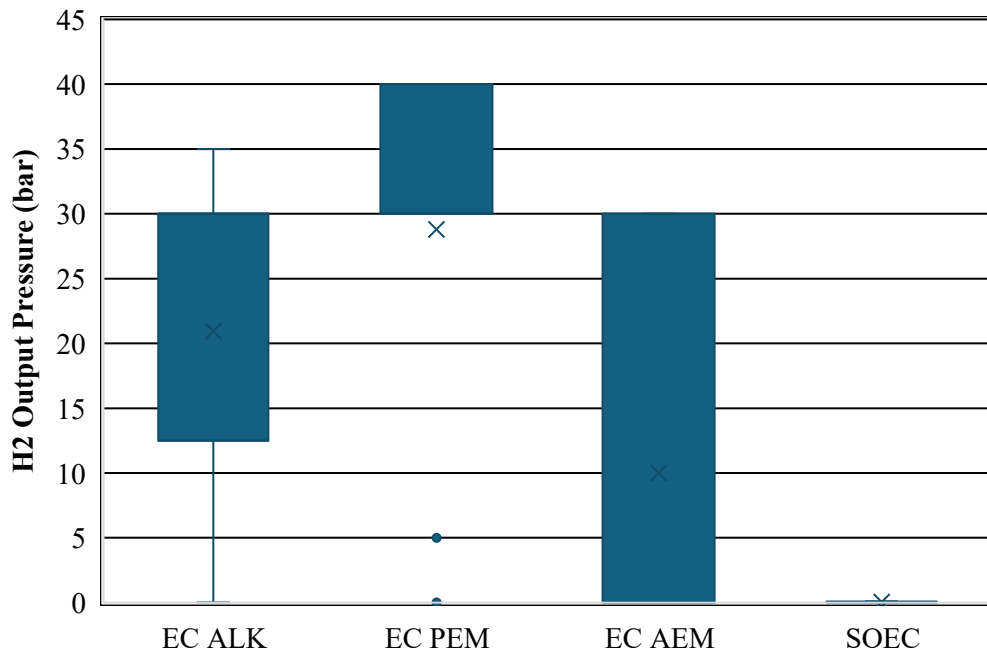


Figure 8.5: Commercial Database: H₂ Output Pressure Boxplot.
 Sources: All references for the Commercial Database sources are available upon request.

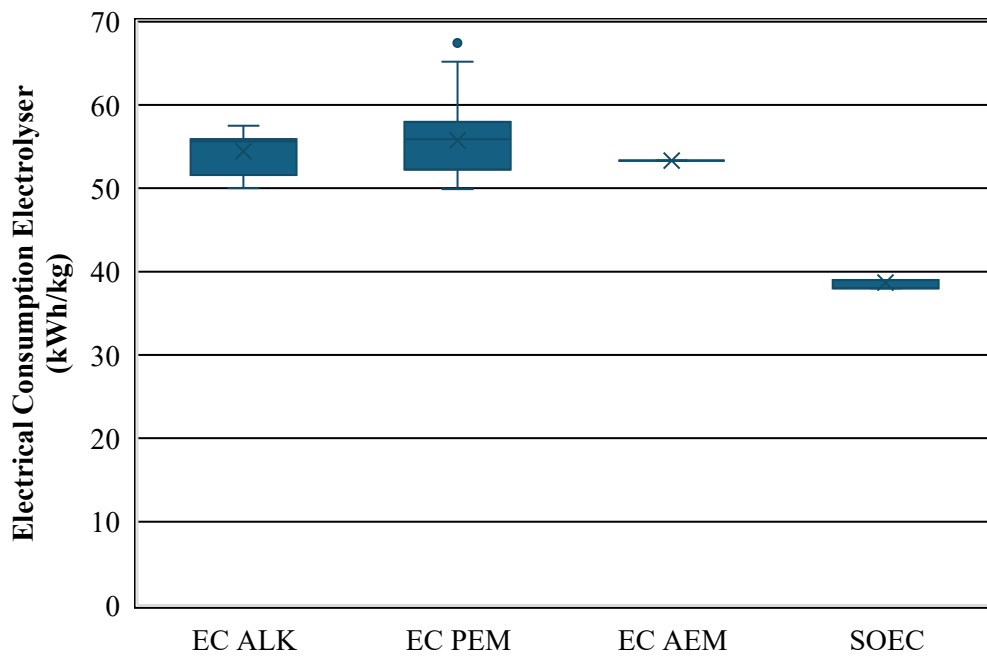


Figure 8.6: Commercial Database: Electrolyser Electrical Consumption Boxplot.
 Sources: All references for the Commercial Database sources are available upon request.

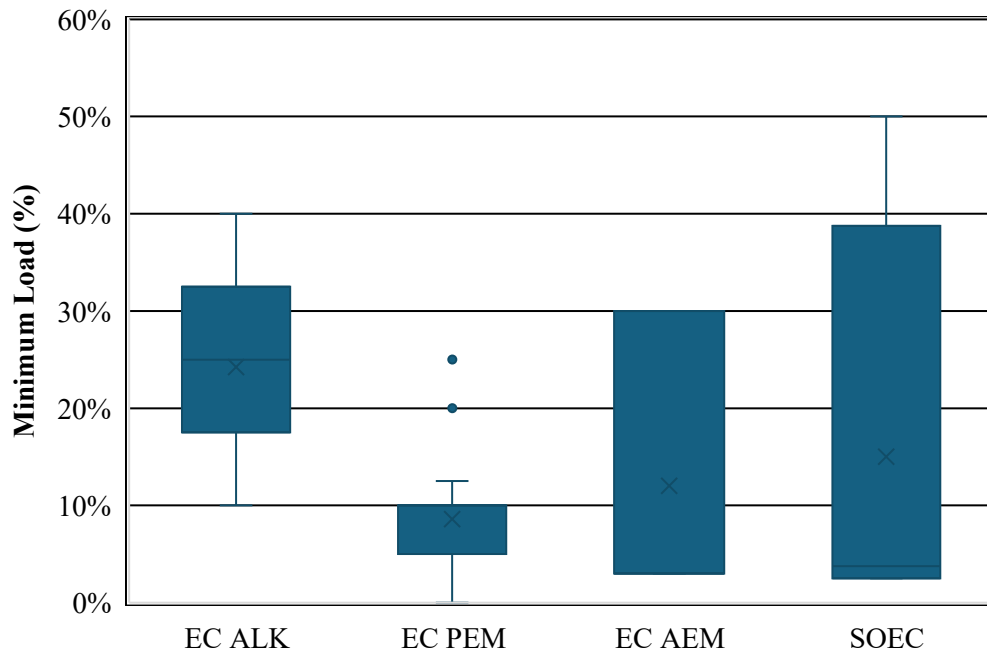


Figure 8.7: Commercial Database: Minimum Load Boxplot.

Sources: All references for the Commercial Database sources are available upon request.

*: Efficiency for AWE, PEM, and AEM is calculated with HHV and SOEC used LHV.

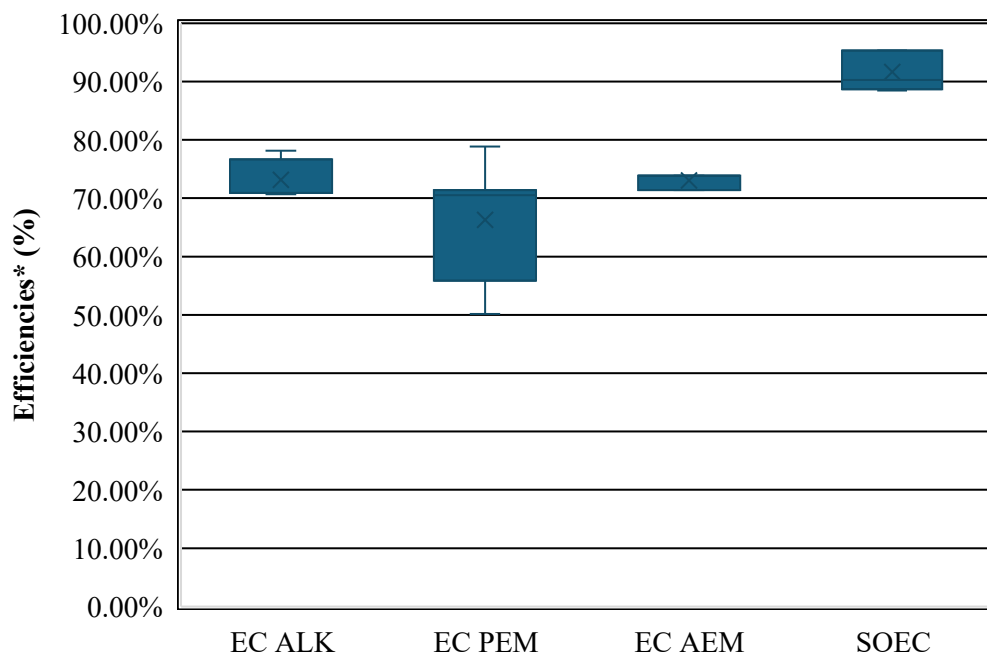


Figure 8.8: Commercial Database: Electrolyser Electrical Efficiency.

Sources: All references for the Commercial Database sources are available upon request.

8.2. Hydrogen Carriers Storage and Transportation

Compressed hydrogen storage is the most established and widely used method due to its simplicity, cost effectiveness, and fast charging and discharging capabilities. It involves pressurizing gas at a range of 350 to 700 bar to increase its density while reducing its volume. This process consumes 5-20% of the hydrogen's energy content and requires control of the temperature and durable tank materials to prevent any leakage or structural failure that can present an explosive risk [1].

There are four main storage tanks that vary according to their material and pressure capacity. Type I tanks are fully metallic, with pressure capacities of 200 bar, which offer good strength but being heavy. Type II tanks use a metal liner with a partial hoop-wrapped composite reinforcement. Type III tanks further enhance this by fully wrapping a metal liner, with capacity of 350 bar. Type IV tanks are the most advanced with a polymer liner fully encased in composite fiber, which offers highest pressure capacity and lowest weight, which is ideal for offshore applications but is the most costly and sensitive to hydrogen permeation [2].

Cryogenic or liquefied hydrogen storage increases hydrogen's volumetric energy density compared to pressurized by cooling it to $-253\text{ }^{\circ}\text{C}$, turning up to 800 liters of gas into one liter of liquid. This method is ideal for large-scale and long-distance transportation, but it must be considered that the liquefaction process consumes around 30-40% of hydrogen's energy content and limits the space efficiency it offers, as well as having specific conditions for its storage [3].

Infrastructure involves complex double-walled and vacuum-insulated spherical tanks with materials that can withstand extreme cryogenic conditions. This can make it suitable for centralized offshore with high capacity but are limited for small-scale applications. Future innovations look for cryo-compressed hydrogen that aim to enhance efficiency and make it more viable for mobile and offshore hydrogen storage [4].

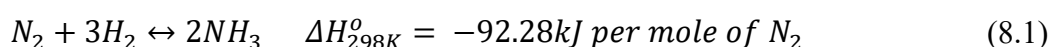
Solid-state hydrogen storage uses primarily metal hydrides by capturing hydrogen within the crystal lattice of alloys to offer exceptionally high volumetric energy densities. Hydrogen molecules dissociate on the alloy surface, allowing atoms to diffuse into interstitial sites and form reversible hydrides. This technology is attractive for offshore where space, safety and compactness are critical, since it operates at low pressures and moderate temperatures. Some of the compounds commonly used are disk-shaped cartridges of MgH_2 . However, some challenges exist in using this technology as hydride cycling degrades the material structure, adds significant weight, and requires a heat input for hydrogen release, as well as problems with

contaminants of O₂ and CO. Despite this, it can be a safe and efficient option when integrated with waste-heat recovery systems [5].

Hydrogen energy carriers are compounds capable of chemically storing and releasing hydrogen in a safe, efficient and compact form. These carriers present a solution towards hydrogen's low volumetric energy density for applications offshore where space and storage efficiency are critical. Hydrogen carriers offer a denser and more manageable alternative in which the hydrogen is stored in a chemical form and released when needed. These carriers can be reversible, for which hydrogen is bonded temporarily and recovered by a reverse reaction, or irreversible, where it is converted into another fuel for direct use [6]. This technology facilitates practical storage while supporting broader hydrogen integration with renewable energy. Some of the most promising hydrogen carriers are liquid organic hydrogen carriers (LOHCs), ammonia, and methanol.

LOHCs are an innovative hydrogen storage method that uses a reversible chemical reaction. These organic compounds absorb hydrogen through an exothermic process at moderate conditions in a range of 100-250 °C in temperature and 30-50 bar of pressure. The reversibility is done via an endothermic reaction at higher temperatures, for which the hydrogen is released and allows for a repeated use of the carrier. These key advantages make it suitable for offshore use due to the compatibility it has with the existing liquid fuel infrastructure, safe handling properties, ease of transport and long-term storage stability, with one of the most suitable for international renewable energy transport being dibenzyl toluene (DBT) [6].

Ammonia (NH₃) is a highly promising hydrogen carrier due to its 17.6% hydrogen content, storing more than 50% of hydrogen per volume than liquid hydrogen. Additionally, the conditions for storage are less extreme, needed either -33 °C at atmospheric pressure or 10 bar at room temperature, making it easier to handle. Ammonia is produced via de Haber-Bosch process as shown in Equation (8.1), and benefits having a mature infrastructure for its handling globally [7]. It is compatible with refrigerated tankers and LNG tanks, making it suitable for offshore hydrogen transport even though it suffers from the drawback of requiring additional equipment [8].



Methanol (CH₃OH) is a versatile hydrogen carrier with 12.5% hydrogen content. It also works as an industrial chemical widely used in the production of plastics, adhesives and alternative fuels like biodiesel. It is synthesized by exothermic reactions from hydrogen and CO or CO₂ at high pressures as seen in Equations (8.2) and (8.3) [9]. It has important advantages for offshore applications such as being a liquid at ambient conditions and having the versatility to be used as marine fuel in internal combustion or through fuel cells or reformed into hydrogen on demand [10].

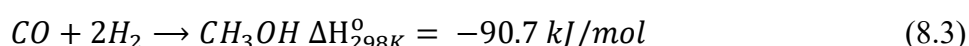
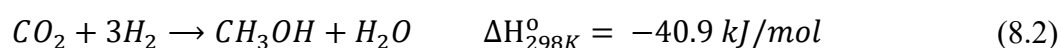


Table 8.1: Pairing of Storage and Transportation of Hydrogen

Storage Type	Paired Transport	Best Use Case	Gravimetric Energy Density [MJ/kg]	Volumetric Energy Density [MJ/L]
Compressed Hydrogen (Type I–IV)	Pipelines, pressurized cylinders	Fast-response storage, mobile/offshore with weight limits	~120	~2.7 (350 bar) ~4.7 (700 bar) [4]
Cryogenic Hydrogen (LH₂)	Insulated tankers, ships	Large-scale offshore or transoceanic transport	~120	~8.5 [11]
Solid-State (Metal Hydrides – MgH₂)	Modular cartridges, containers	Compact, safe offshore buffering on platforms or vessels	~9 [12]	~13.2 [13]
LOHC (DBT)	Liquid tankers, pipelines	Long-term offshore storage, port/maritime infrastructure	~7.5	~6.8 [6]
Ammonia (NH₃)	Refrigerated ships, LNG-type tanks	Offshore shipping, long-distance hydrogen energy transport	~18.6	~12.7 [14]
Methanol (CH₃OH)	Standard fuel infrastructure	Marine fuel, reformed H ₂ source for offshore applications	~19.9	~15.8 [11]

References

- [1] A. Z. Arsad *et al.*, “Hydrogen electrolyser technologies and their modelling for sustainable energy production: A comprehensive review and suggestions,” *Int J Hydrogen Energy*, vol. 48, no. 72, pp. 27841–27871, Aug. 2023, doi: 10.1016/J.IJHYDENE.2023.04.014.
- [2] E. Llera-Sastresa and I. Zabalza, *Hidrógeno: producción, almacenamiento y usos energéticos*. 2011. doi: 10.26754/uz.978-84-15274-94-0.

- [3] A. Lin and G. Bagnato, "Revolutionising energy storage: The Latest Breakthrough in liquid organic hydrogen carriers," *Int J Hydrogen Energy*, vol. 63, pp. 315–329, Apr. 2024, doi: 10.1016/J.IJHYDENE.2024.03.146.
- [4] T. Zhang, J. Uratani, Y. Huang, L. Xu, S. Griffiths, and Y. Ding, "Hydrogen liquefaction and storage: Recent progress and perspectives," *Renewable and Sustainable Energy Reviews*, vol. 176, p. 113204, Apr. 2023, doi: 10.1016/J.RSER.2023.113204.
- [5] E. Nemukula, C. B. Mtshali, and F. Nemangwele, "Metal Hydrides for Sustainable Hydrogen Storage: A Review," *Int J Energy Res*, vol. 2025, no. 1, p. 6300225, 2025, doi: <https://doi.org/10.1155/er/6300225>.
- [6] O. Oner and K. Khalilpour, "Evaluation of green hydrogen carriers: A multi-criteria decision analysis tool," *Renewable and Sustainable Energy Reviews*, vol. 168, p. 112764, Oct. 2022, doi: 10.1016/J.RSER.2022.112764.
- [7] L. Zhai, S. Liu, and Z. Xiang, "Ammonia as a carbon-free hydrogen carrier for fuel cells: a perspective," *Ind. Chem. Mater.*, vol. 1, no. 3, pp. 332–342, 2023, doi: 10.1039/D3IM00036B.
- [8] Q. Song *et al.*, "A comparative study on energy efficiency of the maritime supply chains for liquefied hydrogen, ammonia, methanol and natural gas," *Carbon Capture Science & Technology*, vol. 4, p. 100056, Sep. 2022, doi: 10.1016/J.CCST.2022.100056.
- [9] N. Garg, A. Sarkar, and B. Sundararaju, "Recent developments on methanol as liquid organic hydrogen carrier in transfer hydrogenation reactions," *Coord Chem Rev*, vol. 433, p. 213728, Apr. 2021, doi: 10.1016/J.CCR.2020.213728.
- [10] Methanex, "Marine Fuel - Methanex," <https://www.methanex.com/about-methanol/marine-fuel/>.
- [11] R. Nagar *et al.*, "Recent Developments in State-of-the-art Hydrogen Energy Technologies – Review of Hydrogen Storage Materials," *Solar Compass*, vol. 5, p. 100033, Jun. 2023, doi: 10.1016/j.solcom.2023.100033.
- [12] D. Grant, "Magnesium hydride for hydrogen storage," *Solid-State Hydrogen Storage: Materials and Chemistry*, pp. 357–380, Jan. 2008, doi: 10.1533/9781845694944.4.357.
- [13] X. Zhang *et al.*, "Atomic reconstruction for realizing stable solar-driven reversible hydrogen storage of magnesium hydride," *Nat Commun*, vol. 15, Dec. 2024, doi: 10.1038/s41467-024-47077-y.
- [14] M. Aziz, A. TriWijayanta, and A. B. D. Nandiyanto, "Ammonia as effective hydrogen storage: A review on production, storage and utilization," *Energies (Basel)*, vol. 13, Jun. 2020, doi: 10.3390/en13123062.

8.3. Demonstration and Pilot Projects Overview

Table 8.2: State-of-the-art in industry for hydrogen production platforms.

*: Initial expected operation date for projects currently in development

Project Name	Capacity	Site	Country	Operation Date	Project Scope
SeaLhyfe Project [1]	1 MW	Le Croisic, SEM-REV	France	2022	The world's first offshore hydrogen production pilot, launched in 2022, has completed sea trials and achieved all set objectives by demonstrating the reliability of an electrolyser at sea.
OceanH2 Project [2]	-	Canary Islands	Spain	2023	It is a completed industrial research initiative led by ACCIONA to develop Spain's first offshore green hydrogen plant, aiming to integrate floating wind and photovoltaic technologies.
PosHYdon Project [3]	1 MW	Dutch North Sea	Netherlands	2024	The pilot project currently being successfully tested onshore and be tested offshore located 13 km off the coast of Scheveningen aiming to produce green hydrogen on an operational gas platform integrating offshore wind, gas and hydrogen at the first fully electrified platform in the Dutch North Sea.
China Energy Offshore Platform Pilot [4]	-	Yantai	China	2025	The world's first offshore platform to produce green hydrogen, ammonia, and methanol has been completed, aiming to refuel ocean-going ships at sea. The storage and transportation issues are then resolved by converting hydrogen into methanol and ammonia.
Green Hydrogen Shore Power Demonstrator [5]	-	Leith	Scotland, UK	2025	A green hydrogen shore demonstration project was shown at the Port of Leith, integrating water treatment, waste heat utilization, offshore wind and hydrogen production to provide clean shore power for maritime operations.
OYSTER Project [6]	MW scale	Grimsby	UK	2025	The project aims to develop a marinized electrolyser designed for integration with offshore wind turbines. And conducting planning and permitting work for a larger-scale offshore demonstration. Orsted's withdrawal has impacted the project's scope and was terminated on the 5th of May of 2025.
Hyport Oostende Project [7]	50 MW	Oostende	Belgium	2025*	A demonstration project with an innovative electrolyser of 50 MW expected to be finalized by 2025. It is a shore-based hydrogen production facility using offshore wind as a power source.

H2Mare Project [8]	-	North Sea	Germany	2025*	A German initiative to develop autonomous offshore hydrogen production systems, integrating wind turbines with compact PEM electrolyzers capable of efficient operation under harsh offshore conditions.
HOPE Project [9]	10 MW	North Sea	Belgium	2026*	Aiming to develop, build, and operate the first 10 MW offshore PEM electrolyser unit in the North Sea by 2026, building the continent's first infrastructure for large-scale production of renewable hydrogen offshore.
GET H2 Nukleus Project [7]	300 MW	Lingen	Germany	2027*	RWE is planning to build an electrolysis capacity of 300 MW on the site of a gas-fired power plant, primarily using offshore power. In summer 2024, RWE commissioned a 14 MW (10 ALK + 4 PEM) electrolysis pilot plant on site.
The Salamander Project [10]	200 MW	Peterhead	Scotland, UK	2028*	Proposes 100 MW floating wind + 100 MW onshore battery for hydrogen production on a floating wind platform and transported to shore via pipeline.
HØST PtX Esbjerg Project [11]	1 GW	Esbjerg	Denmark	2028/29*	The project is one of Europe's most advanced Power-to-X projects, focusing on producing green hydrogen with large scale electrolysis powered by renewable energy, primarily offshore wind and solar energy.
H2opZee [12]	500 MW	Dutch North Sea	Netherlands	2030*	Aiming to develop a 500 MW offshore hydrogen production facility in the Dutch North Sea by 2030. The project is currently in the feasibility study phase, was expected to be completed by the end of 2023.
AquaSector Project [12]	300 MW	German North Sea	Germany	2030*	It is a key component of the Aquaventus initiative focusing on large-scale offshore green hydrogen production to be the frontrunner for solving critical technical challenges for gigawatt-scale offshore hydrogen projects.
DOLPHYN Project [13]	4 GW	South Wales & Scotland	UK	2035*	A UK-based project conducting sea trials for offshore hydrogen production technology in South Wales to demonstrate safe and reliable hydrogen production from seawater. It has planned 10 MW Demonstrator, 100-300MW commercial developments for 2028 and expanding to GW-scale by 2035.
AquaVentus Project [14]	10 GW	Helgoland	Germany	2035*	It is an initiative focused on developing and expanding large-scale offshore green hydrogen production in Germany with projects like AquaDuctus, AquaPrimus and SEN-1 area for demonstration area for 1 GW.
NorthH2 [15]	10 GW	North Sea	Netherlands	2035*	The project's aim is to realize a GW-scale green hydrogen factory with which NorthH2 can supply the industry with green hydrogen between 2030 and 2035.

References:

- [1] Lhyfe, “Sealhyfe produces its first kilos of green hydrogen in the Atlantic,” <https://www.lhyfe.com/press/lhyfe-announces-that-sealhyfe-the-worlds-first-offshore-hydrogen-production-pilot-produces-its-first-kilos-of-green-hydrogen-in-the-atlantic-ocean/>.
- [2] ACCIONA, “OCEANH2, the industrial research project coordinated by ACCIONA, launches,” Mar. 2021.
- [3] PosHYdon, “About PosHYdon,” <https://poshydon.com/en/home-en/about-poshydon/>.
- [4] L. Collins, “World’s first offshore platform to produce green hydrogen, ammonia and methanol completed in China,” Apr. 2025.
- [5] A. Habibic, “‘World’s first’ hydrogen shore power demo presented at Port of Leith,” Mar. 2025.
- [6] CORDIS, “Offshore hydrogen from shoreside wind turbine integrated electrolyser,” 2025. doi: 10.3030/101007168.
- [7] DEME, “HYPORT®: green hydrogen plant in Ostend,” <https://www.deme-group.com/news/hyportr-green-hydrogen-plant-ostend>.
- [8] Federal Ministry of Research, Technology and Space, “How the H2Mare project intends to produce hydrogen offshore,” <https://www.wasserstoff-leitprojekte.de/projects/h2mare>.
- [9] Lhyfe, “Offshore Hydrogen Production on a New Scale: HOPE Project,” Jun. 2023.
- [10] Simply Blue Energy, “Salamander Project - Floating Offshore Wind Scotland - Simply Blue Energy,” <https://salamanderfloatingwind.com/>.
- [11] HØST PtX Esbjerg, “About us - HØST PtX Esbjerg,” <https://hoestptxesbjerg.dk/about-host/>.
- [12] RWE, “H2opZee – Demonstration project for green hydrogen in the Netherlands,” <https://www.rwe.com/en/research-and-development/hydrogen-projects/h2opzee/>.
- [13] Dolphyn Hydrogen, “Where We Are,” <https://www.dolphynhydrogen.com/where-we-are#large-scale-commercial-developments>.
- [14] RWE, “AquaVentus – Hydrogen production in the North Sea | RWE,” <https://www.rwe.com/en/research-and-development/hydrogen-projects/aquaventus/>.
- [15] RWE, “NorthH2 | Hydrogen project of RWE,” <https://www.rwe.com/en/research-and-development/hydrogen-projects/north2/>.

8.4. Semi-Submersible Centralized Platform 2D Layout

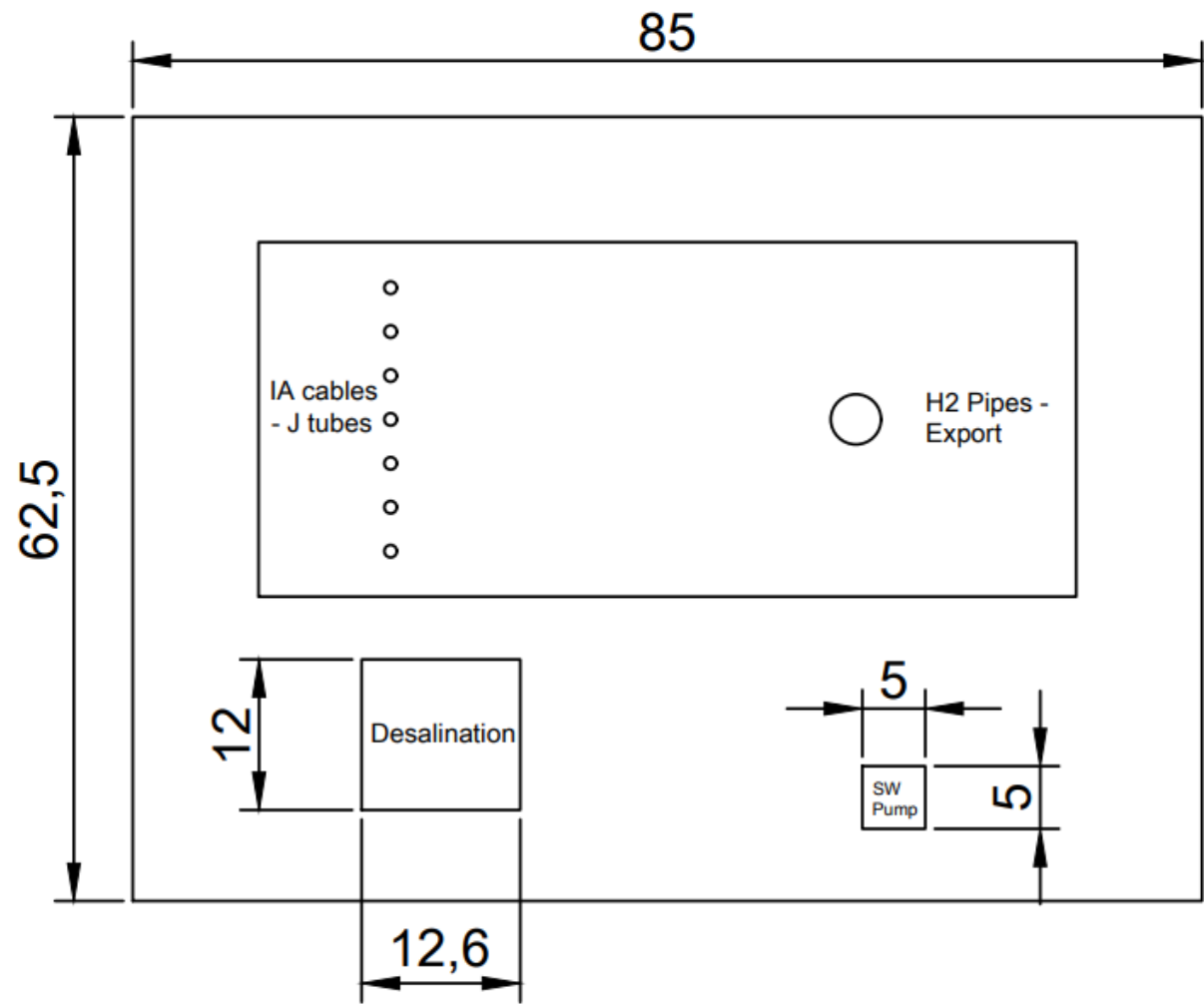


Figure 8.9: Deck #1 2D Layout at 23 meters (Cable Deck)

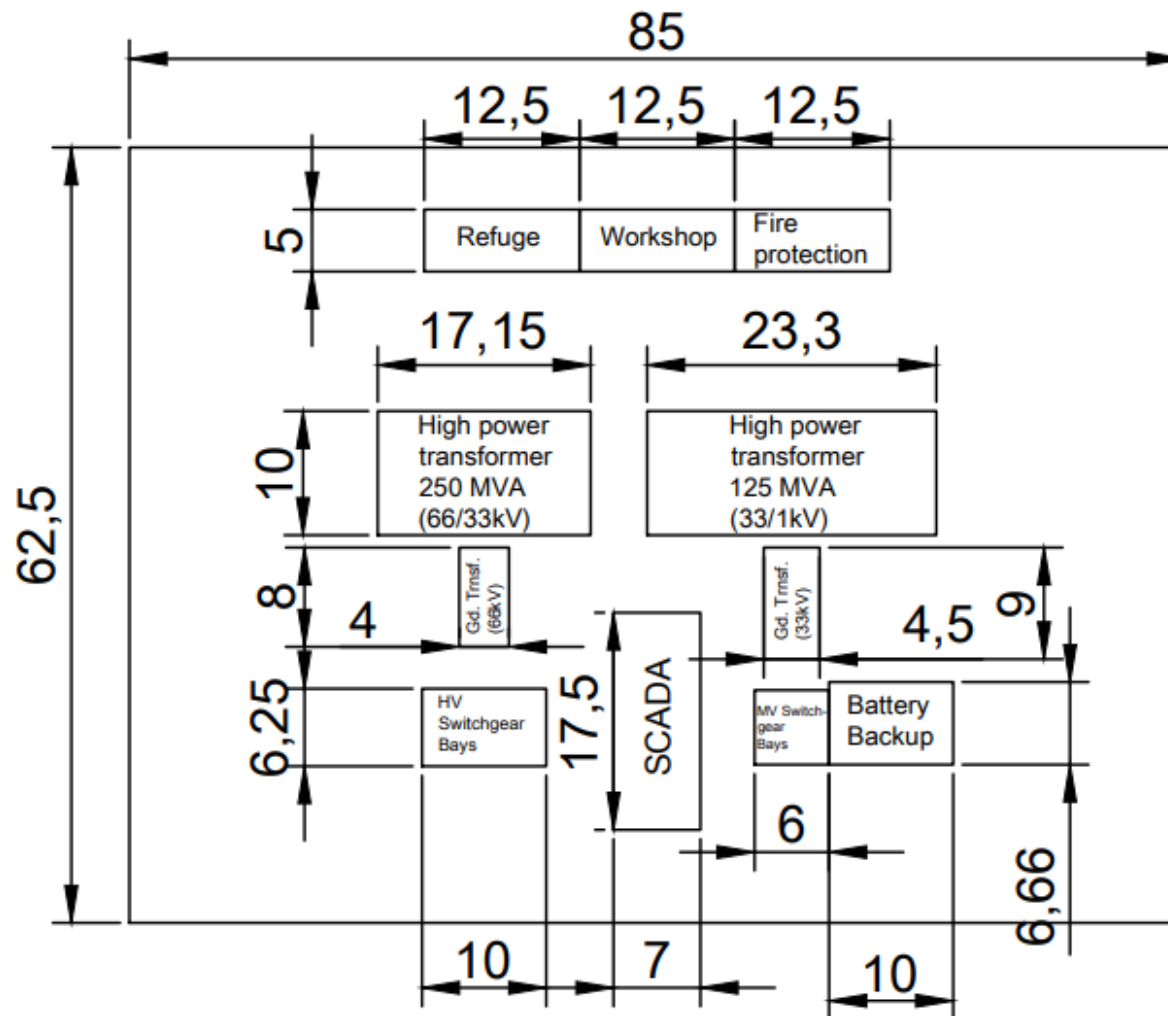


Figure 8.10: Deck #2 2D Layout at 28 meters (Main Deck)

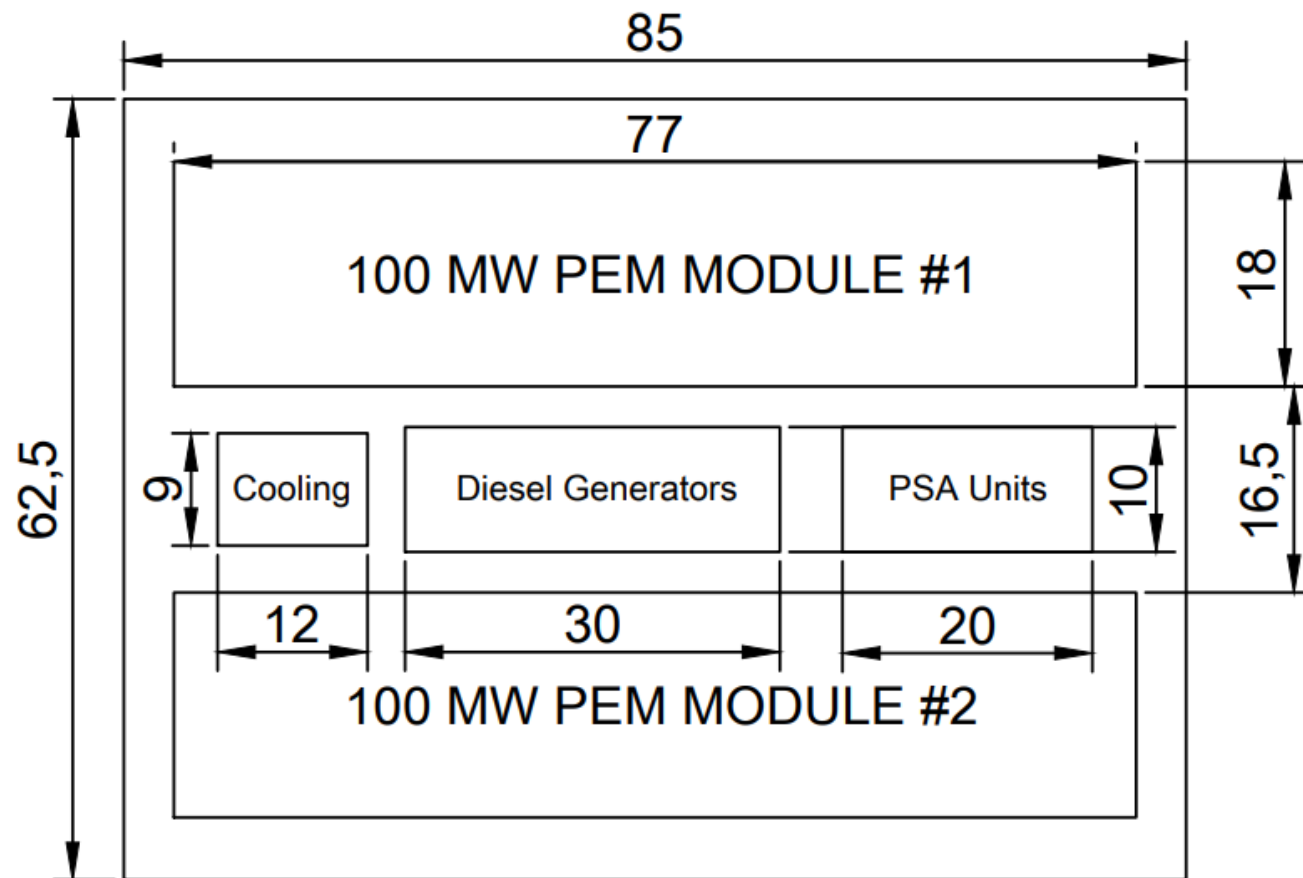


Figure 8.11: Deck #3 2D Layout at 38 meters (PEM Deck #1)

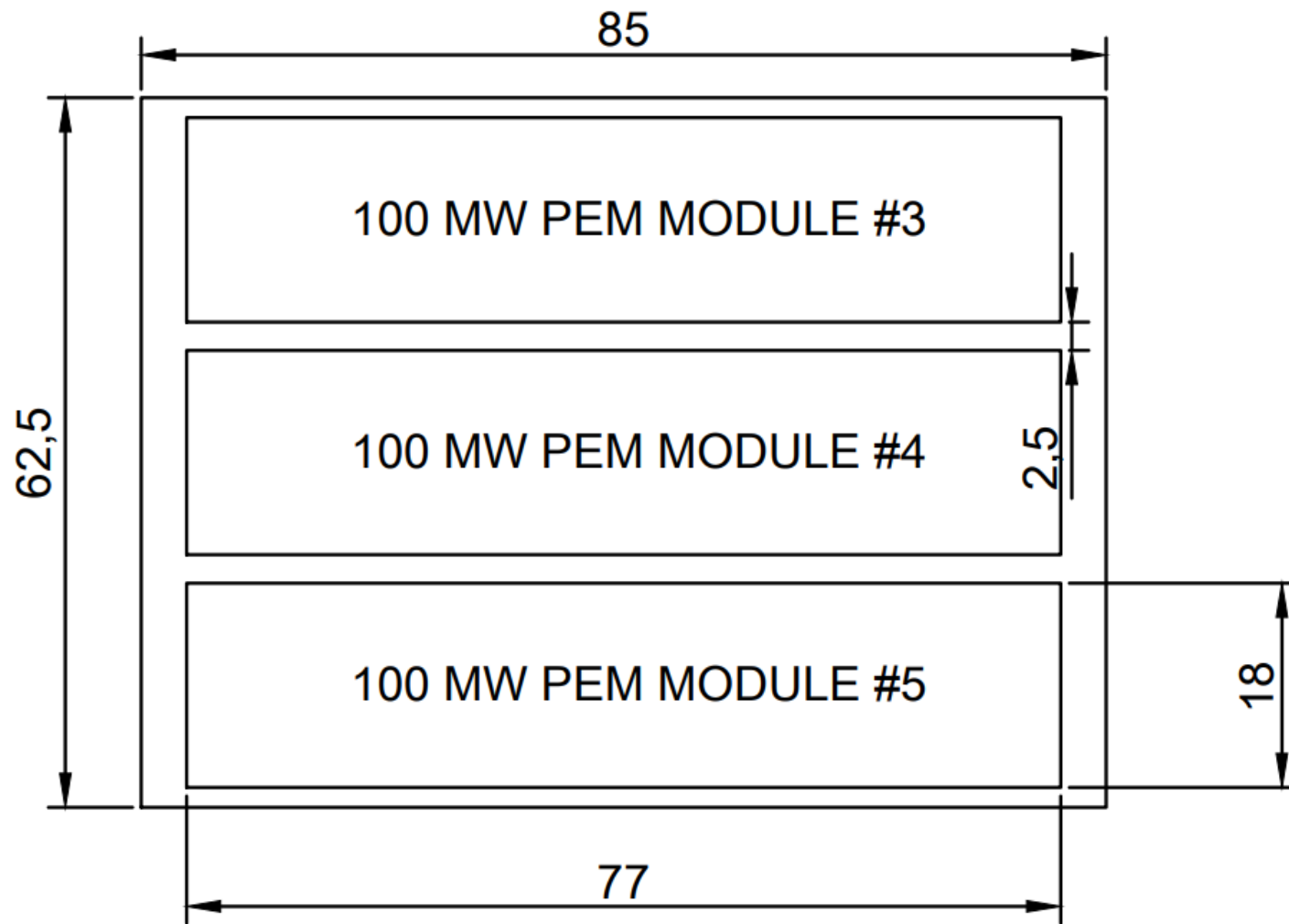


Figure 8.12: Deck #4 2D Layout at 43 meters (PEM Deck #2)

8.5. Semi-Submersible Centralized Platform RAOs for Motion and Acceleration

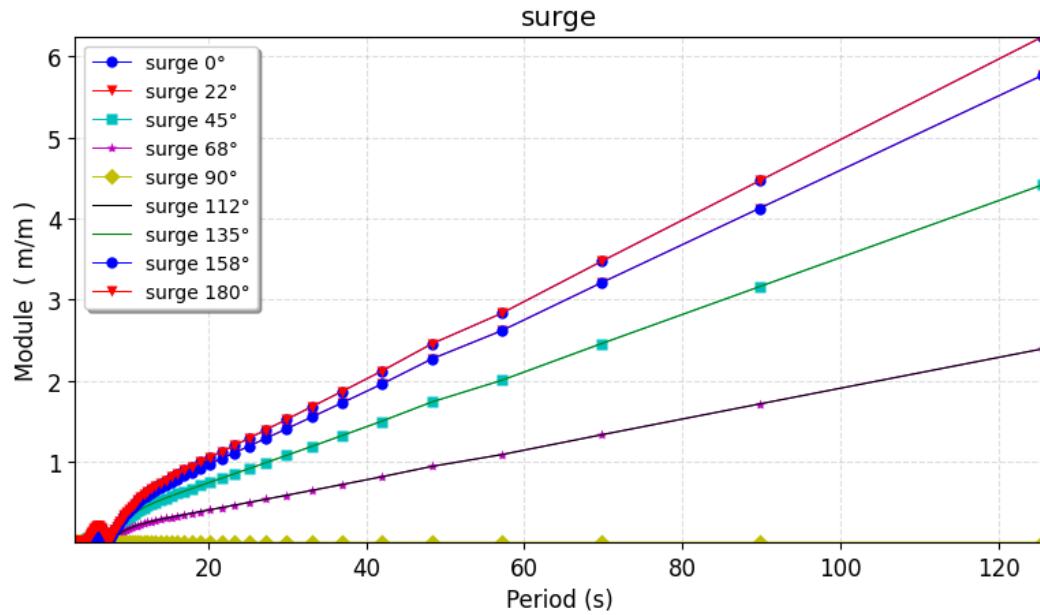


Figure 8.13: Centralized platform Hydrostar RAO for surge

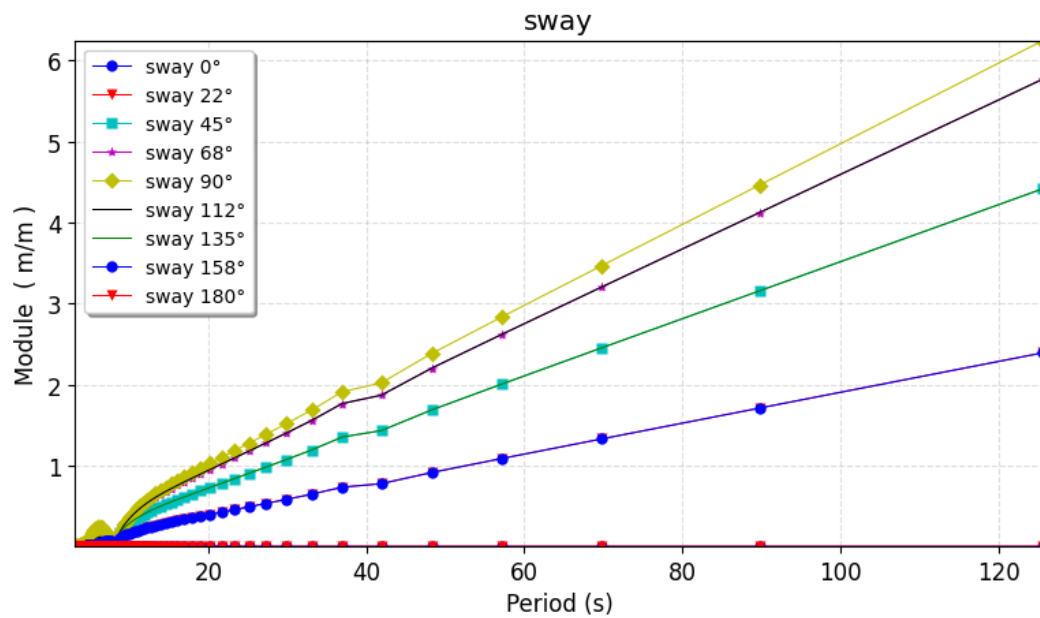


Figure 8.14: Centralized platform Hydrostar RAO for sway

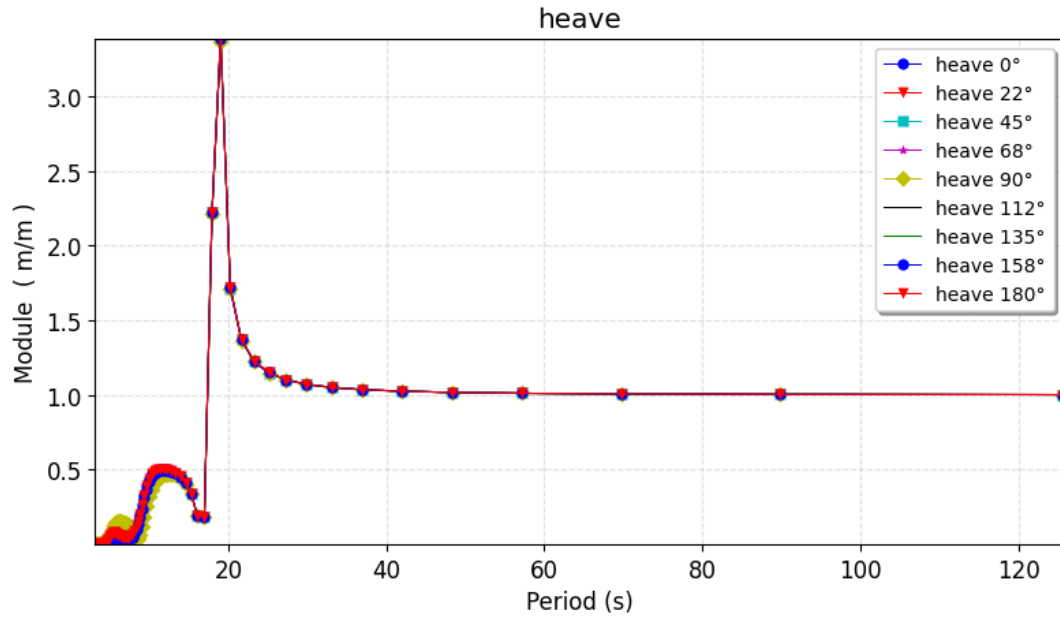


Figure 8.15: Centralized platform Hydrostar RAO for heave

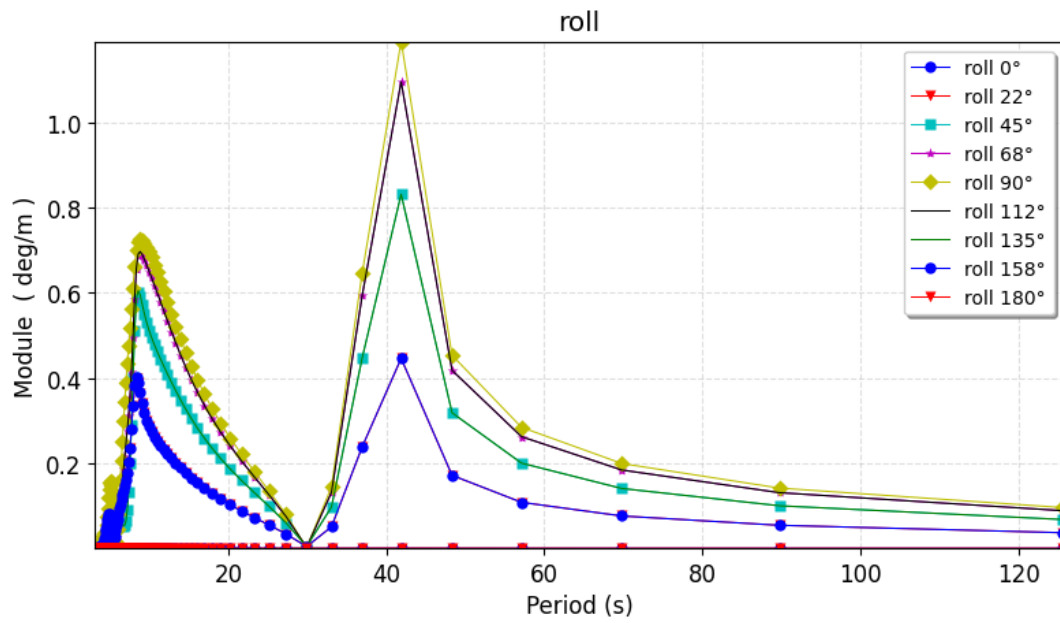


Figure 8.16: Centralized platform Hydrostar RAO for roll

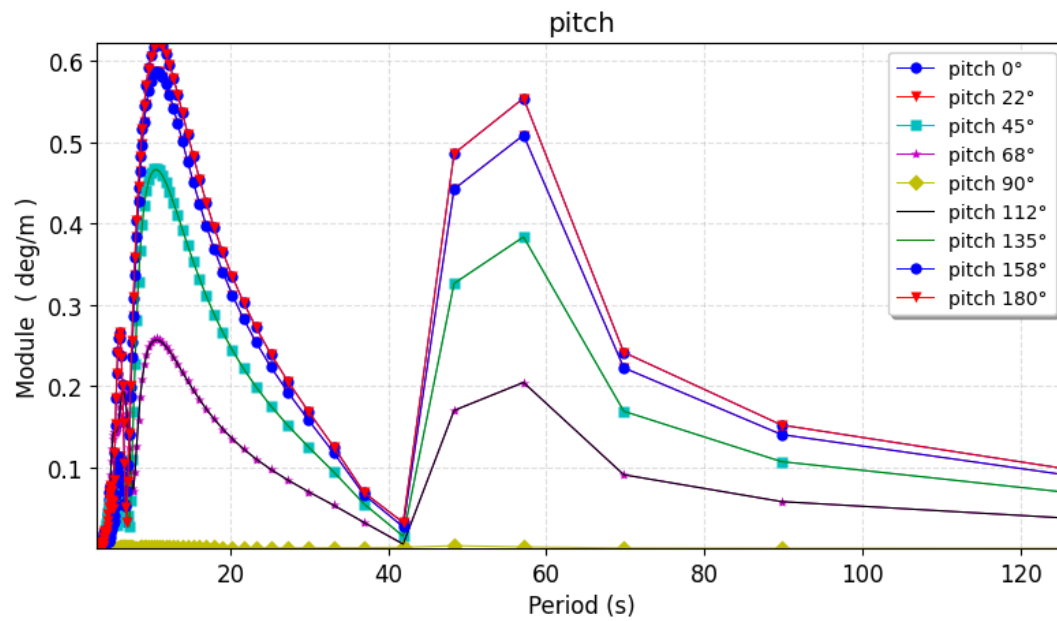


Figure 8.17: Centralized platform Hydrostar RAO for pitch

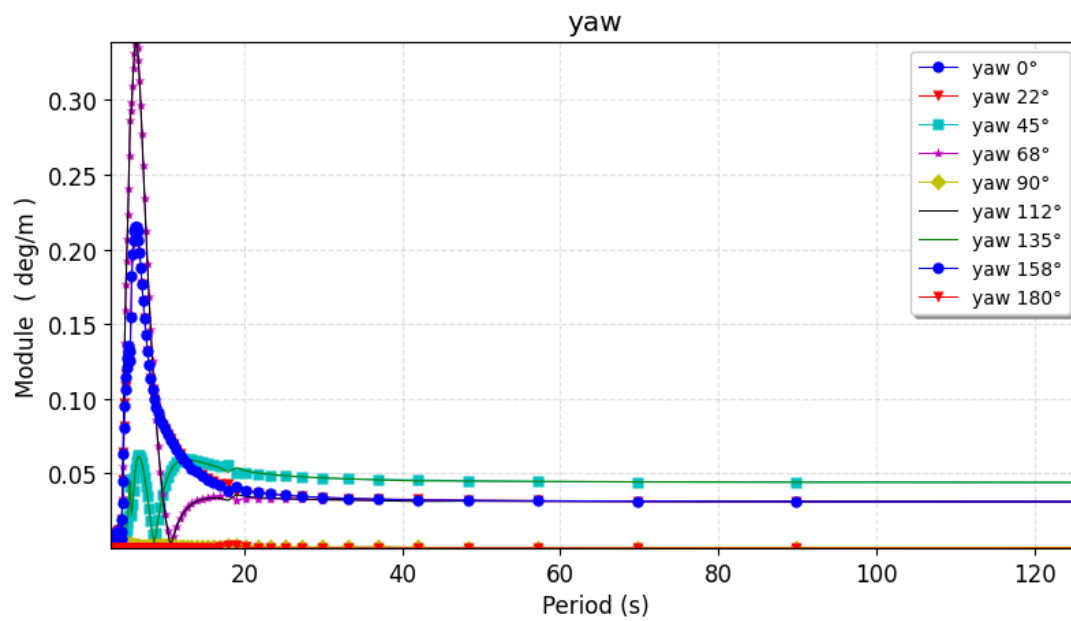


Figure 8.18: Centralized platform Hydrostar RAO for surge

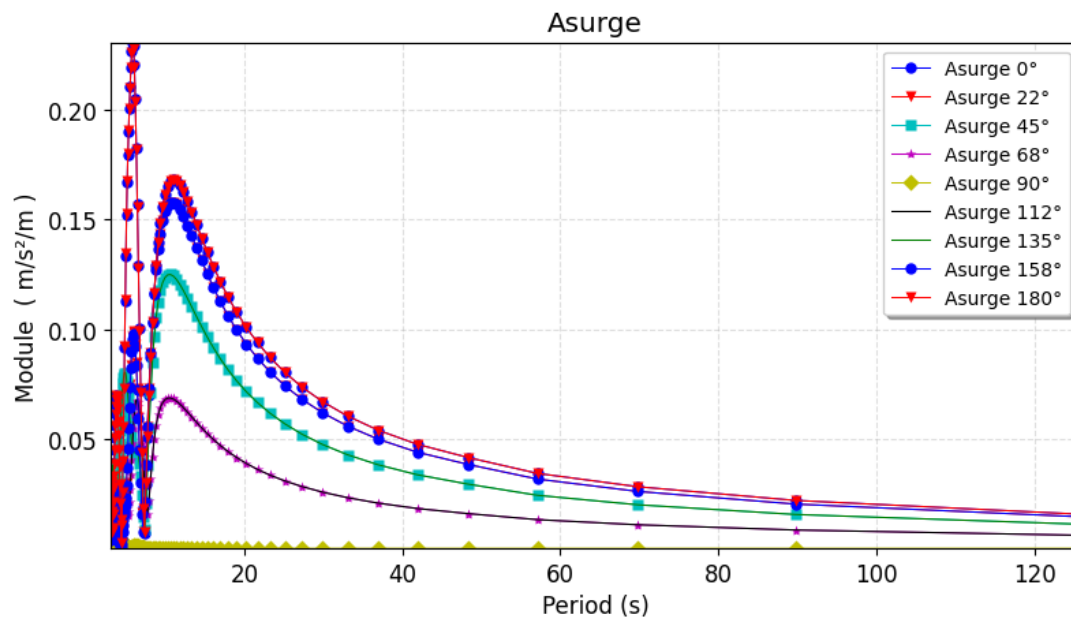


Figure 8.19: Centralized platform Hydrostar RAO for acceleration in surge

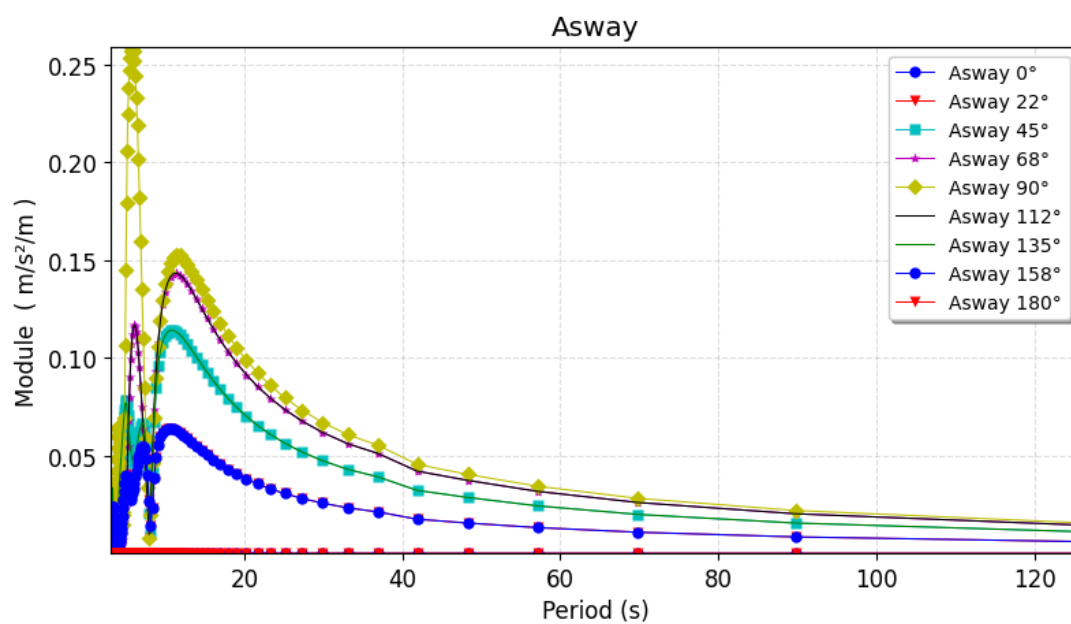


Figure 8.20: Centralized platform Hydrostar RAO for acceleration in sway

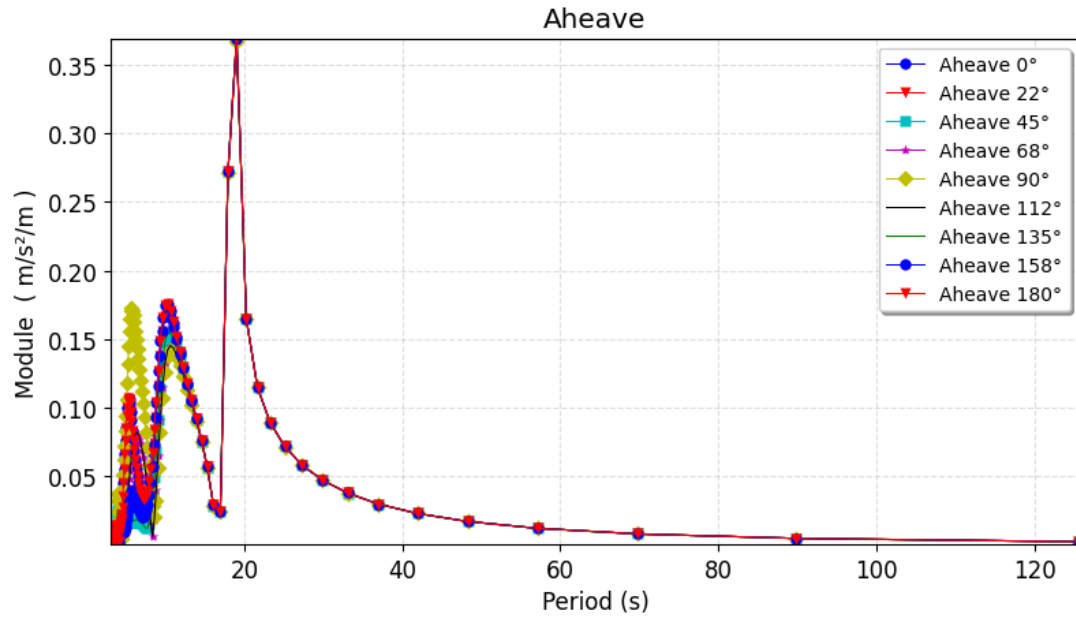


Figure 8.21: Centralized platform Hydrostar RAO for acceleration in heave

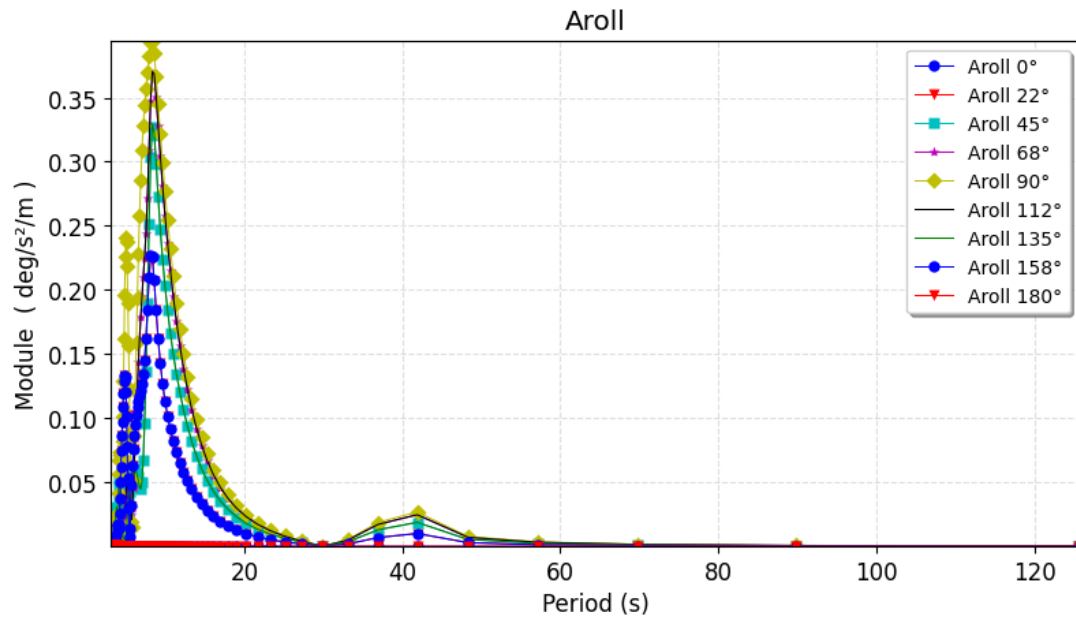


Figure 8.22: Centralized platform Hydrostar RAO for acceleration in roll

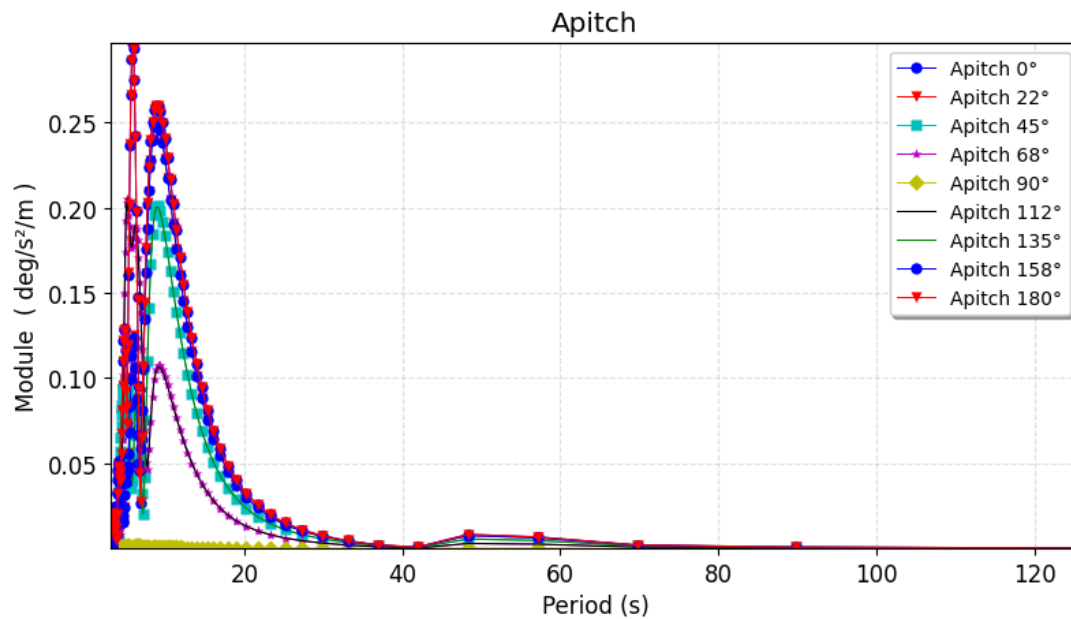


Figure 8.23: Centralized platform Hydrostar RAO for acceleration in pitch

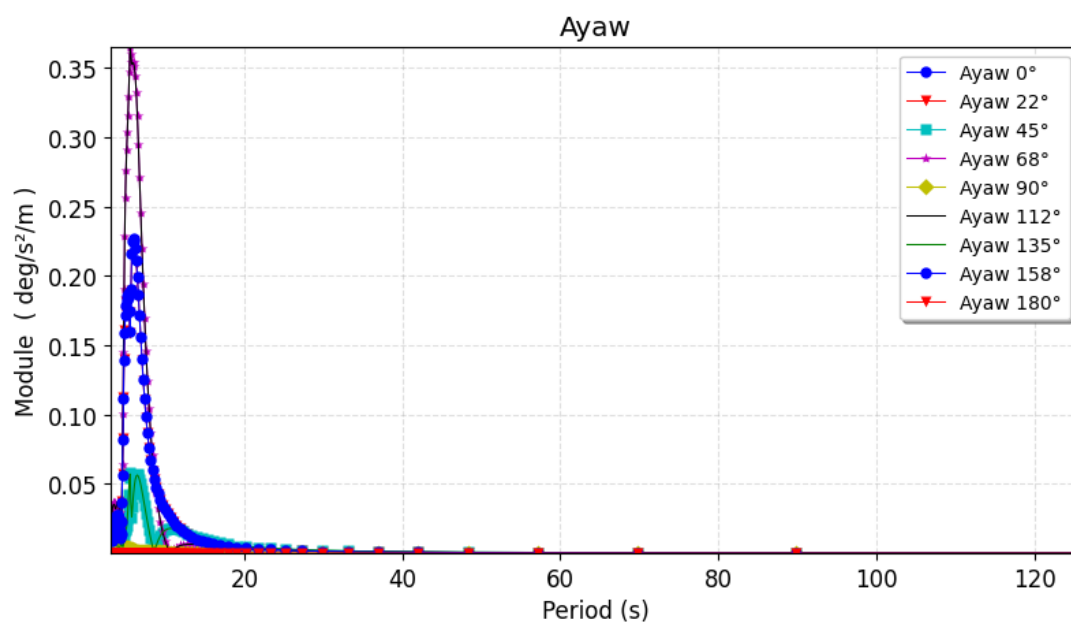


Figure 8.24: Centralized platform Hydrostar RAO for acceleration in yaw

8.6. LCOH Calculations for Case Study

Rate of Return [%]	6.00%	Lifetime [yr]	25	LCOH	Discounted Et w/deg	4.00	€/kg	
Centralized Onshore (On,C)					Discounted Et	3.90	€/kg	
					Undiscounted Et	2.00	€/kg	
Year	CAPEX [M€]	OPEX [M€]	DECEX [M€]	NPV [M€]	Et [MkgH ₂]	Et discounted [MkgH ₂]	η _{st} [%]	Et discounted w/deg [MkgH ₂]
0	77.19	-	-	77.19	-	-	-	-
1	77.19	45.01	-	115.28	35.08	33.09	100.00%	33.09
2	77.19	45.01	-	108.75	34.92	31.07	99.53%	30.93
3	77.19	45.01	-	102.60	34.75	29.18	99.06%	28.90
4	77.19	45.01	-	96.79	34.59	27.40	98.59%	27.01
5	77.19	45.01	-	91.31	34.42	25.72	98.12%	25.24
6	77.19	45.01	-	86.14	34.26	24.15	97.65%	23.58
7	77.19	45.01	-	81.27	34.09	22.67	97.18%	22.03
8	77.19	45.01	-	76.67	33.93	21.29	96.71%	20.59
9	77.19	45.01	-	72.33	33.76	19.98	96.24%	19.23
10	77.19	45.01	-	68.23	33.60	18.76	95.77%	17.97
11	77.19	45.01	-	64.37	33.43	17.61	95.30%	16.78
12	77.19	45.01	-	60.73	33.27	16.53	94.83%	15.68
13	77.19	45.01	-	57.29	33.10	15.52	94.36%	14.65
14	77.19	45.01	-	54.05	35.08	15.52	93.89%	14.57
15	77.19	227.17	-	127.00	34.92	14.57	93.42%	13.61
16	77.19	45.01	-	48.10	34.75	13.68	100.00%	13.68
17	77.19	45.01	-	45.38	34.59	12.84	99.53%	12.78
18	77.19	45.01	-	42.81	34.42	12.06	99.06%	11.95
19	77.19	45.01	-	40.39	34.26	11.32	98.59%	11.16
20	77.19	45.01	-	38.10	34.09	10.63	98.12%	10.43
21	77.19	45.01	-	35.94	33.93	9.98	97.65%	9.75
22	77.19	45.01	-	33.91	33.76	9.37	97.18%	9.11
23	77.19	45.01	-	31.99	33.60	8.80	96.71%	8.51
24	77.19	45.01	-	30.18	33.43	8.26	96.24%	7.95
25	-	45.01	35.57	18.78	33.27	7.75	95.77%	7.42
Total	1,929.71	1,307.36	35.57	1,705.58	853.28	437.75	97.45%	426.59

Figure 8.25: Detailed LCOH calculations across the project's lifetime at Viana do Castelo case study for Centralized Onshore scenario

Rate of Return [%]	6.00%	Lifetime [yr]	25	LCOH	Discounted Et w/deg	4.57	€/kg	
Centralized Offshore (Off,C)					Discounted Et	4.45	€/kg	
					Undiscounted Et	2.28	€/kg	
Year	CAPEX [M€]	OPEX [M€]	DECEX [M€]	NPV [M€]	Et [MkgH ₂]	Et discounted [MkgH ₂]	η _{st} [%]	Et discounted w/deg [MkgH ₂]
0	82.75	-	-	82.75	-	-	-	-
1	82.75	57.98	-	132.76	35.50	33.49	100.00%	33.49
2	82.75	57.98	-	125.24	35.34	31.45	99.53%	31.30
3	82.75	57.98	-	118.16	35.17	29.53	99.06%	29.25
4	82.75	57.98	-	111.47	35.00	27.73	98.59%	27.33
5	82.75	57.98	-	105.16	34.84	26.03	98.12%	25.54
6	82.75	57.98	-	99.21	34.67	24.44	97.65%	23.87
7	82.75	57.98	-	93.59	34.50	22.95	97.18%	22.30
8	82.75	57.98	-	88.29	34.34	21.54	96.71%	20.83
9	82.75	57.98	-	83.29	34.17	20.22	96.24%	19.46
10	82.75	57.98	-	78.58	34.00	18.99	95.77%	18.18
11	82.75	57.98	-	74.13	33.83	17.82	95.30%	16.99
12	82.75	57.98	-	69.94	33.67	16.73	94.83%	15.87
13	82.75	57.98	-	65.98	33.50	15.71	94.36%	14.82
14	82.75	57.98	-	62.24	35.50	15.70	93.89%	14.74
15	82.75	300.26	-	159.81	35.34	14.74	93.42%	13.77
16	82.75	57.98	-	55.40	35.17	13.84	100.00%	13.84
17	82.75	57.98	-	52.26	35.00	13.00	99.53%	12.94
18	82.75	57.98	-	49.30	34.84	12.20	99.06%	12.09
19	82.75	57.98	-	46.51	34.67	11.46	98.59%	11.30
20	82.75	57.98	-	43.88	34.50	10.76	98.12%	10.56
21	82.75	57.98	-	41.39	34.34	10.10	97.65%	9.86
22	82.75	57.98	-	39.05	34.17	9.48	97.18%	9.21
23	82.75	57.98	-	36.84	34.00	8.90	96.71%	8.61
24	82.75	57.98	-	34.76	33.83	8.36	96.24%	8.04
25	-	57.98	33.70	21.36	33.67	7.84	95.77%	7.51
Total	2,068.69	1,691.70	33.70	1,971.35	863.55	443.02	97.45%	431.73

Figure 8.26: Detailed LCOH calculations across the project's lifetime at Viana do Castelo case study for Centralized Offshore scenario

Rate of Return [%]	6.00%	Lifetime [yr]	25	LCOH	Discounted Et w/deg	4.82	€/kg	
Decentralized Offshore (Off,D)					Discounted Et	4.69	€/kg	
					Undiscounted Et	2.41	€/kg	
Year	CAPEX [M€]	OPEX [M€]	DECEX [M€]	NPV [M€]	Et [MkgH ₂]	Et discounted [MkgH ₂]	η _{st} [%]	Et discounted w/deg [MkgH ₂]
0	86.72	-	-	86.72	-	-	-	-
1	86.72	61.53	-	139.86	35.50	33.49	100.00%	33.49
2	86.72	61.53	-	131.94	35.33	31.44	99.53%	31.30
3	86.72	61.53	-	124.47	35.16	29.52	99.06%	29.25
4	86.72	61.53	-	117.43	35.00	27.72	98.59%	27.33
5	86.72	61.53	-	110.78	34.83	26.03	98.12%	25.54
6	86.72	61.53	-	104.51	34.66	24.44	97.65%	23.86
7	86.72	61.53	-	98.60	34.50	22.94	97.18%	22.30
8	86.72	61.53	-	93.01	34.33	21.54	96.71%	20.83
9	86.72	61.53	-	87.75	34.16	20.22	96.24%	19.46
10	86.72	61.53	-	82.78	34.00	18.98	95.77%	18.18
11	86.72	61.53	-	78.10	33.83	17.82	95.30%	16.98
12	86.72	61.53	-	73.68	33.66	16.73	94.83%	15.87
13	86.72	61.53	-	69.51	33.50	15.70	94.36%	14.82
14	86.72	61.53	-	65.57	35.50	15.70	93.89%	14.74
15	86.72	330.52	-	174.10	35.33	14.74	93.42%	13.77
16	86.72	61.53	-	58.36	35.16	13.84	100.00%	13.84
17	86.72	61.53	-	55.05	35.00	13.00	99.53%	12.94
18	86.72	61.53	-	51.94	34.83	12.20	99.06%	12.09
19	86.72	61.53	-	49.00	34.66	11.46	98.59%	11.30
20	86.72	61.53	-	46.23	34.50	10.76	98.12%	10.55
21	86.72	61.53	-	43.61	34.33	10.10	97.65%	9.86
22	86.72	61.53	-	41.14	34.16	9.48	97.18%	9.21
23	86.72	61.53	-	38.81	34.00	8.90	96.71%	8.61
24	86.72	61.53	-	36.61	33.83	8.36	96.24%	8.04
25	-	61.53	23.16	19.73	33.66	7.84	95.77%	7.51
Total	2,168.05	1,807.20	23.16	2,079.29	863.42	442.96	97.45%	431.66

Figure 8.27: Detailed LCOH calculations across the project's lifetime at Viana do Castelo case study for Decentralized Offshore scenario